International
WOCE
Newsletter

Number 39 ISSN 1029-1725 August 2000

IN THIS ISSUE

News from the WOCE IPO

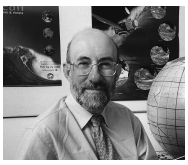

W. John Gould, Director, WOCE IPO and ICPO, Southampton Oceanography Centre, UK. john.gould@soc.soton.ac.uk

Not Long to go Now

Lots of things that I have been dealing with over the period since the last Newsletter have been about activities needed to bring WOCE to a conclusion by the end of 2002. Let me tell you about them.

That Book!

Firstly I have been sending off to Academic Press the completed Chapters for the "WOCE" book now titled "Ocean Circulation and Climate – Observing and Modelling the Global Ocean". Of the 33 Chapters only about 3 need a little more work before they are submitted. All will be completed by the time this newsletter appears on your desks. Unfortunately I still cannot give you information about the price of the book. That will be fixed in September when the publishers have put it all together. It has been an enormous undertaking for the authors, for staff in Hobart and for Roberta Boscolo and Jean Haynes in the WOCE IPO. Gerold Siedler and John Church and I as editors are pleased to see it finally coming together.

Workshops

Today I sent out a final reminder about the deadline for submitting abstracts for the WOCE Workshop in Fukuoka on Variability and Representativeness of the WOCE data sets. We are looking forward to a stimulating meeting. The workshop is co-sponsored by CLIVAR and will provide some important pointers for the ocean sampling strategy that CLIVAR will need to adopt.

There is only one more workshop scheduled in the WOCE AIMS series and that is the one at which the estimates of oceanic transports of heat, freshwater and chemical constituents will be discussed. It will also make progress towards deciding what those transports were during

About WOCE

The World Ocean Circulation Experiment (WOCE) is a component of the World Climate Research Programme (WCRP), which was established by WMO and ICSU, and is carried out in association with IOC and SCOR.

WOCE is an unprecedented effort by scientists from more than 30 nations to study the large-scale circulation of the ocean. In addition to global observations furnished by satellites, conventional in-situ physical and chemical observations have been made in order to obtain a basic description of the physical properties and circulation of the global ocean during a limited period.

The field phase of the project lasted from 1990–1997 and is now being followed by Analysis, Interpretation, Modelling and Synthesis activities. This, the AIMS phase of WOCE, will continue to the year 2002.

The information gathered during WOCE will provide the data necessary to make major improvements in the accuracy of numerical models of ocean circulation. As these models improve, they will enhance coupled models of the ocean/atmosphere circulation to better simulate – and perhaps ultimately predict – how the ocean and the atmosphere together cause global climate change over long periods.

WOCE is supporting regional experiments, the knowledge from which should improve circulation models, and it is exploring design criteria for long-term ocean observing system.

The scientific planning and development of WOCE is under the guidance of the Scientific Steering Group for WOCE, assisted by the WOCE International Project Office (WOCE IPO):

- W. John Gould, *Director*
- Peter M. Saunders, *Staff Scientist*
- N. Penny Holliday, *Project Scientist*
- Roberta Boscolo, *Project Scientist*
- Sheelagh Collyer, *Publication Assistant*
- Jean C. Haynes, *Administrative Assistant*

For more information please visit:
http://www.soc.soton.ac.uk/OTHERS/woceipo/ipo.html

WOCE, whether these estimates differ from and have smaller errors than previous estimates and also towards deciding if we now have a better idea of how to make these estimates in future. I am very pleased to say that Carl Wunsch has agreed to chair the science organising committee for that workshop. It will be held here in Southampton in the last week of June 2001. It will be in conjunction with a related JGOFGS workshop on CO_2 transports that is being organised by Paul Robbins and Rik Wanninkhof. More details of the workshop will be circulated in the coming months.

CD-ROMs Version 2

Over the past months Peter Saunders and Penny Holliday in the IPO and Mark Warner, University of Washington, have been receiving and checking the CD-ROMs submitted by each of the WOCE Data Assembly and Special Analysis Centres that will make up Version 2 of the WOCE CD-ROMs. These have a much more uniform structure and format that the ones issued in 1998 – and most importantly they contain MUCH more data. They will be duplicated by NODC – we are most grateful for their assistance – and will be distributed by the IPO towards the end of 2000. The final set (V3) is scheduled for production in 2002.

Other issues

The WOCE SSG will have its 27th meeting immediately following the Fukuoka Workshop. One topic on the agenda will be the arrangements for a final WOCE Conference. The SSG will be considering how to ensure a balance between a retrospective "What did we achieve?" theme and a focus on "What lessons did we learn?" and "How do we build on WOCE's achievements to improve our ability to understand and predict climate?". We will also once again be discussing the Atlases that we plan to publish based on the WHP One-Time data set. We hope to start the production process very soon.

We plan the next WOCE Newsletter to be issued at the end of the year and to include papers based on the Fukuoka Workshop and a summary of SSG issues. Over the next 2 years the WOCE Newsletter will not appear as frequently as in the past. However I encourage you to submit relevant science articles to the CLIVAR Newsletter – Exchanges.

Farewell to Sheelagh (again)

Sheelagh Collyer, the longest serving member of the WOCE staff formally retires later this month. Sheelagh joined the WOCE Office in November 1988 and was soon known to WOCE scientists around the world as the person who had all the answers at her fingertips. When the IPO moved from Wormley to Southampton in 1994 Sheelagh actually decided to retire and we even held a farewell party for her. But she then decided that she would miss us so much that she moved to Southampton. Since 1998 Sheelagh has been working part-time from home on our publications and you will agree that their quality is a testimony to her attention to detail.

I'm sure you will all join me in saying "Thank you Sheelagh for all you've done for WOCE" and wishing her a long and happy retirement!

Labrador Sea Water in the Iceland Basin: An Overview of the Present Kiel RAFOS Float Programme

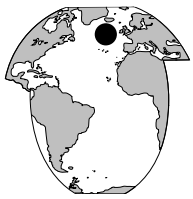

Walter Zenk, Institut für Meereskunde, Kiel, Germany. wzenk@ifm.uni-kiel.de

In 1997 the Institut für Meereskunde started its float programme in the northern North Atlantic. It covers the region north of 50°N and east of the Mid-Atlantic Ridge up to the southern approaches to Iceland (Fig. 1, page 21). In contrast to the open boundary to the south, the deep Iceland Basin is closed to the north. The Iceland–Scotland Ridge acts as a natural barrier for water-mass exchanges between the open North East Atlantic and the Norwegian Sea.

On its eastern margin the upper levels of the water column host warm and salty waters from the northern most extension of the subtropical gyre. Separated by the flow of the North Atlantic Current and its Subpolar Front, the western side of the Basin is dominated by the fresher subpolar regime.

Not only does one find pronounced upper ocean water-mass exchanges across the Subpolar Front, but also between water-masses at intermediate levels (1000–1800 m). The primary water-mass there originates from the Labrador Sea where it has been formed convectively during previous winters. The conventional spreading picture, recently confirmed by a snapshot of the total CFC inventory in the subpolar gyre in the year 1997 (Rhein et al, 2000), suggests this freshly ventilated low-salinity water enters the eastern basins through the Charlie Gibbs Fracture Zone. The latter constitutes a natural gap in the Middle Atlantic Ridge near 52°N.

A second source of mid-depth waters emanates from the warm and salty Mediterranean outflow in the Gulf of Cadiz. How far northward this water-mass can invade the Rockall Trough and the Iceland Basin still remains an open question (see Bower et al., 2000). Finally, Iceland–Scotland Overflow Water at its northern end adds salt to Labrador Sea Water layer. Further mixing components at intermediate depths arise from adjacent strata, i.e. Subpolar Mode Water from above and Lower Deep Water from below.

The main goal of our effort is the circulation and fluctuations in water-masses at the intermediate levels of the Iceland Basin. For our studies we have chosen conventional isobaric RAFOS floats.

Table 1. Details on RAFOS sound sources in the Iceland Basin. The sources are part of the present internationally co-ordinated RAFOS array of the N.E. Atlantic. It dates back to 1990 when the Institut für Meereskunde in Kiel started its first RAFOS observations in the Iberian Basin (Zenk et al., 1992). More information on the array's evolution during the Eurofloat campaign and the other experiments like AMUSE, ARCANE etc. can be found on a web site maintained by Thierry Reynaud from IFREMER, Brest (<http://www.ifremerfr/lpo/eurofloat/index.html>).

Mooring		*Ping time UTC*	*Appr. launch position*		*Launch date*	*Maintenance date*
Code	*IfM No.*		*Lat.*	*Long.*		
IM1	V384	1:00	60° N	25° W	29/5/97	29/6/99
IM2	V385	0:30	57° N	22° W	24/5/97	-
IM3	V388	1:30	53° N	30° W	21/5/97	10/8/98

Table 2. Inventory of cruises in the Iceland Basin in the context of SFB 460 of Kiel University. SFB stands for an accelerated research initiative comprising intensive observations and modelling efforts of fluctuations in the thermohaline circulation in the subpolar gyre of the North Atlantic.

Ship	*Cruise*	*Duration*	*No. of floats launched*
Meteor	39/2	14/5-8/6/97	17
Poseidon	242	2-21/8/98	22
Meteor	45/2	11/6-8/7/99	8
Poseidon	261	planned: July 2000	(10)

Our Lagrangian observations started in the summer of 1997. Three RAFOS sources were moored in the central Iceland Basin (Table 1). With similar instrumentation from the American Atlantic Circulation and Climate Experiment (ACCE), the French ARCANE project and the terminated Eurofloat initiative, these sound sources reflect the backbone for our eddy-resolving observations of circulation patterns at roughly 1500 m depth. So far, we have visited the region three times (Table 2). In total, 47 floats manufactured by SeaScan Inc. of Falmouth, Mass., were launched. 29 instruments surfaced on time, two did not show up, one float was 'deaf'. For all floats but three the nominal target depths was 1500 m. While writing this note (April 2000), 16 floats are still on mission. Presently our data set consists of about 33 float years (fy). Daily readings of instantaneous float positions centred at 01:00 UTC together with on board temperature and pressure observations were processed in the laboratory in Kiel. Pre-programmed mission length varied initially between 15–18 months. More recently they were extended up to two years under water.

At the main entrance for Labrador Sea Water east of Gibbs Fracture Zone delayed releases by multiples of three months were arranged by the newly developed float park

concept (Zenk et al., 2000). A 'park' consists of a number of dual release RAFOS floats. Their first release keeps the instruments temporarily moored on the sea-bed. The second achieves the conventional release of a drop weight at the mission's end.

In the light of this note for the International WOCE Newsletter it is of interest to compare our current harvest of 33 fy with the original requirements of the past WOCE float programme. It had called for 5 fy per $5° \times 5°$ square of the ocean. In our case we count approximately $5° \times 3°$ (longitude × latitude), resulting in 75 necessary fy/box or 44% of the projected coverage. Together with the well-supported float campaigns of our American, British and French colleagues we can already state that the WOCE goals in respect to float coverage in the North Atlantic including the Iceland Basin will definitely be met by the end of the series of on-going experiments.

Fig. 1 (page 21) shows logistical details and some integral results of our observations with floats in the Iceland Basin. Different launch events according to Table 2 are denoted by different symbols (○ 1997, □ 1998, ◇ 1999). The displacement vectors shown connect launch and surface positions of individual floats. Symbols without vectors label floats that are still on mission. Note the general alignment of displacement vectors with the main axis of Maury Channel, i.e. the deep trough on the eastern side of the Iceland Basin. They seem to be antiparallel with a preferred south-westerly direction on the eastern side of the Reykjanes Ridge. At the southern end of our area under investigation a southward export of water is suggested by the vectors. The region represents an extension of the Eurofloat launch sites. This study terminated in 1998 and focused on the frontal exchange at mid depth between the Mediterranean and Labrador Sea Waters in the eastern limb of the subtropical gyre (Speer et al., 1998).

More details are contained in the 'spaghetti' diagram in Fig. 2. We have separated our set of trajectories into two preliminary modes. On the eastern side of the Iceland Basin floats show a well developed tendency towards stagnation or rotation with only little or no significant translations. Here on the more chaotic eddy side of the Basin floats are under the influence of the low-salinity Labrador Sea Water.

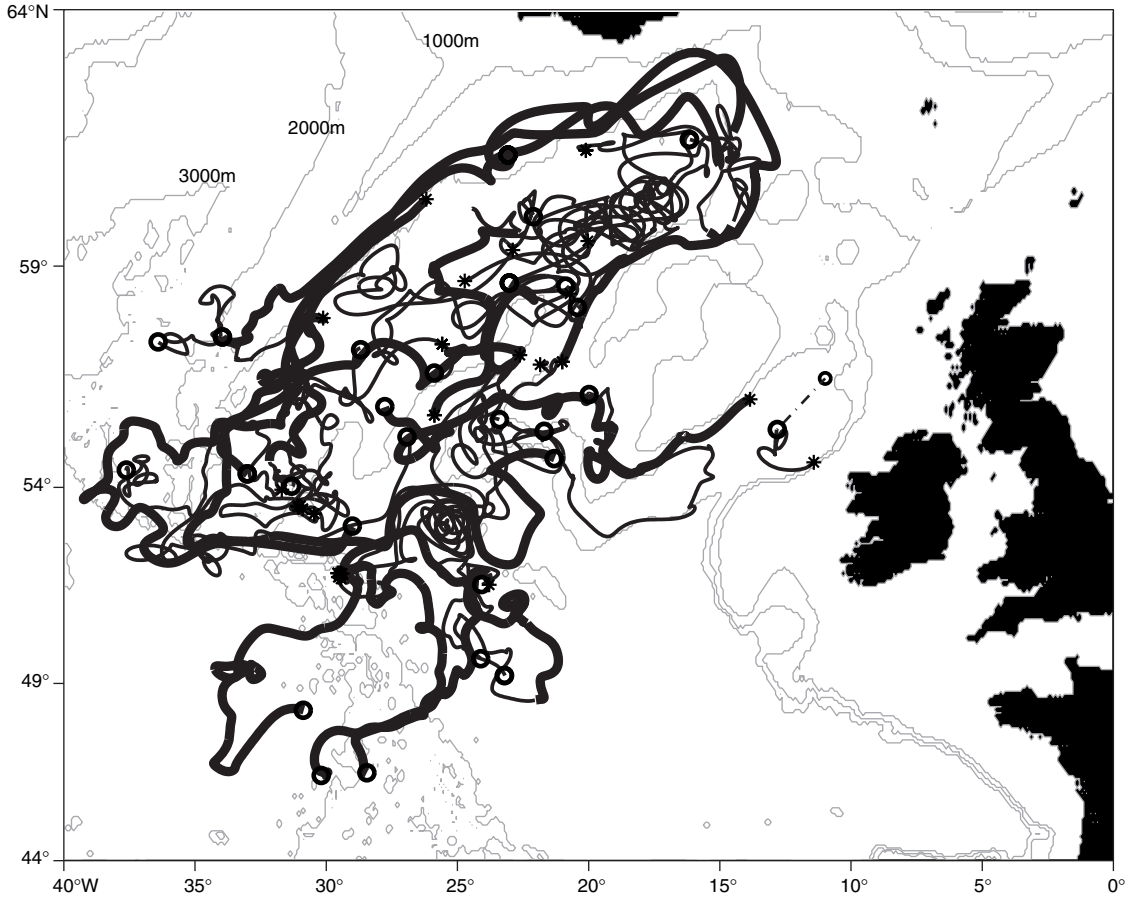

Figure 2. Summary diagram of all available float trajectories (status: April 2000). To enhance the underlying bi-modal structure of the intermediate flow at approximately 1500 m depth we use bold and thinner lines for the plotted pathways. Bold curves denote the preferably steady flow regime on the western side of the Iceland Basin. The more eddy-rich regions in the centre and on the eastern side are represented by thin curves. Black stars stand for launch, big circles for surface positions of RAFOS floats. Where tracking was disturbed we use a thin dashed line. The 1000, 2000, and 3000 m isobaths are included for better orientation.

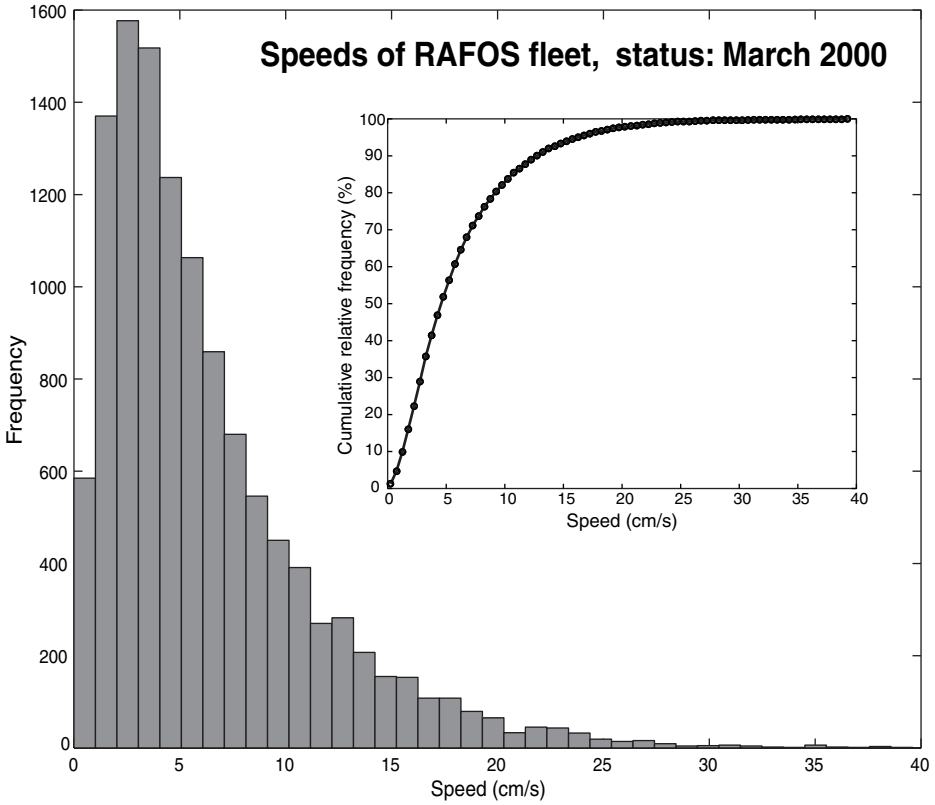

Figure 3. Frequency distributions and its integral (insert) of daily speeds at 1500 m from all floats shown in Fig. 2. Data represent almost 33 float years.

The hydrographic situation differs totally on the western side of the Basin where they are swiftly advected along the Reykjanes Ridge. As a result we infer a well organised steady and swifter flow south of Iceland and along northern portions of the Ridge. The immediate water-mass there consists of Iceland–Scotland Overflow Water which entrains and absorbs the outlying northernmost extensions of Labrador Sea Water. The Lagrangian temperature and pressure time series of our float records will help to study this mixing process in more detail.

A presentation of all daily speed values is given in Fig. 3. We recognise a pronounced peak in the frequency distribution of the whole float fleet in the range $2-4\,\mathrm{cm\,s^{-1}}$. Less frequent speeds of $>11\,\mathrm{cm\,s^{-1}}$ are typical for the northern and north-western rims of the Iceland Basin.

South of about 58°N the Overflow Water still seems to behave like a contour current. While it sinks farther down the flanks of the Ridge our floats at 1500 m depth are detrained from the deeper levels of this fast moving vein when finally reaching Gibbs Fracture Zone. The general cyclonic circulation at the intermediate level in the Iceland Basin is closed potentially by a new vintage of Labrador Sea Water. Once the floats are captured by such a repeat eastward interbasin exchange event they are advected towards the western approaches of Europe again.

It is interesting to note that so far none of our floats north of Gibbs Fracture Zone transgressed permanently from the Iceland Basin into the Irminger Basin. During the forthcoming Poseidon cruise (see Table 2) we will ballast a few floats for deeper levels in order to study the descending

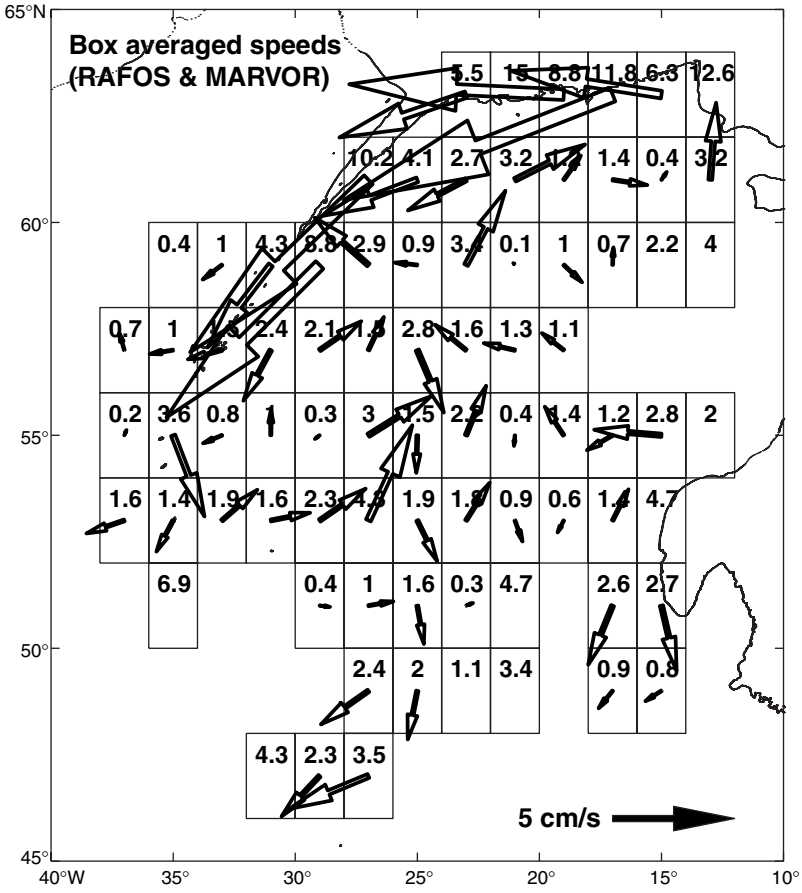

Figure 4. Non-synoptic Eulerian vector averages at approximately 1500 m from our RAFOS data (status: March 2000) and from the MARVOR data set obtained during the first EurofloaT year (Speer et al., 1998). Current speeds are give in addition numerically. As a reference for vector scaling we include the arrow on the bottom right side. For better orientation we repeat the 1000 m isobath (see also Fig. 2).

branch of the Overflow before it can escape to the western subpolar gyre.

Labrador Sea Water reaches the eastern basins through the Gibbs Fracture Zone. Hereafter it diverges into three branches, an eastward limb and two opposite progressing more meridionally aligned limbs, as reported by Paillet and co-workers (1999). In Fig. 4 we demonstrate the kinematics of the Iceland Basin cyclone by preliminary box averages of our Lagrangian vectors supplemented with the Eurofloat data from the first year (Speer et al., 1998). Only boxes with at least two different floats and a minimum residence time of 21 days per $2° \times 2°$ box contain a vector. Its size is proportional to its scalar speed. Independent of duration of float visits and the number of floats per box numerical speeds for all boxes of our data are also included.

The most obvious results obtained for the 1500 m level in the Iceland Basin so far are:

- For the first time we can confirm a well-developed cyclonic circulation by direct long-term Lagrangian current observations.
- The obtained advection pattern can be separated into two different geographical and hydrographical modes. In the centre and on the eastern side of the Basin eddies with little or practically no translation tendency prevail. These regions of chaotic currents enhance local mixing by the availability of eddy kinetic energy. They further degenerate Labrador Sea Water as a characteristic water-mass. On the opposing side, i.e. on the flanks of the Reykjanes Ridge we find persistent currents with higher levels of mean kinetic energy. It is here that the newly formed Iceland–Scotland Overflow Water consolidates after heavy dilution by entrainment farther upstream (Østerhus et al., 1999).
- The outflow core sinks as it parallels the Reykjanes Ridge leaving a level with lower currents behind when approaching the Charlie Gibbs Fracture Zone.

We look forward to receive further data from our experiment which also includes an Eulerian component from five current meters (see Fig. 1, bold stars), and to analyse them jointly with our colleagues and their data from adjacent depths level of this exciting region of the North Atlantic.

Acknowledgements

We thank the nautical crews of the Meteor and the Poseidon for their engaged work in the Iceland Basin. Sylvia Becker diligently tracked our RAFOS floats. Financial support was provided by the Deutsche Forschungsgemeinschaft (SFB 460), Bonn.

References

Bower, A. S., P. L. Richardson, H. D. Hunt, T. Rossby, M. D. Prater, H.-M. Zhang, S. Anderson-Fontana, P. Perez-Brunius, and P. Lazarevich, 2000: Warm-water pathways in the subpolar North Atlantic: An overview of the ACCE RAFOS float programme. Int. WOCE Newsl., 38, 14–16.

Østerhus, S., B. Hansen, R. Kristiansen, and P. Lundberg, 1999: The overflow through the Faroe Bank Channel. Int. WOCE Newsl., 35, 3537.

Rhein, M., J. Fischer, W. M. Smethie, D. Smythe-Wright, R. F. Weiss, C. Mertens, D. H. Min, U. Fleischmann, and A. Putzka, 2000: Labrador Sea Water: pathways, CFC-inventory and formation rates. J. Phys. Oceanogr., submitted.

Speer, K. G., W. J. Gould, and J. Lacasce, 1999: Year-long trajectories in the Labrador Sea Water of the eastern North Atlantic. Deep-Sea Res., II, 46, 1–2, 165–179.

Zenk, W., K. Schultz-Tokos, and O. Boebel, 1992: New observations of Meddy movement south of the Tejo Plateau. Geophys. Res. Lett., 19(24), 2389–2392.

Zenk, W., A. Pinck, S. Becker, and P. Tillier, 2000: The float park: A new tool for a cost-effective collection of Lagrangian time-series with dual release RAFOS floats. J. Atmos. Oceanic Technol., in press.

Is Labrador Sea Water Formed in the Irminger Basin?

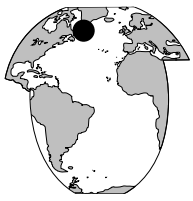

Robert S. Pickart, Woods Hole Oceanographic Institution, USA, and Kara L. Lavender, Scripps Institution of Oceanography, USA. rpickart@whoi.edu

The two major water masses of the mid-depth North Atlantic Ocean are the Mediterranean Water and the Labrador Sea Water. The former is characterised by distinctly high values of salinity, and originates from the outflow through Gibraltar. The latter is recognisable by its weak stratification and is thought to result from convection in the Labrador Sea (hence its name). The Labrador Sea Water (LSW) is particularly important to the ventilation of the Atlantic, and is believed to contribute significantly to the meridional overturning circulation, global heat flux, and modification of the Nordic overflow waters. In this note we explore the possibility that a significant fraction of LSW is actually formed outside of the Labrador Sea, within the Irminger Basin.

This notion is in fact not new – Nansen, Defant, and Sverdrup all argued that deep convection occurred in the Irminger Sea based on oceanographic evidence from the early part of the 20th century. However, at some point between those early measurements and the present day, the conventional thinking changed, and it became commonly accepted that LSW was formed exclusively via convection in the Labrador Basin. Perhaps this change came about as a result of the

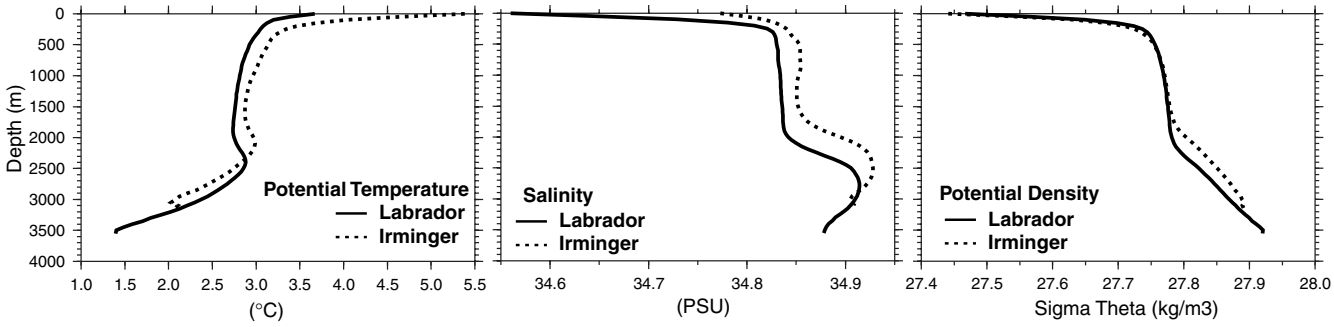

Figure 2. Average vertical profiles in the Labrador and Irminger recirculations, from the 1990s WOCE data.

network of ocean weather ships (OWSs) which was established in the middle of the last century. Included in this network was OWS Bravo in the Labrador Sea, and OWS Alpha in the Irminger Sea. While clear evidence for convection was observed at Bravo (e.g. Lazier, 1980), this was not the case at Alpha. Whether or not this was the reason, the idea eventually emerged that a relatively shallow water mass was formed during winter in the Irminger Sea, as opposed to the deep convected product of the Labrador Sea. Here we present evidence, using modern data, that deep convection occurs in the Irminger Basin as well.

Recently, Lavender et al. (2000) have offered the first-ever view of the absolute mid-depth circulation in the western sub-polar gyre of the North Atlantic (Fig. 1, page 21). This mean streamline map at 700 m, the result of four years of PALACE float data, shows a series of sub-basin scale cyclonic recirculation gyres (four altogether) situated adjacent to the western boundary from east Greenland to Newfoundland. Among other things, these features – which are robust, largely barotropic, and present year-round – serve to "trap" the water to some degree within these areas. During wintertime in the Labrador Sea, cold air blows off the Canadian land mass and cools the surface water, causing convection. In light of the trapping noted above, one would then expect the overturning to occur most readily within the trough of the cyclonic gyre in the western Labrador Sea. This indeed seems to be the case, as seen in Fig. 1, which shows the region of deepest convection observed in winter 1997 (which is the only such basin-wide survey conducted in the Labrador Sea during deep convection). The same pattern is also seen in the PALACE float hydrography (not shown).

In analogous fashion to the Labrador Sea, cold air also blows off of Greenland over the Irminger Sea during winter. Using the same argument, one might expect convection to occur within the cyclonic gyre situated in the western Irminger Sea. However, the atmospheric forcing is generally less there (see below), so convection might only occur during particularly strong winters. The best measure of the "robustness" of a winter is the North Atlantic Oscillation (NAO) index, defined as the normalised sea-level pressure difference between Iceland and the Azores (Hurrell, 1995). A high NAO means stronger westerly winds in the subpolar North Atlantic, a more northerly storm track, and a higher frequency of storms – all of which add up to stronger air-sea forcing in both the Labrador and Irminger Seas. Unfortunately, there are no wintertime surveys of the Irminger Sea during a strong winter, thus we cannot construct a comparable map of mixed-layer depth as

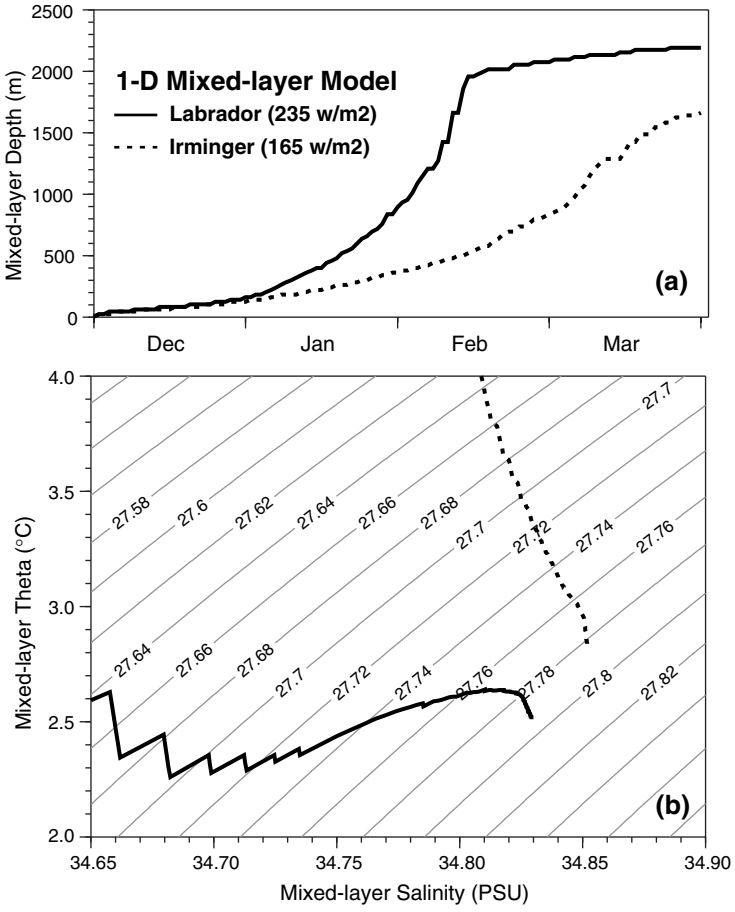

Figure 3. (a) Time evolution of mixed-layer depth in the Labrador and Irminger Seas, using the mixed-layer model with the indicated forcing. (b) Evolution of the mixed-layer potential temperature and salinity.

was shown for the Labrador Sea. However, the A1E hydrographic line of the World Ocean Circulation Experiment (WOCE) spans the southern Irminger Sea, and was occupied numerous times in the 1990s during the recent high NAO period (non-winter occupations). The mean distribution of potential vorticity (PV) along this line, at the density level of the LSW, is included in Fig. 1. Note that the lowest PV water – i.e. the most recently ventilated water – is located precisely within the trough of the Irminger Sea cyclonic gyre. This is analogous to the Labrador Sea scenario, and constitutes strong support for local convection in the Irminger Basin. Note that if the newly ventilated water seen in the A1E section had originated from the Labrador Sea, as is suggested by Sy et al. (1997), the lowest PV signal would appear outside the Irminger gyre, not within it.

In addition to the trapping of water by the recirculation gyres, and the cold wind emanating from the continental boundaries during winter, another critical factor for convection is the pre-conditioning of the water column. In the Labrador Sea, upper-layer isopycnals generally dome upward towards the centre of the basin, allowing more weakly stratified water to reside near the surface. This condition makes it easier for the air-sea forcing to destabilise the water column after the seasonal stratification has been eroded. A similar isopycnal doming occurs in the Irminger Sea, so it is of interest to compare the extent of pre-conditioning in the two seas. This is done in Fig. 2, which shows the springtime mean vertical profiles of potential temperature, salinity, and potential density (referenced to 0 db) in the Labrador and Irminger Seas. The averages were computed from the 1990s WOCE data (the A1E line in the Irminger Sea, and the AR7W line in the Labrador Sea), confined spatially to the region within the respective recirculation gyres (Fig. 1, page 21). Not surprisingly, the water in the Irminger Sea is warmer and saltier. However, these variables compensate each other such that the density profiles are nearly identical over the top 1500 m. Since density is the pertinent variable for overturning, this shows that, in terms of preconditioning, there is nothing special about the Labrador Sea versus the Irminger Sea.

Finally, is the atmospheric forcing strong enough to cause deep overturning of the pre-conditioned water within the Irminger basin cyclonic recirculation? To test this, we applied a simple 1-dimensional mixed-layer model to the average vertical profiles from Fig. 2 for each basin. As mentioned above, the winter air–sea forcing is somewhat less in the Irminger Basin. From a 20-year climatology of National Center for Environmental Prediction (NCEP) meteorological fields, the average total heat flux during winter is $50 - 75\,w / m^2$ stronger at the Labrador AR7W line than the Irminger A1E line. Applying the heat loss for a canonical strong winter to the two average density profiles, overturning occurs to 2000 m in the Labrador Sea and 1500 m in the Irminger Sea, taking roughly a month longer to reach full depth in the Irminger Sea (Fig. 3a). This is further (indirect) evidence that deep convection is likely to occur during high NAO winters in the Irminger Sea. Furthermore, the final water mass product in each basin is quite similar (Fig. 3b), which would make it difficult to distinguish between them any distance away from the Labrador Sea.

In summary, while historical evidence from the early 20th century suggested that deep convection occurred in the Irminger Sea, the notion fell out of favour during modern times. This change might have come about because of the lack of evidence for overturning at OWS Alpha, but we know now that Alpha was located east of the Irminger cyclonic recirculation gyre, away from the expected area of overturning where the water is trapped and subject to the elevated heat loss seaward of Greenland. The recent hydrographic and float data presented here suggest that the historical notion was likely correct, though this needs to be verified with wintertime measurements in the Irminger Sea. If LSW is formed in the Irminger Basin (and is close in properties to that formed in the Labrador Basin), this carries strong ramifications both in terms of interpreting the large-scale hydrography of the North Atlantic, as well as understanding/validating ocean general circulation models.

References

Hurrell, J. W., 1995: Decadal trends in the North Atlantic Oscillation: Regional temperatures and precipitation. Science, 269, 676–679.

Lavender, K. L., R. E. Davis, and W. B. Owens, 2000: Mid-depth recirculation observed in the interior Labrador and Irminger Seas by direct velocity measurements. Nature, accepted.

Lazier, J. R. N., 1980. Oceanographic conditions at Ocean Weather Ship Bravo, 1964–1974. Atmos. Ocean, 3, 227–238.

Sy, A., M. Rhein, J. R. N. Lazier, K. P. Koltermann, J. Meincke, A. Putzka, and M. Bersch, 1997: Surprisingly rapid spreading of newly formed intermediate waters across the North Atlantic Ocean. Nature, 386, 675–679.

Mixing of Antarctic Intermediate Water from the Atlantic and Indian Ocean at the Agulhas Retroflection

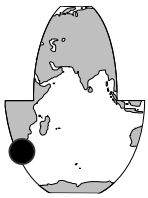

Olaf Boebel, University of Rhode Island, USA; Charlie Barron, Naval Research Laboratory, Stennis Space Center, USA; Phil Richardson, Woods Hole Oceanographic Institution, USA; Johann Lutjeharms, University of Cape Town, South Africa; and Russ Davis, Scripps Institution of Oceanography, USA. oboebel@gso.uri.edu

The exchange of water between the Atlantic and Indian Oceans south of Africa is strongly depth dependent. While the influx of Indian Ocean Central Water from the Indian to the Atlantic Ocean has been documented by observational studies (e.g. Gordon et al., 1992), the behaviour of the deeper layers is less clear. On the average, North Atlantic Deep Water and bottom waters are expected to flow in the opposite direction, i.e. to escape from the Atlantic to the Indian Ocean, while the fate of Antarctic Intermediate Water (AAIW) is least known (Shannon and Hunter, 1988).

AAIW forms a layer about 500 m thick between the Central and Deep Waters and is clearly characterised by a vertical salinity minimum near the $27.2\,\sigma_\theta$ isopycnal surface. On this surface, distinctly different minimum salinities are observed in the Indian (S = 34.40) and Atlantic (S = 34.25) Oceans, but despite this unmistakable tracer signal, it is difficult to determining the inter-ocean transport. The problem is due to the strong mixing of these water types and the underlying intense mesoscale flow field which defeats a climatological description by a few sections. The amount of influx of Indian Ocean intermediate water into the Atlantic however is a crucial parameter in the characterisation of the global thermohaline circulation since the added heat and salt from the Indian Ocean help to precondition the Atlantic for deep convective events. Hence, open questions revolve around salt, heat and freshwater inter-ocean transports and the mechanisms responsible.

The main inter-ocean exchange mechanism for Central Water is undoubtedly the formation of Agulhas Rings at the Agulhas Retroflection region. (Lutjeharms, 1996), but this is arguable for the intermediate depth layer. Ring shedding involves closing of the Agulhas Retroflection onto itself, a process that requires an increasing narrowing of the Retroflection loop. This can either be triggered by the intruding cold core wedges of subantarctic origin from the south or via boundary trapped pulses of the Agulhas Current. Shoaling isotherms within these features also produce low surface temperatures which are discernible in AVHRR images. Since these processes were mostly observed by remote SST imagery, the vertical extent of these features is unclear. Due to enhanced atmospheric cooling of the warm Indian Ocean inflow the SST-contrast quickly dissolves in the interior Cape Basin, where Indian Ocean water is expected to drift north and to mix its high salinity signal into the surrounding fresher Atlantic Waters (Fig. 1).

To obtain a mesoscale resolving, multi-year estimate of the subsurface flow field, an international team of scientists collaborated within KAPEX (Cape of Good Hope Experiments; (Boebel et al., 1998)) to deploy a total of 114 RAFOS floats in the region around southern Africa.

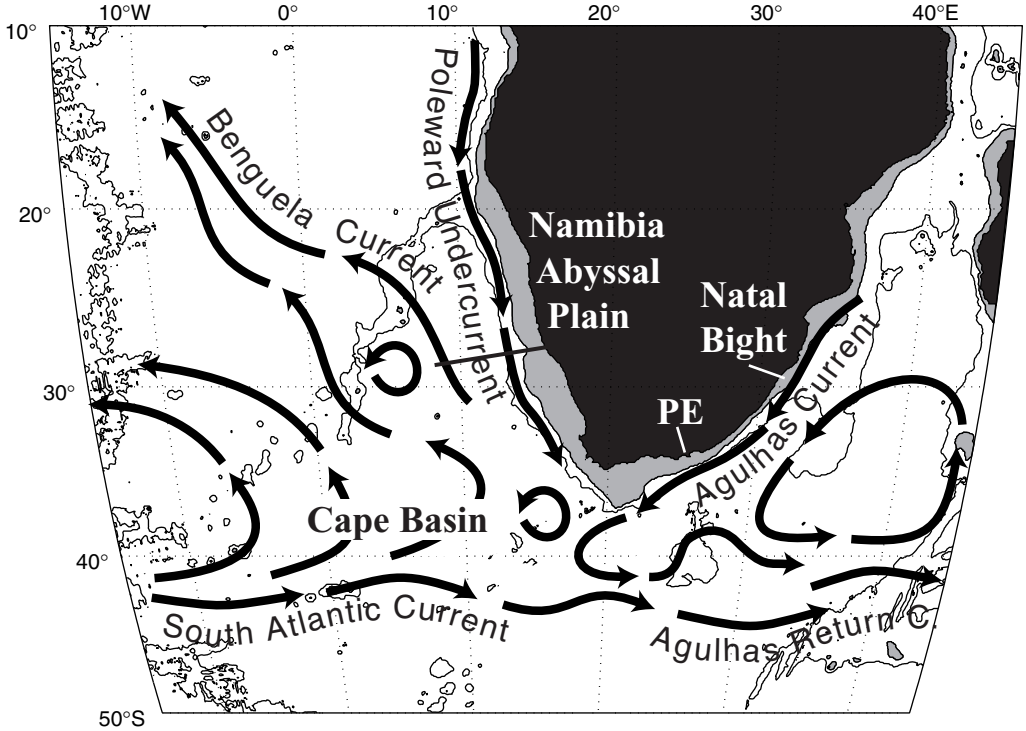

Figure 1. Schematic of intermediate flow paths in the KAPEX region. The areas shallower than 1000 m are lightly shaded. The 3000 m isobath in indicated by a dashed line.

These instruments (Rossby et al., 1986) are designed to drift passively at intermediate depth, while recording their distance to moored sound sources and pressure and temperature at regular intervals. Returning to the sea-surface after pre-programmed subsurface mission periods, the floats transmit the collected data via satellite to the researcher, who can determine the floats trajectories and hydrographic environment.

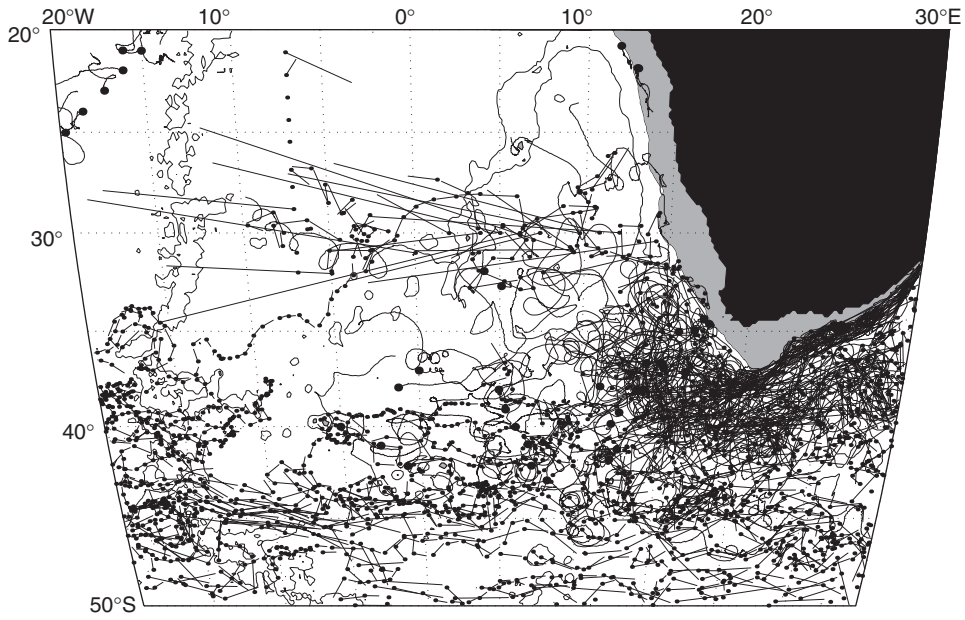

Figure 2. Trajectories and displacement vectors from 47 ALACE and 114 RAFOS floats in the region around southern Africa. Start positions are indicated by small dots.

KAPEX RAFOS floats

Between March 1997 and October 1999, KAPEX collaborators deployed the RAFOS floats and moored 11 sound sources in the region. Isobaric RAFOS floats (67) were launched to capture the inflowing South Atlantic Current and the outflowing Benguela Current, and 47 isopycnal RAFOS floats were launched into the Agulhas Current (Fig. 2).

The isobaric floats (Rossby et al., 1986) were individually ballasted to drift at the depth of the local salinity minimum which is characteristic for the intermediate waters of the region. Its depth varies between 800 m for intermediate water of South Atlantic origin, and 1200 m for intermediate water stemming from the Indian Ocean. Isopycnal floats (Rossby et al., 1985) were ballasted for the 26.8 and 27.2 σ_θ surfaces. The latter isopycnal surface is a close proxy for the minimum salinity surface, regardless of the water parcel's Atlantic or Indian Ocean origin.

Most floats sampled position, temperature and pressure at 12 h intervals. Of the total of 114 floats launched, 105 returned to the surface and successfully transmitted their recorded data. In support of the sea-going activities, the KAPEX hydrographic database was assembled, which combined CTD and XBT data from numerous databases.

The mean flow at intermediate depth

A first estimate of the mean flow at intermediate depth was made by box averaging all float data located between 650 and 1050 dbar. The box size was 4° longitudinal by 2° meridional. Data for this effort included all tracked KAPEX RAFOS floats (75 floats), and launch to surface position displacement vectors from KAPEX floats yet untracked (29 floats). While the use of these displacement vectors enhances the mean flow estimates, it prohibits the calculation of second order statistics and the error based thereupon at this stage. Additional data from 47 ALACE floats that drifted into the area from the Atlantic and Indian Oceans consist of displacement vectors spanning periods between 10 and 25 days.

The analysis (Fig. 3, page 22) shows eastward velocities south of 40°S, associated with the South Atlantic and Antarctic Circumpolar Currents (red arrows). No clear kinematic distinction between these two currents is visible. In the Atlantic, between 35°S and 25°S, the westward flow in the northern limb of the intermediate depth subtropical gyre is obvious (blue arrows). Along the Indian Ocean coast of southern Africa, the Agulhas Current is represented by swift south-westward flow (long blue arrows), which dissolves near 40°S, 20°E at the Agulhas Retroflection. From there, the Agulhas Return Current (red arrows) emerges, carrying intermediate water eastward, after a northern circumnavigation of the Agulhas Plateau. A separation between the Agulhas Return Current and the combined South Atlantic/Antarctic Circumpolar Currents is indicated east of 20°E by the diffuse flow field between 40–45°S.

The superposition of the mean velocity field and climatological position of isohalines (green lines in Fig. 3) on $\sigma_\theta = 27.2$ as obtained from the KAPEX hydrographic database reveals a strong association of the westward flow field with the $S = 34.3$ to 34.4 regime in the Namibia Abyssal Plain and southern Angola Basin. A continuous advective connection between the eastward flowing southern limb of the subtropical gyre (i.e. the South Atlantic Current) and the Benguela Current, as it was presupposed at the beginning of this project (Fig. 1, curling arrows between 10°W and 10°E), is not apparent in our data. This is indicated by a zone of sluggish and undirected flow around 40°S in the Cape Basin. The source of the water flowing in the Benguela Current appears to be rather an approximately equal mixture of Indian Ocean and Atlantic intermediate

waters which converge at the Agulhas Retroflection.

A northeast- to northward increase of salinity is observed in the Cape Basin and across the Benguela Current (Fig. 3). This could be due to an increased Indian Ocean influence on the Benguela Current along its coastal (eastern) side, but it also could be a residue from the objective mapping, which produces such a isohaline distribution per se due to high salinities in the tropical gyre to the north and the long correlations scales employed to overcome the data sparseness. Hence, to understand the mechanisms responsible for the formation of the westward flowing type of AAIW of increased salinity, the observation of the flow and salinity fields at mesoscale resolution appears necessary.

MODAS and the mesoscale field

The Naval Research Laboratory and Naval Oceanographic Office at Stennis Space Center use the Modular Ocean Data Assimilation System (MODAS) (Carnes et al., 1996) to produce, as one of several products, global, daily, $\frac{1}{8}^\circ$ resolution maps of sea-surface steric height anomalies relative to 1000 m. Steric height anomaly is the difference in the height of a given water column and the height of an ideal 0°C, 35 salinity column, where the heights are integrated between specified pressure surfaces. MODAS daily global estimates of steric height anomaly begin with optimal interpolation (OI) of TOPEX and ERS-2 altimetry. The OI uses a mesoscale-tuned estimate of the error covariance (Jacobs and Barron, submitted) to develop a field of height deviation from the altimetric mean. The final steric height anomaly is produced by adding the deviation field to two others, a MODAS climatological mean steric height anomaly and a correction for the difference between the altimetric and climatological means. The climatological steric height anomaly is computed by integrating from the climatological pressure at 1000 m to the surface (for more details, see http://www7300.nrlssc.navy.mil/altimetry). The steric height anomaly is a true height and will be referred to as SSH.

Animated visual comparison of float trajectories with the evolution of the MODAS-SSH field revealed a strong agreement between the location and propagation of mesoscale features as depicted by floats and SSH. This is illustrated in Fig. 4 (page 22), where strong positive (red) and negative (blue) SSH anomalies coincide with anticyclonic and cyclonic float trajectory segments, respectively. Four features stand out in this image. An anticyclonic Agulhas Ring is observed near 36°S, 14°E, which is separated from the Agulhas Retroflection (38°S, 20°E) by an cyclonic eddy (37°S, 16°E). Simultaneously a meander in the Agulhas Current trapped a cyclonic eddy (37°S, 22°E) along the continental shelf break.

The floats traced such features for extended periods of time, as can be viewed in a movie that can be downloaded by anonymous ftp (37 Mbytes; pogo.gso.uri.edu/pub/oboebel/agulhas_ssh.zip). The strong association of floats with the SSH signal indicates that the trapping depth of mesoscale features extend to at least 27.2 σ_θ isopycnal (between 800 and 1200 m depth) in this area. The combined float/SSH data set enabled us to continuously observe the evolution of mesoscale features in the greater Agulhas region, results of which are discussed for the two major mesoscale events known for the region, Agulhas Rings and Natal Pulses.

Table 1. Observation period and site of first identification of cyclonic Agulhas Current meanders.

Observation period	*Formation site*
February - April 1997	Port Elizabeth
November - December 1997	Port Elizabeth
July - September 1998	Natal Bight
March - May 1999	Port Elizabeth
October - November 1999	Port Elizabeth

Agulhas Current meanders and Rings

During the 3 years of the experiment, we observed 5 major and 6 minor cyclonic events along the inshore side of the Agulhas Current. Minor cyclonic events occurred in April, June and September 1997, April and November 1998 as well as February 1999. The occurrence of major cyclones that propagated downstream and were finally shed at the tip of the Agulhas Bank are listed in Table 1. The total number of shelf-trapped cyclonic events (11 in 3 years) is similar to earlier estimates of Natal Pulse frequency (14 in 4 years, de Ruijter et al., 1999). Most of the meanders we resolved were only discernible from Port Elizabeth downstream. This is in contrast to the belief that all major meanders, Natal Pulses, are formed in the Natal Bight.

While the 6 minor cyclonic events did mostly remain stagnant near the widening shelf of the Agulhas Bank, the 5 major Agulhas Current meanders translated south-westward along the continental shelf break at similar speeds, averaging to $11.6 \pm 0.8\,\mathrm{cm\,s^{-1}}$. This is in contrast to earlier observations by other authors (Lutjeharms and Roberts, 1988), who found a propagation speed of $15 - 20\,\mathrm{cm\,s^{-1}}$ for the region north-east of Port Elizabeth and $5 - 6\,\mathrm{cm\,s^{-1}}$ to the south-west of Port Elizabeth.

Eddies embedded in major meanders of the Agulhas were shed from their captured position between the coast and the Agulhas Current at the southernmost tip of the Agulhas Bank. In all cases this involved a pinching off of a juvenile Agulhas Ring, which is why the region adjacent to the tip of the Agulhas Bank can be viewed as a cross-road in which Agulhas Rings translate north-westward and cyclonic eddies drift west- or south-westward. This has also been noted recently in a high resolution numerical model of this region (Penven and Lutjeharms, in preparation).

Similar to the study of Agulhas Current Pulses, the combined float/SSH data set enabled us to continuously observe the events leading to the shedding of Agulhas Rings. During the 3 year experimental period we observed 16 rings to drift through the Cape Basin. This number is at the lower end of earlier estimates (4–9 per year, Lutjeharms,

1996), however the identification of a ring shedding event is inherently difficult, due to numerous rings re-attaching to the Agulhas Retroflection or merging together during their early stage. The phase propagation of the positive SSH anomalies associated with rings was 5.2±1.7 cm/s, which is lower than estimates in the literature (6–9 cm/s, Olson and Evans, 1986).

Acknowledgements

Excellent support from all officers and crews of vessels involved in KAPEX is greatly appreciated. These are, in alphabetical order, SA KUSWAG I, SA KUSWAG V, RV Seward Johnson and RV Polarstern. Further participants of KAPEX, i.e. Chris Duncombe Rae, Dave Fratantoni, Silvia Garzoli, Tom Rossby, Claudia Schmid and Walter Zenk provided indispensable support and valuable scientific discussions throughout the project. Essential technical and scientific contributions were made by I. Ansorge, S. Becker, R. Berger, P. Bouchard, D. Carlsen, J. Fontaine, S. Fontana, H. Hunt, J. Kemp, M. Nielsen and C. Wooding. Support from the National Science Foundation, USA, the Foundation for Research Developments, RSA, the Ministerium für Bildung, Wissenschaft, Forschung und Technologie, Germany, the Alexander-von-Humboldt Foundation, Germany, and the Alfred-Wegener-Institut, Germany is acknowledged.

References

Boebel, O., C. Duncombe Rae, S. Garzoli, J. Lutjeharms, P. Richardson, T. Rossby, C. Schmid, and W. Zenk, 1998: Float experiment studies interocean exchanges at the tip of Africa. EOS, 79(1), 1, 6-8.

Carnes, M. C., D. Fox, and R. Rhodes, 1996: Data assimilation in a north Pacific Ocean monitoring and prediction system. In: Modern Approaches to Data Assimilation in Ocean Modeling, P. Malanotte-Rizzoli (ed.), pp. 319–345, Elsevier, New York.

de Ruijter, W. P. M., P. J. van Leeuwen, and J. R. E. Lutjeharms, 1999: Generation and Evolution of Natal Pulses: Solitary meanders in the Agulhas Current. J. Phys. Oceanogr., 29 (12), 3043–3055.

Gordon, A. L., R. F. Weiss, W. M. Smethie, and M. J. Warner, 1992: Thermocline and intermediate water communication between the South Atlantic and Indian Ocean, J. Geophys. Res., 97 (C5), 7223–7240.

Jacobs, G. A., and C. N. Barron: The Mesoscale Scale. J. Geophys. Res., submitted.

Lutjeharms, J. R. E., 1996: The exchange of water between the South Indian and South Atlantic Oceans. In: The South Atlantic: present and past circulation, G. Wefer, W., H. Berger, G. Siedler, and D. J. Webb (eds.), pp. 122–162, Springer-Verlag, Berlin-Heidelberg.

Lutjeharms, J. R. E., and H. R. Roberts, 1988: The Natal Pulse: an extreme transient of the Agulhas Current. J. Geophys. Res., 93(C1), 631–645.

Olson, D. B., and R. H. Evans, 1986: Rings of the Agulhas Current. Deep-Sea Res., 33(1), 27-42.

Penven, P., and J. R. E. Lutjeharms. Formation and behaviour of cyclonic eddies attendant on the Agulhas Current. J. Phys. Oceanogr., in preparation.

Rossby, H. T., E. R. Levine, and D. N. Connors, 1985: The isopycnal Swallow Float – a simple device for tracking water parcels in the ocean. Prog. Oceanogr., 14, 511–525.

Rossby, T., D. Dorson, and J. Fontaine, 1986: The RAFOS System. J. Atmos. Oceanic Technol., 3, 672–679.

Shannon, L. V., and D. Hunter, 1988: Notes on Antarctic Intermediate Water around southern Africa. S. African J. Mar. Sci., 6, 107–117.

The Role of the Southern Ocean in the Upwelling of North Atlantic Deep Water

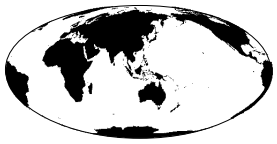

Pedro de Vries and Sybren Drijfhout, Royal Netherlands Meteorological Institute (KNMI), The Netherlands; and Andrew C. Coward, Southampton Oceanography Centre, UK. pvriesde@knmi.nl

The flow of North Atlantic Deep Water (NADW) is part of a global circulation cell that is thought to be a thermohaline circulation (THC). Several models have described the THC in terms of loss and gain of buoyancy, where the latter is provided by interior mixing giving rise to uniform upwelling of NADW (Stommel, 1958). In this case, a scaling relation between circulation strength, buoyancy forcing and diffusion coefficient for interior mixing can be established (Bryan, 1987). It has been shown (Marotzke, 1997) that these scaling results are fairly insensitive to assumptions about the spatial distribution of the interior mixing.

The view that the THC is (exclusively) driven by buoyancy differences has been challenged by several authors (Warren, 1990; Toggweiler and Samuels, 1995). For instance, Toggweiler and Samuels point out that the equatorward Ekman transport at the northern boundary of Drake Passage almost equals the strength of the THC and argue that the compensating deep poleward flow consists of NADW. In this formulation, NADW ventilates in a region of upward Ekman pumping and buoyancy gain at the surface, the latter being a far more efficient process than buoyancy gain by interior mixing. The THC would thus be driven mainly by Southern Ocean winds and NADW would almost exclusively upwell southward of 57°S, which is the tip of South America. Eddy-related transports have to be taken into account, however, since they can also compensate the northward Ekman flow. By parameterising the eddies in the Southern Ocean, Gnanadesikan (1999)

derived a new scaling relation that includes all the above processes.

Here, we present results on the upwelling behaviour of NADW using the high-resolution global ocean model OCCAM (Webb et al., 1997). We employed data from a run in which the wind forcing was defined by the re-analysed six-hourly ECMWF winds. Both model climatology and an evaluation of the eddy contributions were derived from archived five-day averages covering a three-year model run. Our flow field was constructed by transforming the five-day averaged velocities from z to density coordinates, determining the averaged mass transport within fixed isopycnals and, finally, transforming this quantity back to z coordinates. In this way, we obtain a velocity field that contains both the annual-mean component as well as an eddy-induced component, i.e. an effective velocity due to the time-varying mass transports.

In a previous study on NADW upwelling, Döös and Coward (1997) calculated Lagrangian trajectories using annual-mean velocities only. In eddy-active regions such as the Southern Ocean, however, the spreading of water-masses cannot be represented by the mean flow only. This can be appreciated by considering Figs. 1a and 1b, which show zonally-integrated streamfunctions as a function of density corresponding to, respectively, the annual-mean velocities and the eddy-induced mass transports obtained as described above. At potential densities larger than $\sigma_2 = 36.8$ we see the southward flow of NADW from the Atlantic equator. Above this density level the northward spreading of the NADW return flow is seen. The streamfunction in Fig. 1a also exhibits an extra recirculation cell of about 10 Sv between 35° and 60°S. The downwelling of 10 Sv between 35° and 45°S is not realistic. This recirculation is akin to the so-called Deacon cell that results spuriously from averaging transports in z instead of density coordinates (Döös and Webb, 1994). The latter type of

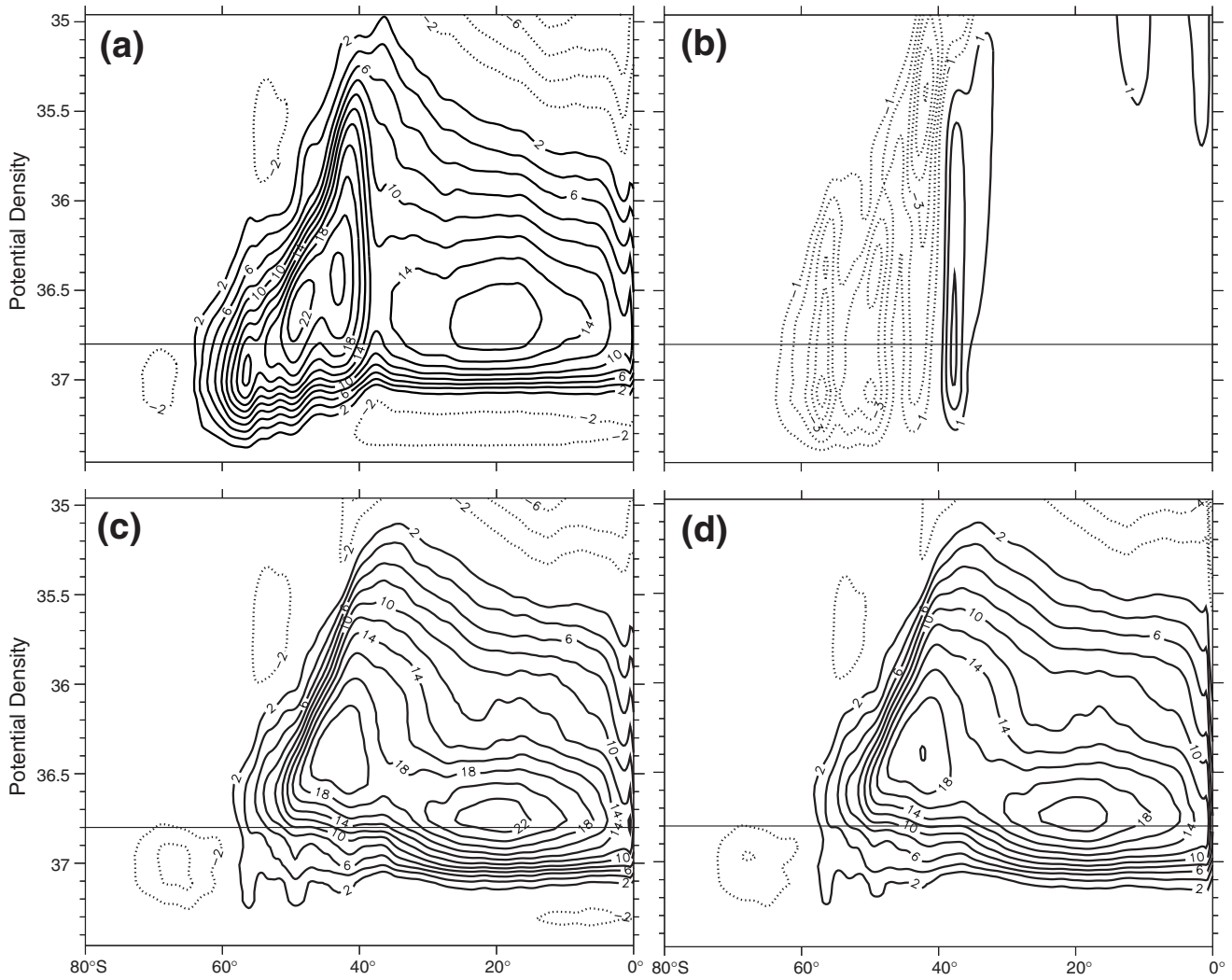

Figure 1. Zonally-integrated streamfunctions as a function of latitude and potential density σ_2 for the (a) annual-mean velocity field, (b) eddy-induced transports, (c) flow field averaged over density surfaces and including the correction for model drift and (d) summed transports through each grid cell of the calculated NADW trajectories. Contours are in Sverdrups. The density dividing NADW and light water is also indicated.

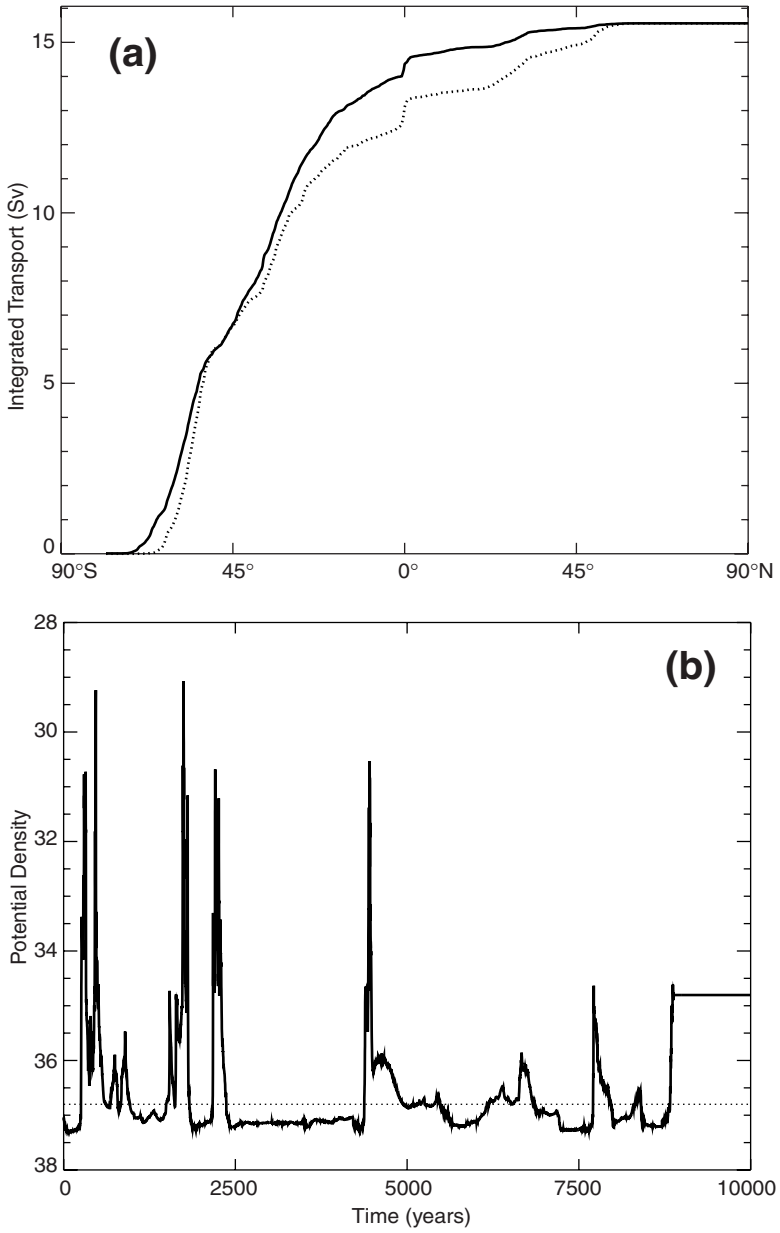

Figure 2. (a) Zonally and meridionally-integrated upwelled transports as a function of latitude. Drawn (dotted) curve corresponds with the first (last) upwelling of NADW. The total transport of NADW is 15.6 Sv. (b) Variation of potential density σ_2 of one NADW trajectory as a function of time. Trajectory starts (t = 0) at Atlantic equator flowing southwards and finally returns with $\sigma_2 < 36.8$.

averaging is more appropriate here, since water masses move along isopycnals. Due to this recirculation, upwelling of NADW as calculated from annual-mean velocities will occur preferably in this region. It is apparent from Fig. 1b that the eddy-induced mass transports reduce this recirculation cell and shift it towards shallower levels.

We have also accounted for the effect of model drift on mass transport. The long-term mass transformation rates of in- and deflating density layers were evaluated and from these a flow field was constructed in which the mean drift of each layer is removed. Details of this method will be reported elsewhere. Now, the recirculation cell in corresponding overturning streamfunction (Fig. 1c) is reduced further to about 3 Sv and is now mainly confined to the upper 1000 m. Employing this corrected flow field we calculated Lagrangian trajectories associated with the flow of NADW. About 15.6 thousand trajectories starting at the Atlantic equator were traced until they returned representing light water. The spreading paths and upwelling sites of NADW in the model immediately confirms the role of the several key processes mentioned above in driving the THC. In particular, the extent to which the upwelling is biased to the region south of 57°S points to the relevance of the scenario advocated by Toggweiler and Samuels. We distinguish between NADW and lighter waters by defining upwelling as a mass transfer through the density surface with potential density $\sigma_2 = 36.8$. This interface typically lies at 2000 m depth in most parts of the global ocean, but surfaces at high latitudes.

The tracing technique utilised here was originally developed by Döös (1995) and Blanke and Raynaud (1997). For a given velocity field the particle displacements are solved analytically within each grid cell. This method is computationally very efficient and allows us to calculate thousands to millions of trajectories for very long periods. The validity of the tracing technique can be demonstrated by calculating a streamfunction by summing the mass transport associated with each computed trajectory through each grid cell of the model. The resulting overturning streamfunction is shown in Fig. 1d, where the flow of NADW appears to almost fully capture the one of Fig. 1c.

Almost 25% (3.6 Sv) of NADW upwells southwards of 57°S, see Fig. 2a. The total amount of NADW upwelling southwards of 45°S, being the latitude of maximal wind stress and the northern boundary of the upward Ekman pumping, is approximately 45% (6.7 Sv). These numbers indicate that the scenario of Toggweiler and Samuels is indeed important in driving the THC, but also that interior diapycnal mixing as driving agent cannot be neglected. The fact that the THC is driven by two completely different physical mechanisms may have important implications for its stability characteristics. Calculations also show that after NADW has upwelled it generally does not return directly to the North Atlantic as light water. Water parcels are subject to many upwellings and downwellings during their course through the global ocean. This behaviour is illustrated by the fate of one particular NADW trajectory in Fig. 2b. Calculated transports (Fig. 2a) through $\sigma_2 = 36.8$ differ for the first and last upwelling event of NADW. At 45°S the difference is zero. When employing transports from the annual-mean flow only the difference between these two

events can be very pronounced: 5 Sv at 45°S. By taking into account eddy-induced transports and model drift this is reduced by 70% and 30%, respectively. The recurrent upwelling and multiple connection between upper and lower branch of the THC is currently the subject of further research.

Acknowledgements

This work is financially supported by the European MAST-III project TRACMASS (contract MAS3-CT97-0142). Computational facilities were supplied by the Southampton Oceanography Centre.

References

Blanke, B., and S. Raynaud, 1997: Kinematics of the Pacific Equatorial Undercurrent: An Eulerian and Lagrangian approach from GCM results. J. Phys. Oceanogr., 27, 1038–1053.

Bryan, F., 1987: Parameter sensitivity of primitive equation ocean general circulation models. J. Geophys. Res., 17, 970–985.

Döös, K., 1995: Interocean exchange of water masses. J. Geophys. Res., 100, 13499–13514.

Döös, K., and A. C. Coward, 1997: The Southern Ocean as the major upwelling zone of North Atlantic Deep Water. Int. WOCE Newsl., 27, 3–4.

Döös, K. and D. J. Webb, 1994: The Deacon cell and the other meridional cells of the Southern Ocean. J. Phys. Oceanogr., 24, 429–442.

Gnanadesikan, A., 1999: A simple predictive model for the structure of the oceanic pycnocline. Science, 283, 2077–2079.

Marotzke, J., 1997: Boundary mixing and the dynamics of the three-dimensional thermohaline circulations. J. Phys. Oceanogr., 27, 1713–1728.

Stommel, H., 1958: The abyssal circulation. Deep-Sea Res., 5, 80–82.

Toggweiler, J. R., and B. Samuels, 1995: Effect of Drake Passage on the global thermohaline circulation. Deep-Sea Res., 42, 477–500.

Warren, B. A., 1990: Suppression of deep oxygen concentrations by Drake Passage. Deep-Sea Res., 37, 1899–1907.

Webb, D. J., A. C. Coward, B. A. de Cuevas, and C. S. Gwilliam, 1997: A multiprocessor ocean general circulation model using message passing. J. Atmos. Oceanic Technol., 14, 175–183.

Changes in the Deep and Bottom Waters of the Scotia Sea, 1995–1999

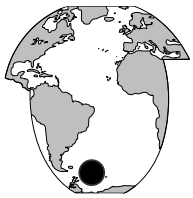

Michael P. Meredith and Alberto C. Naveira Garabato, School of Environmental Sciences, University of East Anglia, UK; David P. Stevens, School of Mathematics, UEA, UK; Karen J. Heywood, School of Environmental Sciences, UEA, UK; and Richard J. Sanders, Environmental Sciences, UEA (now at Southampton Oceanography Centre, UK).
m.meredith@uea.ac.uk

The Scotia Sea is the region immediately to the east of Drake Passage, and is bounded meridionally by the North and South Scotia Ridges (Fig. 1). Its eastern limit is the South Sandwich Arc, at approximately 25–30°W. Since the region is directly downstream of the greatest constriction of the Antarctic Circumpolar Current (ACC; Fig. 1), there is a consequent strong divergence of the ACC fronts occurring across the area (e.g. Orsi et al., 1995). A component of the Weddell Sea Deep Water (WSDW) formed on the Antarctic shelves spills over the South Scotia Ridge as part of its northward progression towards the Argentine Basin (Locarnini et al., 1993; Naveira Garabato et al., 2000); the Orkney Passage in particular is believed to be important for this overflow (McDonagh et al., 2000). The remaining fraction of WSDW and the underlying Weddell Sea Bottom Water are topographically restricted to flowing south of the South Scotia Ridge and east of the South Sandwich Arc. The complex bathymetry and bottom-reaching ACC fronts in the region exert strong influences on the circulation and mixing of these waters (Arhan et al., 1999).

In 1995, the WOCE A23 section (Antarctica to Brazil) was performed from RRS James Clark Ross on a meridional line nominally along 35°W. As part of this cruise, stations were occupied between 8 and 12 April in the eastern Scotia Sea between South Georgia and the South Scotia Ridge (Fig. 1). Exactly four years later (8–12 April 1999), the stations in the Scotia Sea were repeated as part of the Antarctic Large-scale Box Analysis and the Role of the Scotia Sea (ALBATROSS) project (Heywood and Stevens, 2000; see also http://www.mth.uea.ac.uk/ocean/ALBATROSS/). This enabled a study of changes in the water mass properties and circulation in this region between the times of the two occupations (Meredith et al., 2000). In this article, we outline the main differences observed in the deep and bottom waters, and discuss their most likely causes.

Observations

Figs. 2a and 2b (page 22) show the potential temperature fields for 1995 and 1999, respectively. In both sections, the Southern ACC Front (SACCF) is present close to South

Georgia, at approximately 55.5°S. In 1995, the Southern Boundary (SB) of the ACC is observed at approximately 58.5°S; in 1999 it was slightly further south (approximately 59°S). Particularly striking in each section is the presence of a narrow recirculation close to 57°S. Following the original WOCE A23 section, this was suspected to be a transient eddy or meander of the SB, though the subsequent 1999 section hints at a longer-term presence. Whilst we suspect topographic effects to be important in the apparent persistence of the feature, we have not yet identified any bathymetric features which might explain such a recirculation.

The most obvious difference between the two sections concerns the Warm Deep Water (WDW) layer south of the SB at approximately 500 m depth. This is derived from the Circumpolar Deep Water (CDW) of the ACC which has entered the eastern Weddell Gyre, circulated cyclonically around the Weddell Sea, and subsequently fed through to the Weddell–Scotia Confluence region. The change is clearly demonstrated in Fig. 3, which shows that the WDW layer has warmed by approximately 0.1–0.2°C during the four-year interval. The core of the WDW layer in 1999 has a marginally higher salinity as well, though the spread of salinity values is also larger due to greater mixing with ACC waters. The main cause of this change is increased WDW potential temperatures in the Weddell Sea itself, which Fahrbach et al. (2000) showed was related to an

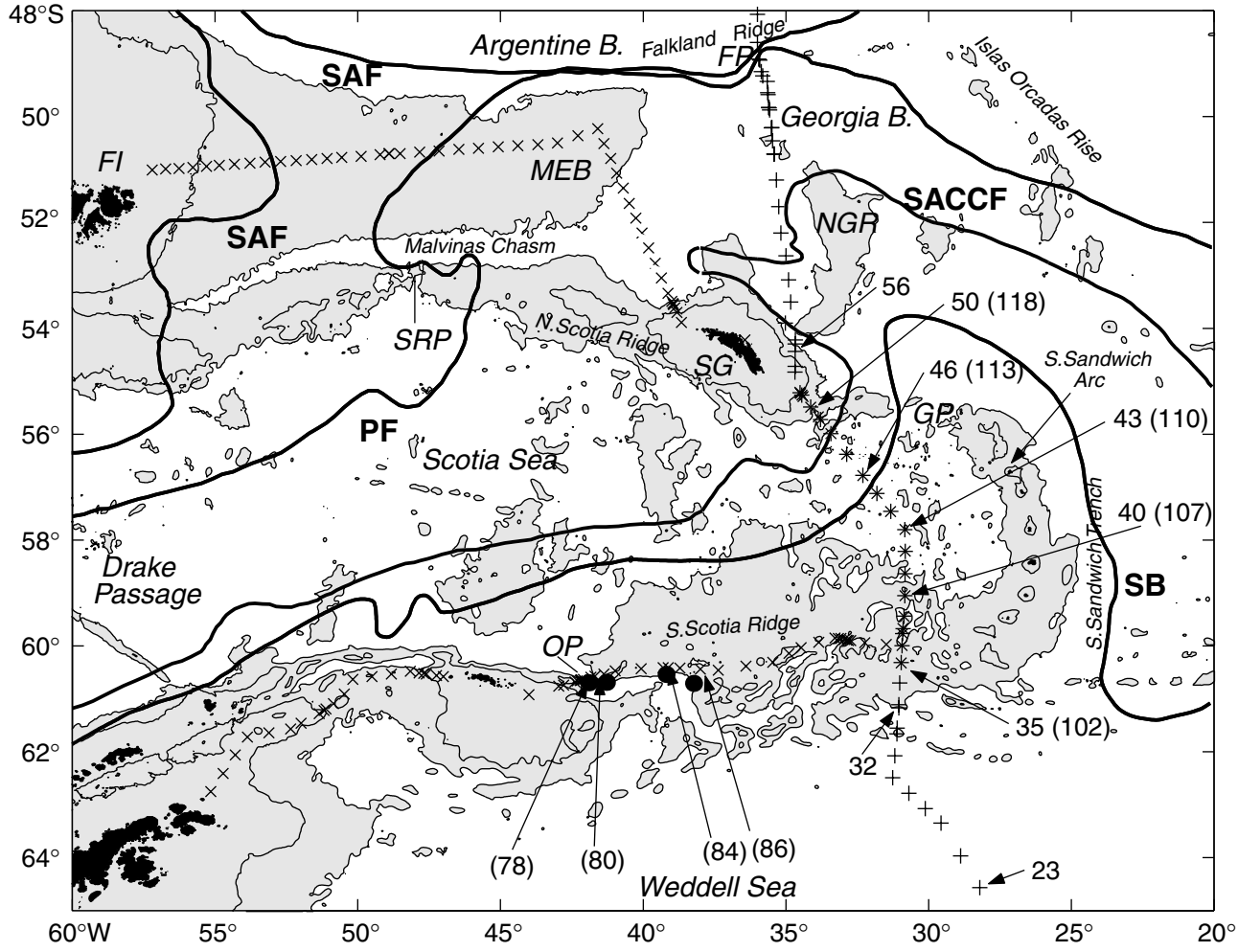

Figure 1. Bathymetry of the Scotia Sea and surrounding environs. The 1000 and 3000 m isobaths are marked; regions shallower than 3000 m are shaded. Stations in the region undertaken as part of WOCE section A23 (1995) are marked with plusses; stations undertaken as part of the ALBATROSS cruise (1999) are marked with crosses. Asterisks denote A23 stations repeated during ALBATROSS. Selected stations from the WOCE A23 section are numbered unbracketed; selected stations from the ALBATROSS cruise are numbered bracketed. Dots on the South Scotia Ridge mark selected stations from the WOCE S4 section (1990). Various topographic features are marked by their initials: FP Falkland Passage; MEB Maurice Ewing Bank; FI Falkland Islands; NGR North-east Georgia Rise; SRP Shag Rocks Passage; SG South Georgia; GP Georgia Passage; OP Orkney Passage. Frontal patterns of the ACC in the region are marked: SAF Subantarctic Front; PF Polar Front; SACCF Southern ACC Front; SB Southern Boundary of the ACC. Patterns adapted from Arhan et al. (1999); originally drafted by R. Locarnini.

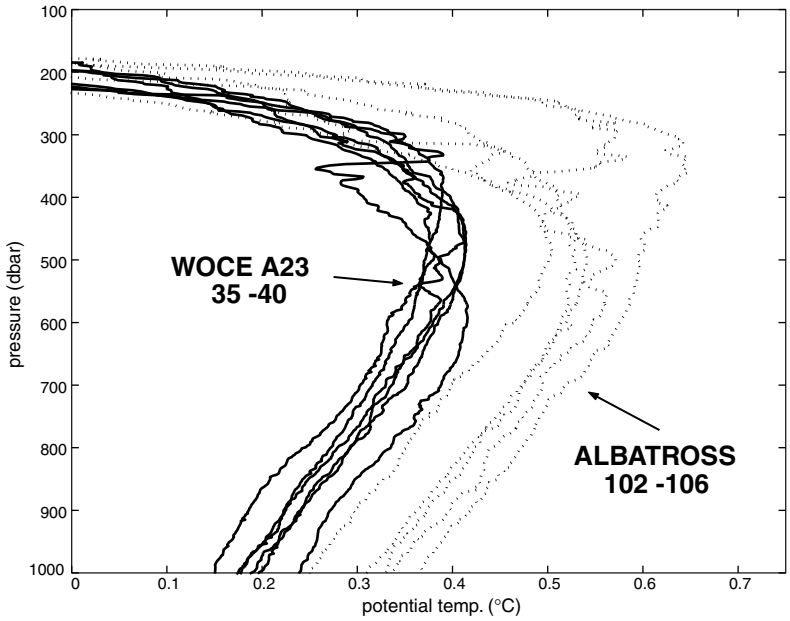

Figure 3. Potential temperature versus pressure from CTD data for stations south of the Southern Boundary. Solid lines are stations 35 to 40 from WOCE section A23; dashed lines are stations 102 to 106 from the ALBATROSS cruise (see Fig. 1 for station locations). Note the significant difference in potential temperature at its maximum (the core WDW layer).

anomalously strong inflow of CDW to the eastern Weddell Gyre between 1984 and 1992. This increase in temperature is now being seen in the Weddell–Scotia Confluence waters of the Scotia Sea. The change in WDW temperature is also apparent in a comparison of our 1999 South Scotia Ridge stations with those occupied nearby in 1990 as part of the WOCE S4 section (station locations in Fig. 1); a general increase of approximately 0.3°C at the potential temperature maximum of the WDW is found.

Other significant changes in the Scotia Sea are observed in the WSDW layer (nominally waters below the WDW or CDW in the Scotia Sea, with potential temperature below 0°C). A warming of around 0.05°C is apparent in this water mass across the whole meridional extent of the sections (example profiles of this are shown in Fig. 4). There is an accompanying change in salinity, so that the potential temperature–salinity curves for the 1999 data overlie those of the 1995 data (but terminate at warmer, more saline levels). There is thus an apparent removal of the bottom layer of WSDW between 1995 and 1999, with a consequent downward shifting of property isopleths. The bottom-reaching ACC fronts in the Scotia Sea are known to be subject to significant variability in position: meanders, shifts and/or eddies of the fronts could in theory explain the changes in WSDW potential temperature and salinity (though the difference in location of the SB in the 1995 and 1999 sections does not seem great enough to explain the large change in bottom water properties; Fig. 2). Measurements of dissolved oxygen (not shown) do not refute this possibility. However, measurements of dissolved silicate in 1995 and 1999 indicate that this is not the case. For example, Figs. 5a and 5b (page 23) show that the bottom waters of the Scotia Sea in 1999 had higher dissolved silicate levels in 1999 than in 1995, whereas a simple downward displacement of properties between these times (such as would be associated with a southward meander of the SB) would imply lower silicate levels. Consequently, we conclude that there has been a change in the characteristics of the inflowing WSDW crossing the South Scotia Ridge some time between 1995 and 1999, with warmer, more saline water (with higher dissolved silicate) being the densest overflowing layer. This is consistent with known WSDW properties upstream in the Weddell Sea, which show an increase in dissolved silicate associated with an increase in potential temperature between the Weddell Sea Bottom Water and WSDW layer (Fig. 6).

The cause of this change in WSDW properties is

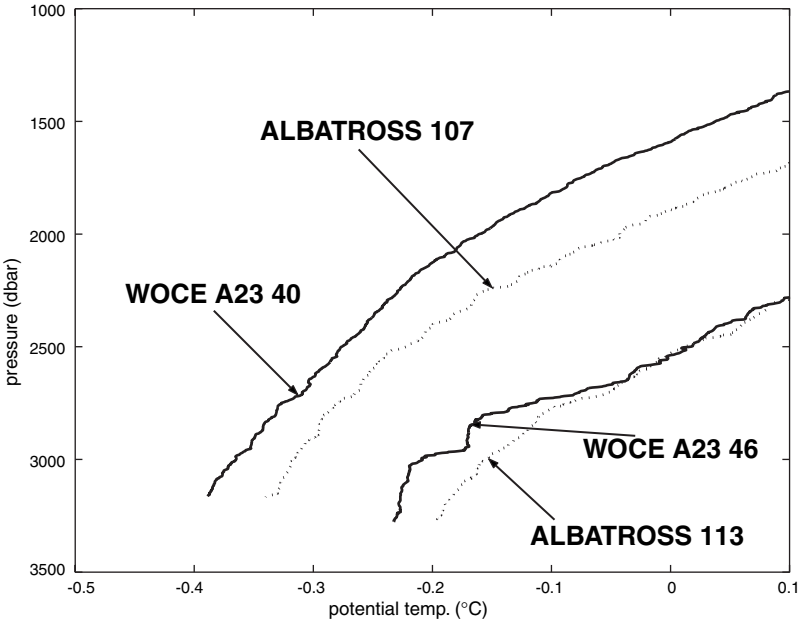

Figure 4. Potential temperature versus pressure for WOCE A23 stations 40 and 46, and ALBATROSS stations 107 and 113. Paired stations are from the same locations. Note the warmer WSDW in 1999 (dotted) compared to 1995 (solid). North of the SB, warming is present only in the WSDW layers, but extends higher in the water column further south due to the WDW warming there (e.g. Fig. 3).

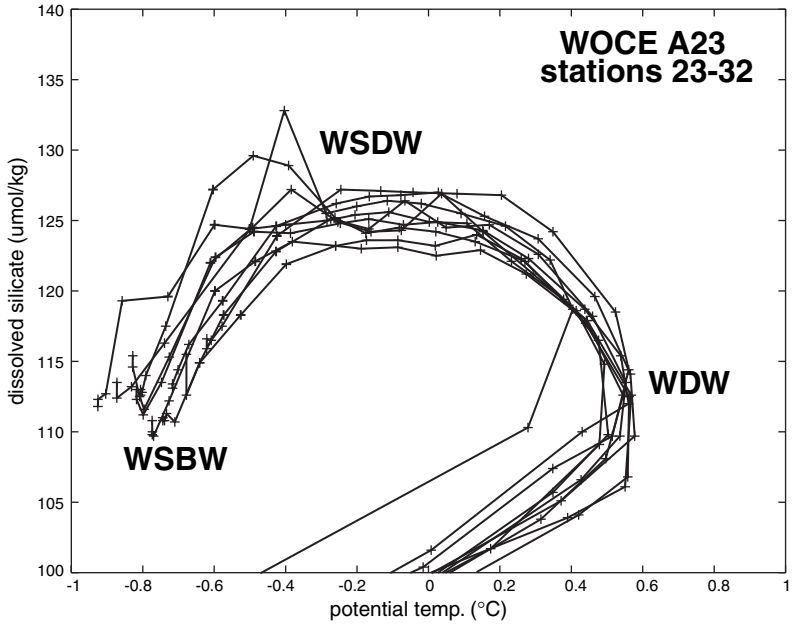

Figure 6. Potential temperature versus dissolved silicate for WOCE A23 stations 23 to 32 in the northern Weddell Sea. Note the lower silicate values towards lower potential temperatures between WSDW and WSBW; an inflow of anomalously cold water to the Scotia Sea would thus feature lower dissolved silicate values.

not known unambiguously, but the comparatively short interval between section occupations (4 years) suggests that it is unlikely to be due to a change in actual formation rate or formation properties of the water. Instead, we suspect that the influence of changes in the intensity of Weddell Gyre circulation on water mass properties at the depth of the South Scotia Ridge overflows is important, as argued previously by Coles et al. (1996). In essence, a period of increased wind stress curl over the Weddell Gyre would lead to enhanced geostrophic current speeds in the northern and southern limbs of the gyre, and hence a steepening of the isopycnals supporting the geostrophic flow. This would lead to the isopycnals intersecting the topography of the South Scotia Ridge at deeper levels, and hence a reduction in the density of the water at the deepest overflow level.

A second change affecting the WSDW of the Scotia Sea is apparent solely for waters denser than $\sigma_4 = 46.09\,\mathrm{kg/m^3}$ (the Lower WSDW (LWSDW) layer; Arhan et al., 1999). These waters are present only at the southern side of the Scotia Sea, and the stations containing LWSDW south of the SB display a change very different to the warming noted above. In 1995, the potential temperature–salinity curves for these stations were essentially linear, indicating simple mixing of WSDW from over the South Scotia Ridge with overlying WDW (Fig. 7a). However, in 1999, there is a distinct inflection in the curves at the level of the $\sigma_4 = 46.09$ isopycnal, with waters below this level featuring higher salinity for a given potential temperature than in 1995 (Fig. 7b). Rather than being a change in properties of the South Scotia Ridge overflows, this is a reflection of a change in the direction of the very bottom flow in the Georgia Passage (just south-east of South Georgia; Fig. 1). LWSDW constrained to flow south of the South Scotia Ridge and east of the South

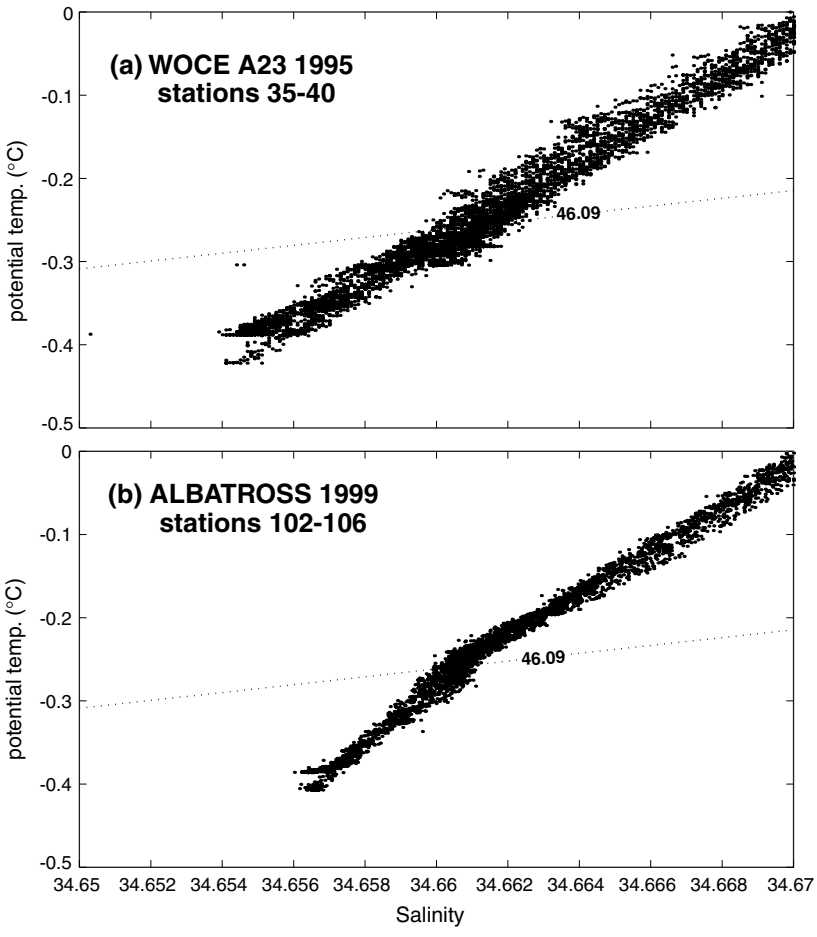

Figure 7. Salinity versus potential temperature for (a) WOCE A23 stations 35 to 40, and (b) ALBATROSS stations 102 to 106. Note the discontinuity in the ALBATROSS curves around $\sigma_4 = 46.09$ (the division between Lower WSDW and Upper WSDW). In comparison to the WOCE A23 curves, the ALBATROSS curves divert towards higher salinity below this density.

Sandwich Arc is known to be more saline for a given potential temperature than that overflowing the South Scotia Ridge (e.g. Arhan et al., 1999; Gordon et al., 2000). In 1995, the water mass properties we observed were consistent with a north-eastward flow of WSDW through Georgia Passage, i.e. an outflow from the Scotia Sea at all levels. Whilst this passage must remain an important outflow location for higher levels, the enhanced salinity of the very bottom layer within the Scotia Sea in 1999 indicates a thin, abyssal inflow through Georgia Passage of the more saline LWSDW that has circulated around the southern and eastern flanks of the South Scotia Ridge and Scotia Island Arc.

Two possible reasons for this change in circulation are suspected. Firstly, it has been observed at other locations that meanders and shifts of the ACC fronts can have significant effects on the speed and direction of bottom water throughflow in narrow passages (e.g. Zenk, 1981). Consequently, meanders and shifts of the SB across the Georgia Passage might act to preclude or permit flow from the northeast. However, such meanders are likely to occur predominantly at mesoscale frequencies, and it seems doubtful that the entire LWSDW layer south of the SB would be so strongly affected as a result. A second possibility is that changes in the density of the WSDW overflowing the South Scotia Ridge (and hence, ultimately the density of the WSDW exiting the Scotia Sea through the Georgia Passage) could be responsible. A less dense overflow across the South Scotia Ridge (such as was observed above) could be associated with a weaker, less dense outflow through the Georgia Passage, and hence a greater possibility of a reverse-direction inflow in the densest layer.

Discussion

The measurements we have made reveal that very significant changes in water mass properties can occur in the Scotia Sea between 500 m depth and the bottom over a period as short as 4 years. Further, in addition to water mass properties, circulation pathways can also be affected. The complex bathymetry of the region, with narrow inflow and outflow passages and large meridional and zonal barriers, interacts with the bottom-reaching fronts of the ACC to create large spatial and temporal variability. The water masses discussed here are components of the global thermohaline circulation, and thus important in more than just a regional sense. Consequently, we suggest that further measurements would be valuable in better understanding such processes and their effects on a much larger scale.

A fuller description of this work is currently available at:

http://www.uea.ac.uk/~e151/a23repeat_2col.pdf

Acknowledgements

We are grateful to the officers, scientific party and crew of RRS James Clark Ross for their assistance during the fieldwork phase of this work. WOCE section A23 was funded by the Natural Environment Research Council (NERC) through grant number GST/02/575. ALBATROSS was funded through NERC grant GR3/11654. MPM was funded via NERC fellowship GT5/99/MS/17.

References

Arhan, M., K. J. Heywood, and B. A. King, 1999: The deep waters from the Southern Ocean at the entry to the Argentine Basin. Deep-Sea Res., 46, 475–499.

Coles, V. J., M. S. McCartney, D. B. Olson, and W. M. Smethie, 1996: Changes in Antarctic Bottom Water properties in the western South Atlantic in the late 1980s. J. Geophys. Res., 101(C4), 8957–8970.

Fahrbach, E., R. Meyer, G. Rohardt, M. Schroder, and R. A. Woodgate, 2000: Gradual warming of the Weddell Sea Deep and Bottom Water. J. Geophys. Res., submitted.

Gordon, A. L., M. Visbeck and B. Huber, 2000: Export of Weddell Sea Deep and Bottom Water. J. Geophys. Res., submitted.

Heywood, K. J. and D. P. Stevens, 2000: ALBATROSS Cruise Report. UEA Cruise Report series No. 6, UEA Publications, Norwich, UK.

Locarnini, R. A., T. Whitworth, III, and W. D. Nowlin, Jr., 1993: The importance of the Scotia Sea on the outflow of Weddell Sea Deep Water. J. Mar. Res., 51, 135–153.

McDonagh, E. L., A. C. Naveira Garabato, K. J. Heywood, D. P. Stevens, and R. J. Sanders, 2000: On the flux of deep water from the Weddell Sea. Deep-Sea Res., II, in preparation.

Meredith, M. P., A. C. Naveira Garabato, D. P. Stevens, K. J. Heywood, and R. J. Sanders, 2000: Deep and Bottom Waters in the Eastern Scotia Sea: Rapid changes in properties and circulation. J. Phys. Oceanogr., submitted.

Naveira Garabato, A. C., K. J. Heywood, and D. P. Stevens, 2000: Modification and pathways of the deep waters of the Antarctic Circumpolar Current in the Scotia Sea. Deep-Sea Res., submitted.

Orsi, A. H., T. Whitworth, III, and W. D. Nowlin, Jr., 1995: On the meridional extent and fronts of the Antarctic Circumpolar Current. Deep-Sea Res., 42, 641–673.

Zenk, W., 1981: Detection of overflow events in the Shag Rocks Passage, Scotia Ridge. Science, 213, 1113–1114.

Impact of 4D-Variational Assimilation of WOCE Hydrography on the Meridional Overturning Circulation of the Indian Ocean

Bruno Ferron, Laboratoire de Physique des Océans, France; and
Jochem Marotzke, Southampton Oceanography Centre, UK.
Bruno.Ferron@ifremer.fr

The deep meridional overturning circulation of the Indian Ocean still represents a dilemma to oceanographers. Estimates either from hydrographic sections or from general circulation models (GCMs) differ significantly in the structure and rate of the overturning. Depending on hydrographic lines considered and details of inverse methods used, the northward transport below 2000 m ranges from 3.6×10^6 m^{3}s^{-1} (Fu, 1986) up to $(27 \pm 10) \times 10^6$ m^{3}s^{-1} (Toole and Warren, 1993). The most recent estimate from Ganachaud et al. (2000), which includes recent WOCE sections, gives a deep inflow of $(11 \pm 4) \times 10^6$ m^{3}s^{-1}. In contrast, GCMs only produce weak deep overturnings (Wacongne and Pacanowski, 1996; Lee and Marotzke, 1997, 1998; Garternicht and Schott, 1997; Zhang and Marotzke, 1999).

Inconsistencies between the two type of estimates may be attributed to deficiencies of either of the methods. On the one hand, inverse model results depend on error estimates which should in principle include errors present in the model itself. For instance, inverse models typically assume steady state, whereas the Indian Ocean has a strong seasonal cycle and has probably an interannual cycle due to El Niño events. This temporal variability has to be part of errors in the inversion process, especially when the inversion combines several hydrographic lines taken at different seasons or years (Ganachaud et al., 2000, include this variability in their error estimates). On the other hand, GCMs are initialised from climatologies which are smoothed and miss the real thermal wind. Integrating in time perfect GCMs with perfect forcings would probably converge to what is observed even if the spin-up is done from a climatology. But forcing fields are far from perfect, and the subgrid-scale physics of GCMs are parameterised. Hence, GCMs may fail to represent the basic circulation of the Indian Ocean circulation.

In order to test whether initial conditions closer to observations change the deep circulation of a GCM, we present here some preliminary results of a 4D-variational approach which combines the dynamics of a GCM and the WOCE hydrography. The assimilation changes some independent variables (e.g. initial conditions) of the GCM to correct the trajectory of the model so that the resulting estimated circulation (i.e. dynamics) is consistent with observations within some error bars.

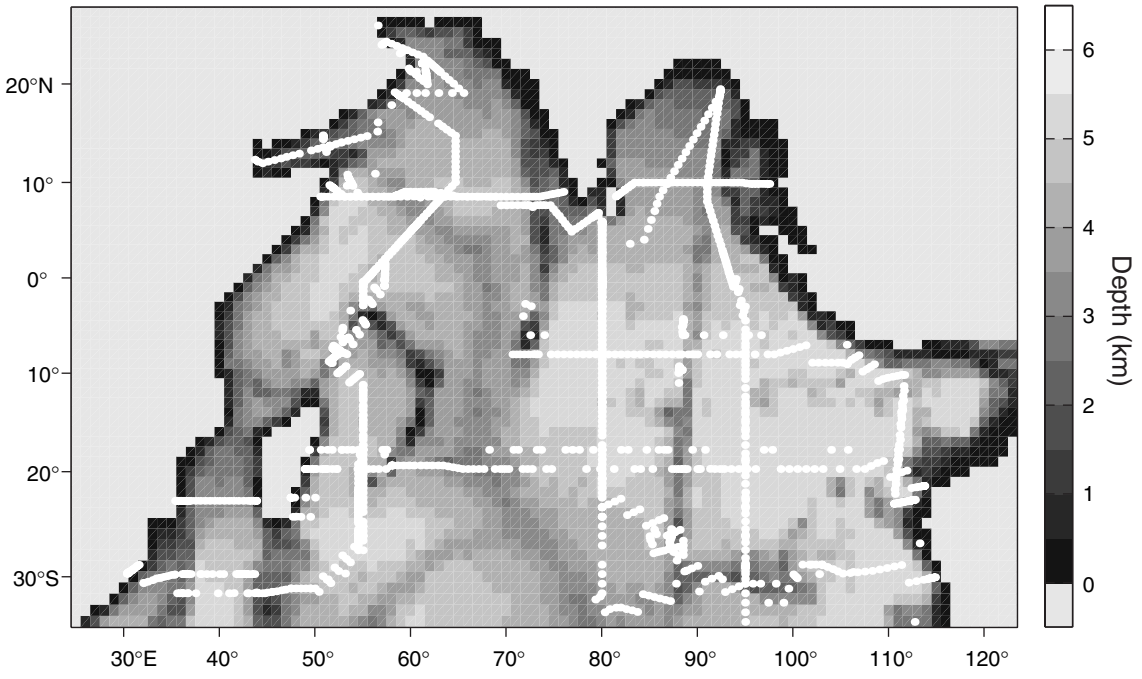

Figure 1. Gridded bathymetry of the model and the WOCE CTDs collected during 1995 (white dots).

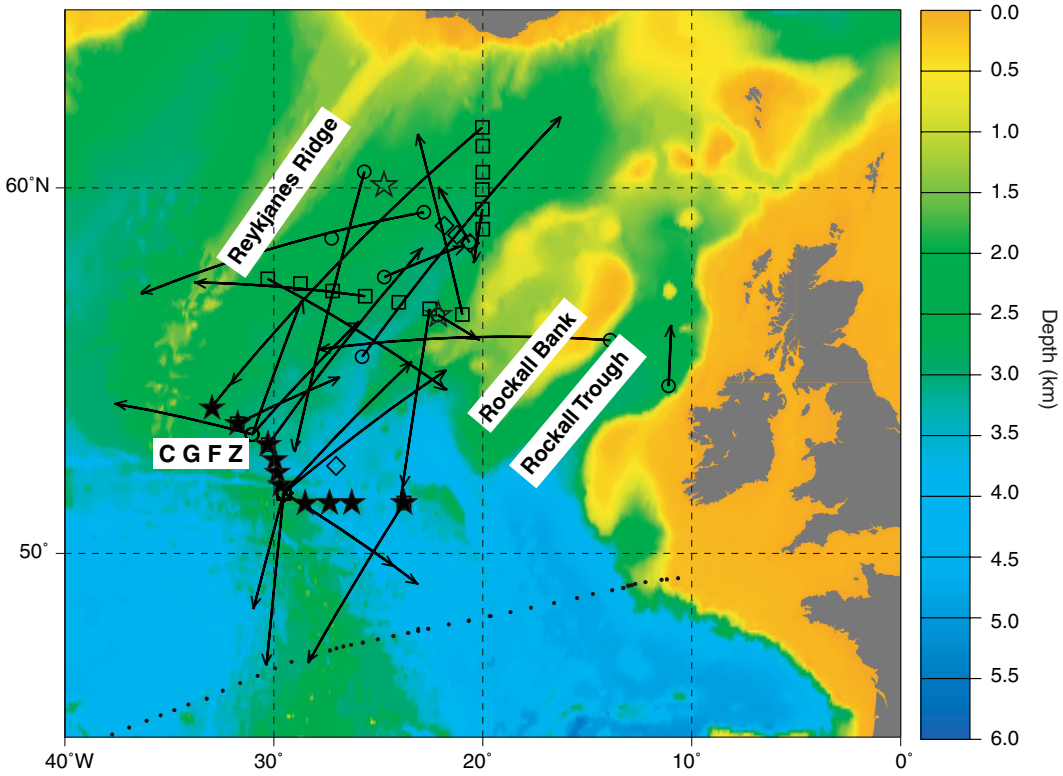

Zenk, page 3, *Figure 1. Topographic chart of the Iceland Basin. Included are locations featuring RAFOS sound sources (open stars) and current meter mooring sites (bold stars), launch (open symbols) and surface positions (arrow tips) from three float seeding cruises according to Tables 1 and 2. On the average displacement vectors represent mission length of 15 months. The lower dotted line denotes WOCE section A2.*

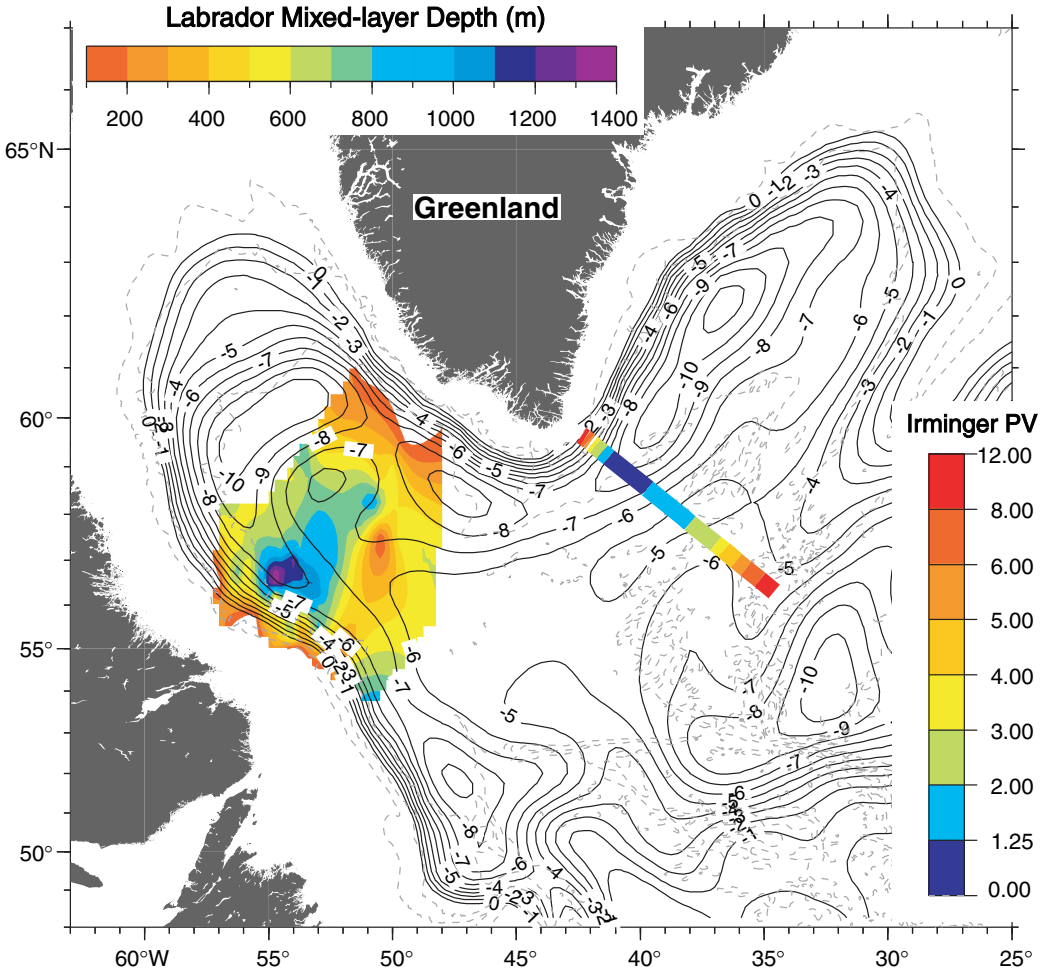

Pickart and Lavender, page 6, *Figure 1. Absolute geostrophic pressure at 700 m (contours in cm) from Lavender et al. (2000). Overlaid on this is the Labrador Sea mixed-layer depth (m) in winter 1997, and the average potential vorticity ($1/(ms)\times 10^{-12}$) of the LSW in the Irminger Sea during the 1990s (see text).*

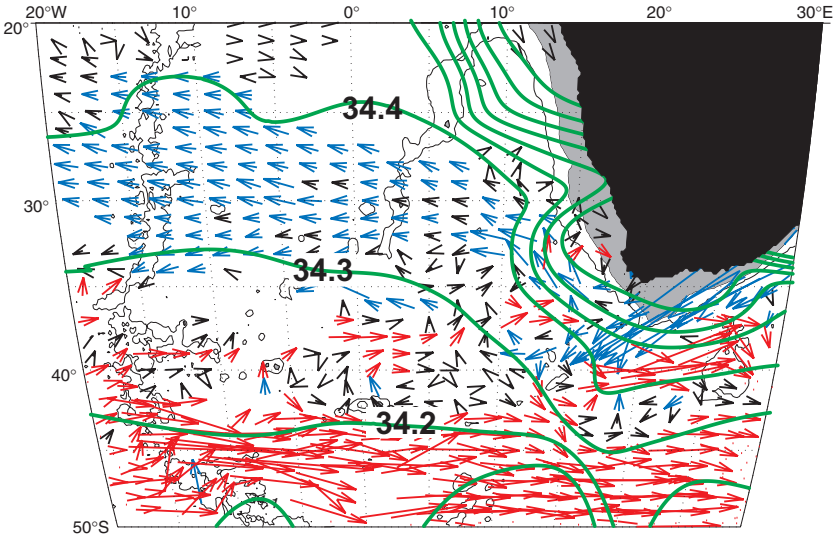

Boebel et al., page 9, *Figure 3. Mean flow and superposed salinity on $\sigma_\theta = 27.2$ surface. Arrows are black if speeds are less than $2.5\,cm\,s^{-1}$ and in colour if greater. Red and blue arrows indicate eastward and westward zonal components, respectively. Green lines indicate isohalines.*

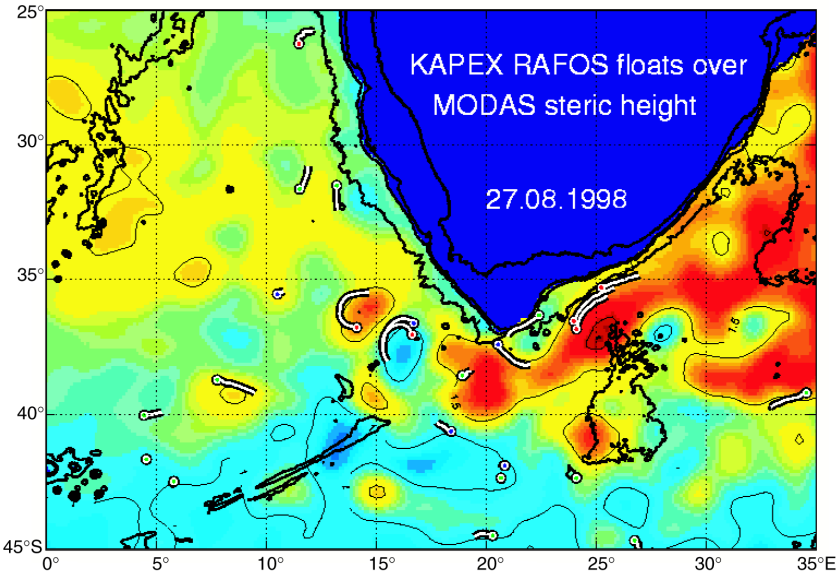

Boebel et al., page 9, *Figure 4. KAPEX RAFOS float trajectories over MODAS steric height anomaly. Trajectory segments span 7 days centred on 27 August 1998. A trajectory segment of 1° length corresponds to a velocity of $18\,cm\,s^{-1}$. Thick solid lines represents isobaths at 0, 500, 1000 and 3000 m depth. Steric height anomaly contours (thin black lines) are at 1, 1.5 and 2 m, located over cyan, yellow and red background colour respectively. This movie can be downloaded by anonymous ftp (39 Mbytes) from pogo.gso.uri.edu/pub/oboebel/agulhas_movie.zip.*

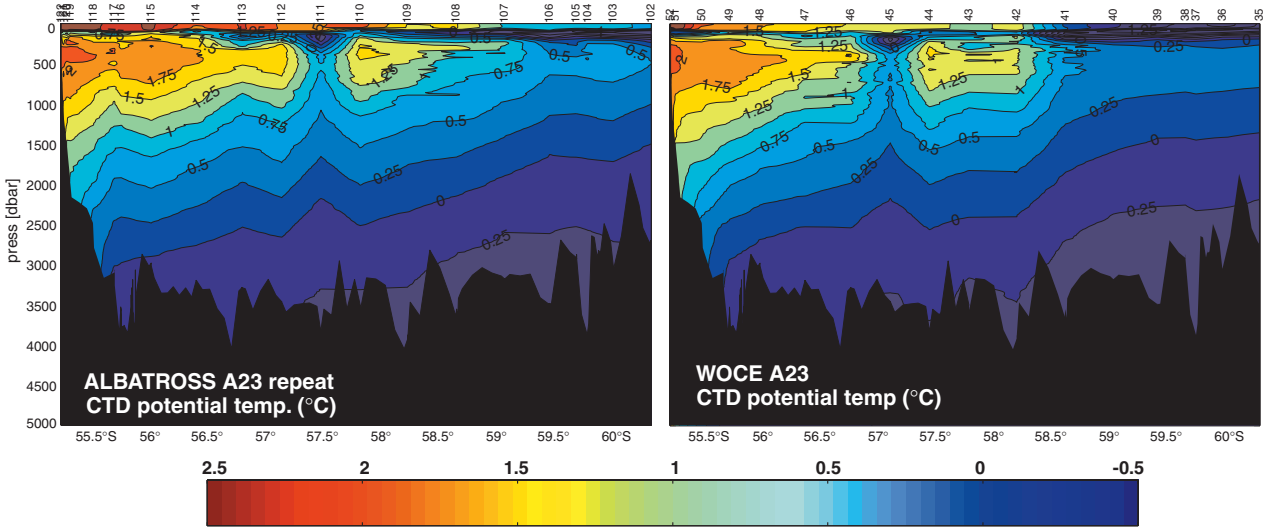

Meredith et al., page 15, *Figure 2. Potential temperature in the eastern Scotia Sea from CTD measurements. Right panel is from the WOCE section A23 in 1995; left panel is from the ALBATROSS cruise in 1999. Station locations are marked by cruise station numbers above the uppermost horizontal axis.*

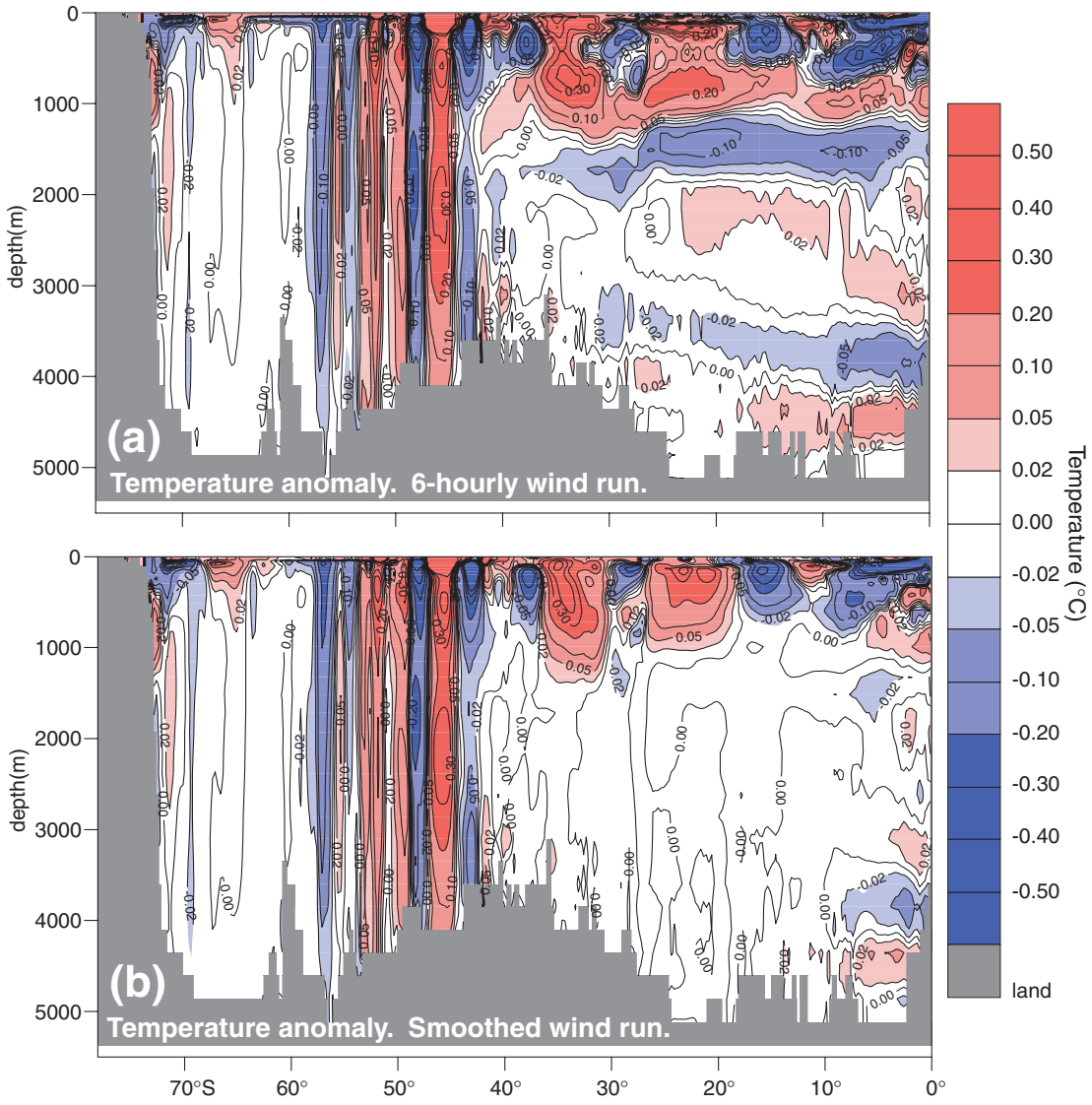

Fox et al., page 27, *Figure 3. OCCAM temperature deviations after one year for (a) the ECMWF 6-hourly wind run, and (b) the smoothed wind run. Deviations are relative to the reference run driven by monthly climatological winds and show the effects of internal waves on deep ocean mixing in OCCAM.*

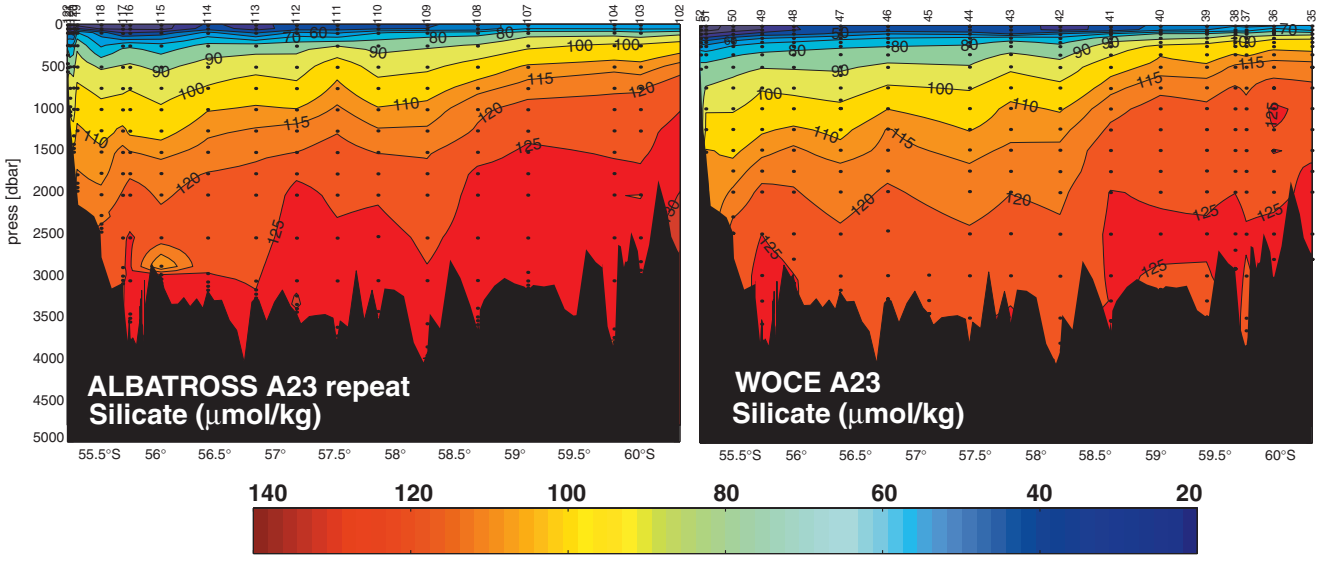

Meredith et al., page 15, *Figure 5. As for Fig. 2, but for dissolved silicate. Locations of discrete water samplings are marked with dots.*

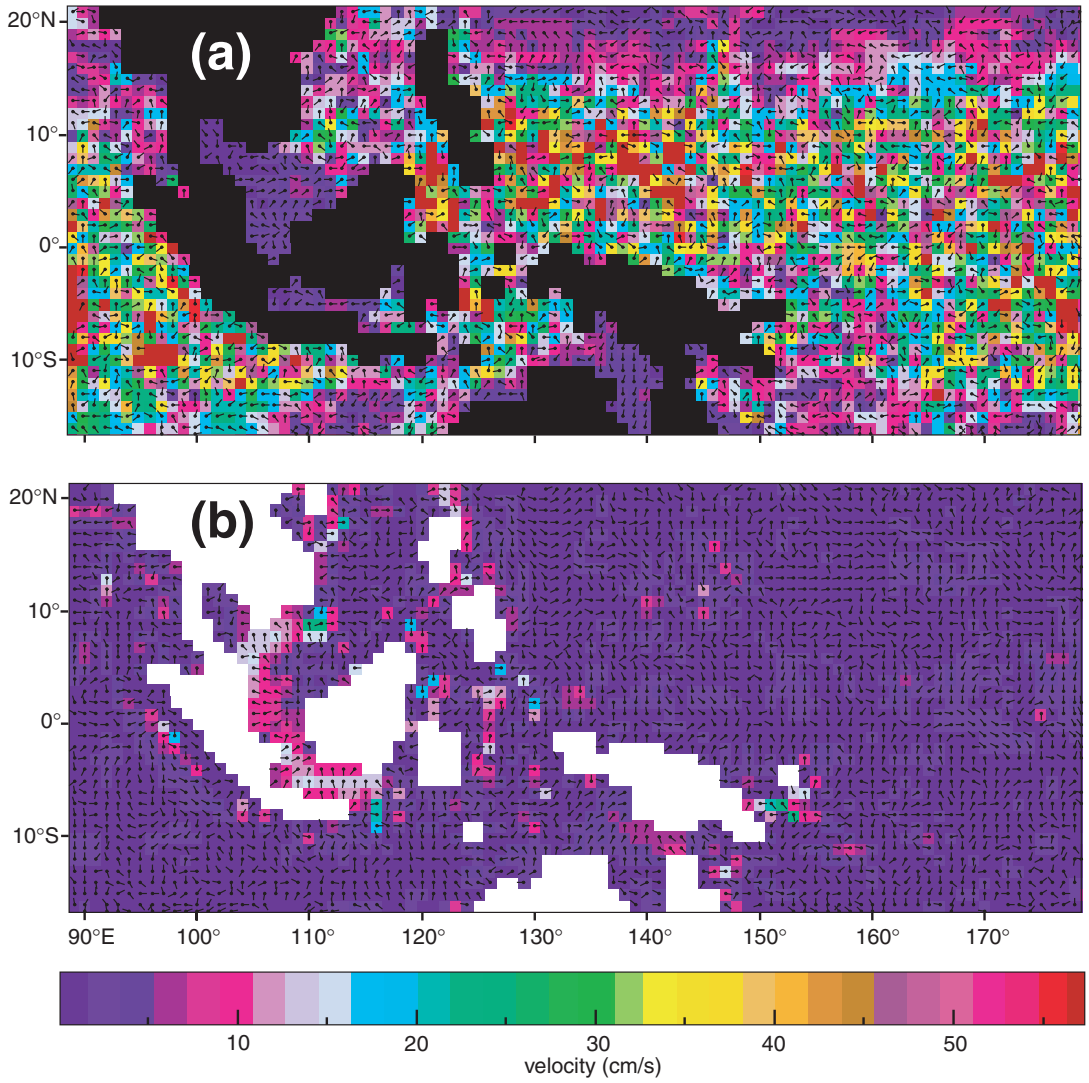

Nurser et al., page 34, *Figure 3. BBL velocity field for (a) standard Killworth and Edwards run (direction of arrow from blob shows direction of flow; colour scale shows speed in* cms^{-1}*) (b) BBL velocity field using new pressure gradient formulation.*

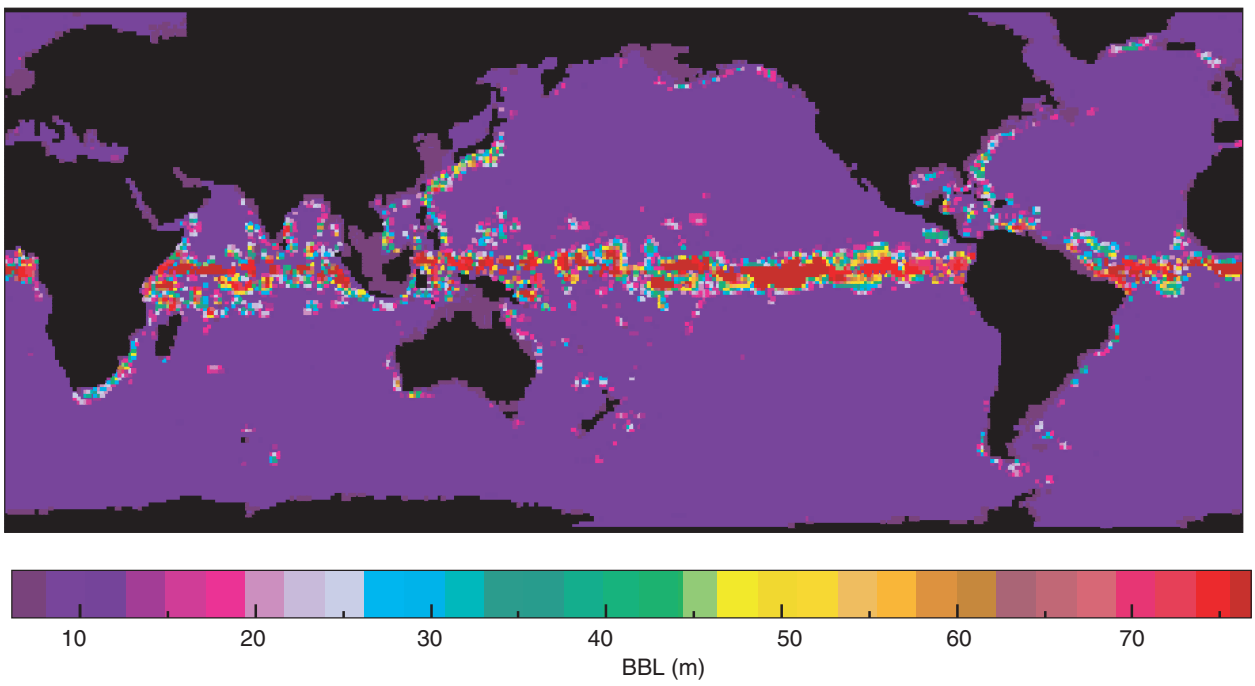

Nurser et al., page 34, *Figure 4. Global plot of BBL thickness, in m.*

Configuration of the model - Spin-up

We use Marshall et al. (1997a,b) primitive equation model (also known as MIT model). Its adjoint is derived with the Tangent Linear and Adjoint Model Compiler (Giering and Kaminski, 1998), as described in Marotzke et al. (1999). The resolution is $1° \times 1°$ horizontally with 23 vertical levels. The model uses Laplacian diffusion in the horizontal and the vertical. A convective algorithm ensures a stable stratification. The domain is regional (Fig. 1); open boundaries are prescribed at 35°S (South Africa–Australia) and 122°E (Indonesian Throughflow) and conserve the Indian Ocean volume. Velocity fields at the open boundary are interpolated from Stammer et al.'s (1997) global assimilation. The surface forcing comes from the National Center for Environmental Prediction (NCEP). Since most of the WOCE hydrography (CTDs) of the Indian Ocean was measured during year 1995, surface and lateral forcing correspond also to year 1995.

The model is spun up from rest, with T and S in the interior and at the open boundaries taken from Levitus. The model undergoes 10 cycles of slightly modified year-1995 forcing. The first-guess initial conditions used in the subsequent optimisation corresponds to the end of year 4 of the spin-up.

Control variables - Cost function

The control vector XX represents the independent variables that are modified to obtain a better fit of the GCM with observations. XX is composed of open boundaries, surface forcings and the first guess (i.e. the initial conditions on T, S, U and V).

The cost function measures the misfit between the model and WOCE CTD data, weighted by some specified variances, but also measures the magnitude of the XX. Errors in the hydrography were calculated as variances of CTD temperature and salinity within a model grid box to account for the coarse resolution of our model. A background error is added to represent the effect of internal waves on CTD data. Errors in the wind stress are computed from statistics between NCEP and ERS products. Errors in the heat and in the evaporation–precipitation are constant over the domain. Since the modelled temperature and salinity deviate significantly from

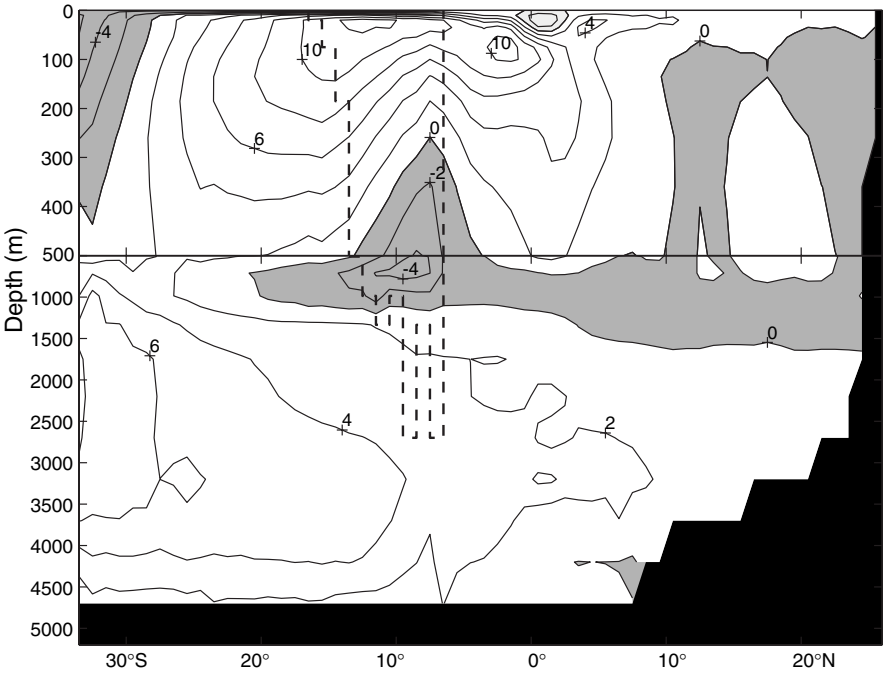

Figure 2. Annual mean meridional overturning after a 5-year spin-up started from Levitus fields and Stammer (1997)'s velocity fields at the open boundaries (positive = counter-clockwise). The dashed lines indicate the location of the Indonesian Throughflow.

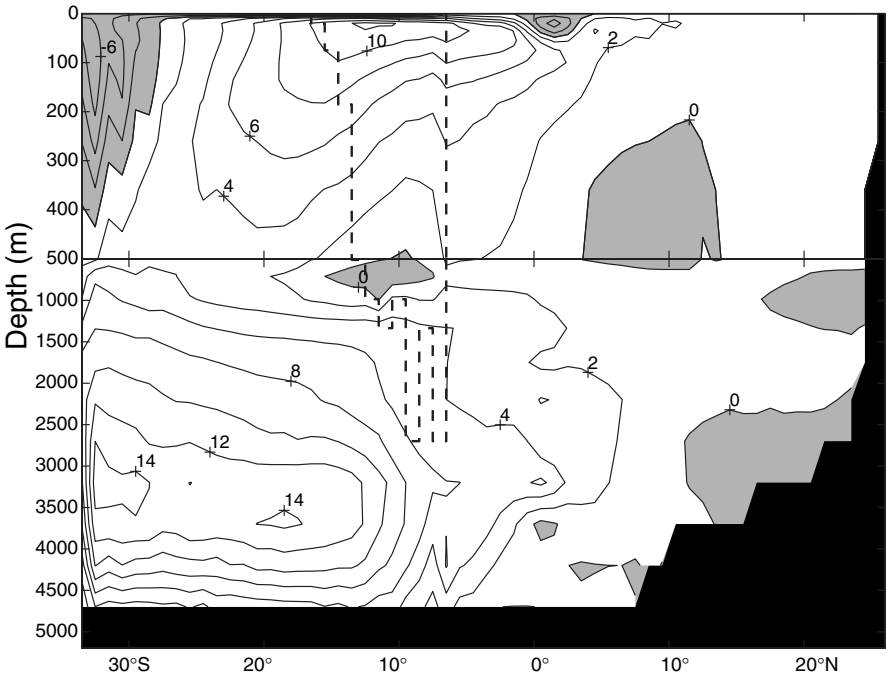

Figure 3. Estimated annual mean meridional overturning after the assimilation of WOCE CTD data (12 iterations with the forward and adjoint models).

observations, the assumed error in the first guess is large; hence it is downweighted. Temperature and salinity at the open boundaries are also weakly constrained which is not the case for velocities at the open boundaries.

Preliminary results

Fig. 2 presents the a priori annual mean meridional overturning based on an average of the monthly fields. Note that in the region of the Indonesian Throughflow which carries 4.5×10^6 m^{3}s^{-1} westward (area bounded by the dashed line), the flow is divergent and isolines represent constant transports integrated from the bottom. Our first guess is similar to previous studies. The circulation is intensified in the first 1000 m with a weak overturning cell at depth. The southern open boundary tries to force a deep overturning of 8×10^6 m^{3}s^{-1} but the interior flow does not allow for more than 4×10^6 m^{3}s^{-1} north of 27°S.

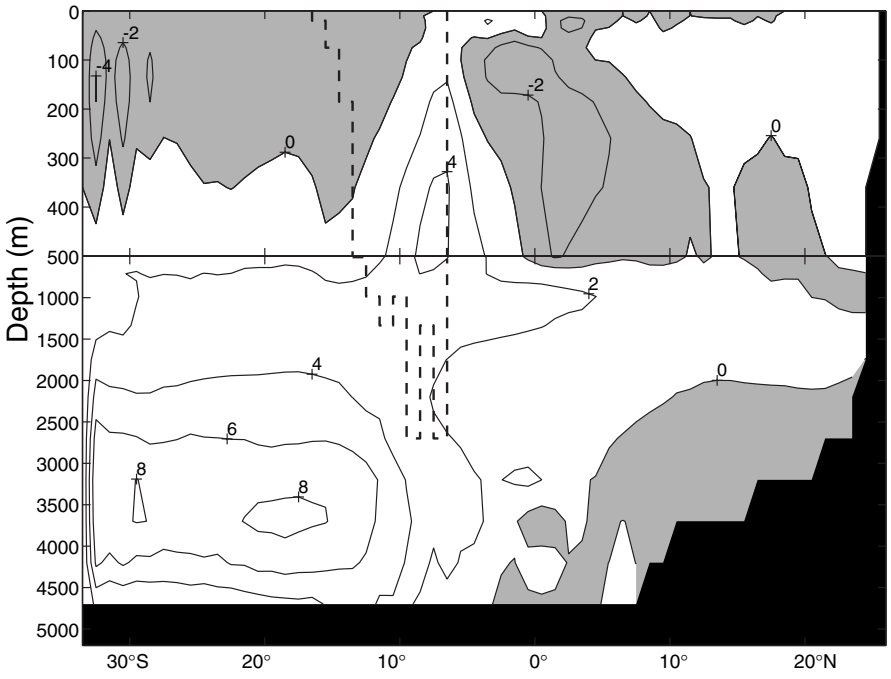

Figure 4. Difference between the estimated and the a priori overturning circulations.

Fig. 3 shows the meridional circulation obtained after a three year-run started from the new initial conditions and forcings generated by twelve iterations of assimilation. The estimated solution is not statistically consistent yet (especially in the first hundred metres), although it is three times more consistent than the first guess. The deep circulation is remarkably modified after the assimilation of WOCE hydrography as Fig. 3 shows. The deep overturning now reaches more than 12×10^6 m^{3}s^{-1} and penetrates up to 12°S. Other experiments based on different constraints (i.e. error bars) on the first guess fields and different initial conditions systematically develop a deep overturning of more than 10×10^6 m^{3}s^{-1}. Such a pattern for the deep circulation of the Indian Ocean is consistent with the hydrographic inversions calculated by Robbins and Toole (1997), Macdonald (1995) and Ganachaud et al. (2000). The significant contrast in the deep circulation between the previous GCM circulations and ours emphasises the drawbacks of smoothed climatologies and the difficulties of GCMs to improve it even when integrated over long timescales.

The difference between the estimated and the a priori overturning circulations (Fig. 4) shows that the CTD data have mainly modified the deep circulation. However, one can note a significant weakening of the circulation at and north of the Equator. The few modifications brought to the upper ocean may be attributed to the shorter correlation time of the circulation at the surface compared to what is observed at depth. Because of limitations in adjoint derivations, our model is too simplistic in the surface physics parameterisation. Hence, this could also limit the impact of assimilating CTDs in the upper ocean, since the assimilation may try to correct for the coarse physics. A better upper ocean physics would exploit the CTD data to a higher degree. Moreover, the lack of upper ocean physics is not taken into account in the variances that weight the model-data misfit. This may explain the statistical inconsistency we observe in the first ocean levels. Choosing variances adequately with the upper ocean physics of the GCM may solve the statistical consistency issue. This work is still ongoing. Although CTDs did not produce any significant change in the Indonesian Throughflow (Fig. 3 shows that open boundaries are weakly constrained by the CTD data), first results from the inclusion of altimetric data in the assimilation seems to be promising for constraining the open boundaries. Details of this study will be published elsewhere.

Acknowledgements

The authors would like to thank all the PIs, their teams and the crews for providing the excellent WOCE data set. This project received support from the National Science Foundation. BF is now supported by the CNRS. Calculations were performed at the San Diego NPACI facilities and at the French IDRIS center.

References

Fu, L.-L., 1986: Mass, heat and freshwater fluxes in the south Indian Ocean. J. Phys. Ocean., 16, 1683–1693.

Ganachaud, A., C. Wunsch, J. Marotzke, and J. Toole, 2000: The meridional overturning and large-scale circulation of the Indian Ocean. J. Geophys. Res., in press.

Garternicht, U., and F. Schott, 1997: Heat fluxes of the Indian Ocean from a global eddy-resolving model. J. Geophys. Res., 102, 21147–21159.

Giering, R., and T. Kaminski, 1998: Recipes for adjoint code construction. ACM Trans. Math., 24, 437–474.
Lee, T., and J. Marotzke, 1997: Inferring meridional mass and heat transports in the Indian Ocean by combining a general circulation model with climatological data. J. Geophys. Res., 102, 10585–10602.
Lee, T., and J. Marotzke, 1998: Seasonal cycles of meridional overturning and heat transport of the Indian Ocean. J. Phys. Ocean., 28, 923–943.
Macdonald, A., 1995: Oceanic fluxes of mass, heat, and freshwater: a global estimate and perspective. PhD dissertation. MIT/WHOI Joint Program in Oceanography. 326 pp.
Marotzke, J., R. Giering, K. Q. Zhang, D. Stammer, C. Hill, and T. Lee, 1999: Construction of the adjoint MIT ocean general circulation model and application to Atlantic heat transport sensitivity. J. Geophys. Res., 104, 29529–29547.
Marshall, J., C. Hill, L. Perelman, and A. Adcroft, 1997a: Hydrostatic, quasi-hydrostatic, and non-hydrostatic ocean modeling. J. Geophys. Res., 102, 5733–5752.
Marshall, J., A. Adcroft, C. Hill, L. Perelman, and C. Heisey, 1997b: A finite-volume, incompressible Navier-Stokes model for studies of the ocean on parallel computers. J. Geophys. Res., 102, 5753–5766.
Robbins, P. E., and J. M. Toole, 1997: The dissolved silica budget as a constraint on the meridional overturning circulation of the Indian Ocean. Deep-Sea Res., 44, 879–906.
Stammer, D., C. Wunsch, R. Giering, Q. Zhang, J. Marotzke, J. Marshall, and C. Hill, 1997: The global ocean circulation estimated from TOPEX/POSEIDON altimetry and a general circulation model. Center for Global Change Science Report, 49, MIT, 40 pp.
Toole, J. M., and B. A. Warren, 1993: A hydrographic section across the subtropical south Indian Ocean. Deep-Sea Res., 40, 1973–2019.
Wacongne, S., and R. Pacanowski, 1996: Seasonal heat transport in a primitive equations model of the tropical Indian Ocean. J. Phys. Oceanogr., 26, 2666–2699.
Zhang, Q., and J. Marotzke, 1999: The importance of open-boundary estimation for an Indian Ocean gcm-data synthesis. J. Mar. Res., 57, 305–334.

Modelling Internal Waves with a Global Ocean Model

Alan D. Fox and Keith Haines, Department of Meteorology, University of Edinburgh, UK; and Beverly A. de Cuevas, Southampton Oceanography Centre, UK.
A.D.Fox@ed.ac.uk

Internal inertia-gravity waves are a ubiquitous feature of the oceans existing on spatial scales from tens of metres up to hundreds of kilometres, and with timescales ranging from a few minutes to the local inertial period. Such waves are generated by the action of the wind at the surface and by the interaction of currents – both tidal and wind-driven – with topography. Whatever the mechanism producing the internal waves, arguably their most important role in ocean circulation is in energy transport. For example, energy input by the wind at the surface can be transported to the deep ocean where it is dissipated in turbulence and mixing. This deep ocean mixing in turn forms an important component of the ocean general circulation. In this way internal waves, although small-scale, influence the largest scales of motion in the ocean.

Until recently the resolution of global ocean general circulation models has been too coarse to resolve even the largest scales of internal waves. Together with global models being almost exclusively run with no tidal currents and purely low-frequency wind forcing, this produces models with little or no internal wave activity. The representation of the effects of internal waves is therefore limited to parameterisations of sub-gridscale processes. However, with increasing computer power, global models are now being run which are able to resolve the large-scale, low-frequency part of the internal wave spectrum. When driven with high-frequency global wind fields these models then contain an explicit representation of the near-inertial frequency, wind-driven part of the internal wave spectrum. Here we describe some results obtained by forcing the UK NERC OCCAM (Ocean Circulation and Climate Advanced Modelling project) $\frac{1}{4}^\circ$ global ocean model with ECMWF 6-hourly global wind fields. First it is useful to highlight some important features of the near-inertial frequency internal wave field in the ocean.

Observations of inertial waves in the ocean

Current meter records demonstrate the presence of internal waves at all depths in the ocean. These observations show a peak in the energy spectrum at frequencies just above the inertial frequency, f. These are generally termed near-inertial frequency waves, or 'inertial waves'. Observation and theory reveal the following basic characteristics of inertial waves (for more details see for example Fu, 1981; Gill, 1982):

1. Generation is predominantly by travelling wind fields, for example eastward moving depressions. This surface generation is confirmed by the dominant downward energy propagation.
2. Currents are almost horizontal (purely horizontal when $\omega = f$) and rotate with time in an anticyclonic direction. Current speeds can be as high $70\,\mathrm{cm\,s^{-1}}$ in the surface layer, decreasing with depth below the thermocline to $3-4\,\mathrm{cm\,s^{-1}}$ near the bed (Sanford, 1975). Vertical displacements of tens of metres in the thermocline have been commonly observed.
3. Intermittent – waves are observed to persist locally for 3–20 wave periods, this observation does not preclude waves persisting for longer periods having

propagated away from the generation region.

4. The observed horizontal coherence scale varies from a few kilometres to nearly 500 km (see e.g. Fu, 1981; Thomson and Huggett; 1981).
5. The near-inertial frequency spectral peak is broad and often contains secondary peaks at frequencies larger than f.
6. The dispersion relation for frequency ω is given by

$$\omega^2 - f^2 = N^2 \frac{k_h^2}{m^2} \qquad (1)$$

where k_h and m are the horizontal and vertical wavenumbers respectively and N is the buoyancy frequency.

Global modelling

The OCCAM model has been run for several years, beginning in 1992, forced by ECMWF 6-hourly wind data. Figs. 1 and 2 show examples of the modelled inertial wave field. Fig. 1 is a global map of temperature anomaly at a depth of 300 m. Fig. 2 is a time-latitude plot showing the sea surface height anomaly associated with the waves along a meridional section at 35°W in the North Atlantic. Although these waves are predominantly internal, with large vertical displacements within the water-column, a small sea surface height signal is also present. Anomalies are calculated relative to a 20-day mean (to aid plotting, the anomalies have also been filtered to remove large (>600 km) spatial scales).

We can examine the modelled waves in terms of the observations and theory outlined above. The most striking feature of the modelled wave field is the spatial pattern of the waves, with crests aligned almost zonally and along-crest coherence scales of several thousand kilometres. This contrasts markedly with the shorter coherence scales found in observations but the discrepancy may be due to the difficulty in observing such along-crest coherence using isolated current meter moorings. Fig. 2 highlights the equatorward propagation of the waves with generation in the 40–60° latitude band, period of around 15–18 hours and propagation speeds decreasing towards lower latitudes. These features are due to generation by eastward travelling wind fields which are moving rapidly compared to the wave propagation speed. The zonal wavelength is governed by the wind field propagation speed and remains approximately constant as the wave travels equatorwards. The meridional wavelength varies according to the dispersion relation (eq. 1): generation is at frequencies, ω, close to f, which corresponds to long wavelengths (small horizontal wavenumber, k_h); as the wave propagates equatorwards it retains the same frequency (see Fig. 2) and vertical wavenumber but the local inertial frequency decreases, therefore k_h must increase corresponding to reduced meridional wavelength (this effect is initially rapid since $\omega \approx f$ and the rate of change of k_h with latitude depends upon $\left(\omega^2 - f^2\right)^{-\frac{1}{2}}$); the combined behaviour of

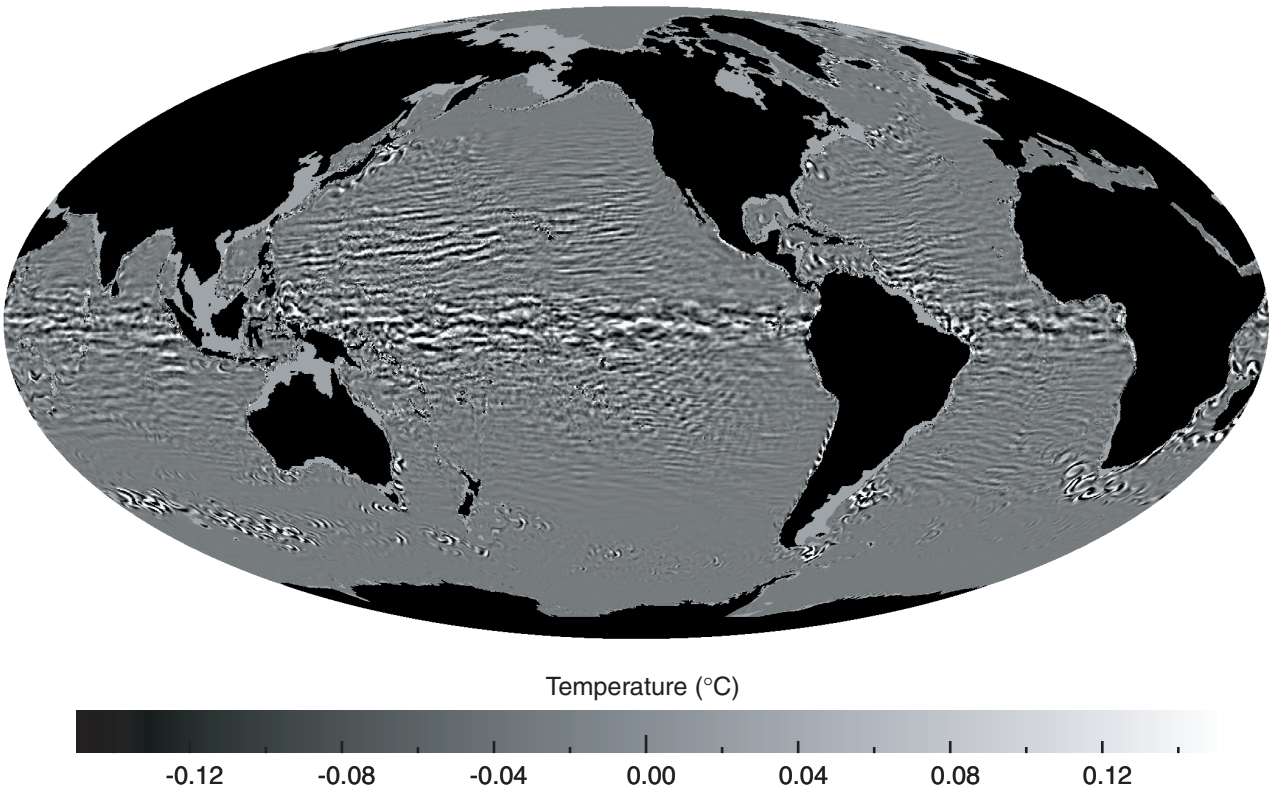

Figure 1. OCCAM temperature anomaly (°C) at 300 m, 9 March 1992. OCCAM is being forced by ECMWF 6-hourly wind fields. Anomalies are relative to a 20-day mean temperature and large (>600 km) spatial scales have also been removed.

zonal and meridional wavelengths then produces the modelled, near-zonal orientation of the crests. It should also be noted that poleward propagation far from the generation region is not possible as f would quickly become greater than ω, instead poleward travelling waves are reflected at the latitude where $\omega = f$ (the 'turning latitude') and join the southward propagating waves.

At low latitudes the wave field appears to be dominated by waves propagating equatorwards from higher latitudes rather than by locally generated waves. This is partly because we are examining vertical displacement fields rather than currents, locally generated waves would be near their turning latitude where currents are nearly horizontal, and vertical displacements are small. However, Fig. 2 suggests that the largest amplitude waves are being generated by the highly variable wind field in the 40–60° latitude band. The obvious equatorward propagation explains the broad spectral peak at near-inertial frequencies and the often observed secondary peaks at frequencies larger than f. Clearly more investigation is required to assess the realism of the modelled wave field. In particular, previous modelling studies (e.g. D'Asaro, 1995) suggest possible problems obtaining realistic dissipation rates.

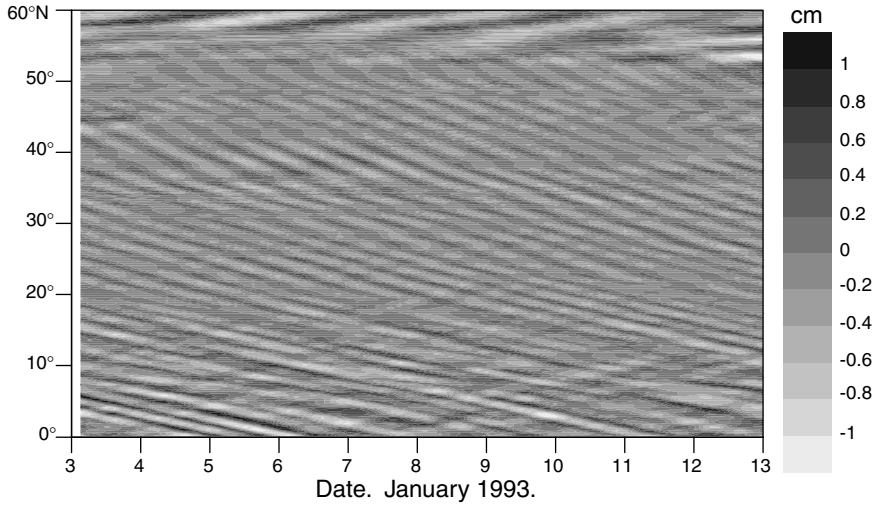

Figure 2. OCCAM sea surface height anomaly along 35°W in the North Atlantic for 10 days in January 1993. Anomalies are relative to a 20-day running mean sea surface height and large spatial scales have also been removed.

Diapycnal mixing

An important property of internal waves is their ability to transfer energy input at the ocean surface by winds to be dissipated via turbulence and diapycnal mixing in the deep ocean. In the real ocean this release of energy is via non-linear wave/wave and wave/current interaction, transfer of energy to higher frequencies and subsequent breaking of high-frequency internal waves. This is a process which is clearly still not included in even the highest resolution global model. However, it is still useful to explore the effects of internal waves on mixing within OCCAM as there will be implications for how these unresolved processes are parameterised. Current global ocean models were designed to work well at lower resolution and as resolution is increased it is important to reassess model numerics and parameterisations.

To investigate the effects of inertial waves in OCCAM, three parallel runs were performed, one with ECMWF 6-hourly wind forcing, a second forced by smoothed ECMWF winds, and a third using monthly climatological winds. The smoothing used a Hamming filter with a 3-day window, which practically eliminated the generation of inertial waves in the model polewards of around 10°. The model was run for one year (1992) with each of the three forcings starting from identical initial conditions. The idea was to isolate the effects of internal waves from other effects of using a more realistic wind field. Results along a section at 20°W in the South Atlantic are presented in Fig. 3 (page 23). This figure shows the deviations of the temperature fields in the 6-hourly and smoothed wind runs from the climatological run. A large increase in mixing at depth due to the inertial wave field is found, this is evident in the increased deviations of the 6-hourly wind run temperature fields from the climatological wind run fields at depths below the thermocline and equatorwards of 40°S.

Given that the model lacks a realistic physical mechanism for this wave-induced mixing, what exactly is the mechanism within the model? Unfortunately, the increased mixing is due to numerical diffusion associated with the vertical advection scheme. The advection scheme used in OCCAM is the modified split QUICK scheme of Webb et al. (1997). This contains a diffusive component which is dependent on the vertical current speed. In the open ocean the vertical currents associated with internal waves in the model can be two orders of magnitude greater than other vertical currents (up to $10^{-1}\,\mathrm{cm\,s^{-1}}$ rather than $10^{-3}\,\mathrm{cm\,s^{-1}}$). A simple 1-D advection model suggests that the resulting vertical diffusion is approximately equivalent to using a diffusion coefficient of $10 - 100\,\mathrm{cm^2\,s^{-1}}$ in the deep ocean, this compares with the explicit background vertical diffusion in OCCAM with a coefficient of $0.5\,\mathrm{cm^2\,s^{-1}}$ and measured estimates of $0.1 - 1.0\,\mathrm{cm^2\,s^{-1}}$. We also note that energy supplied for mixing in this way, leading to an increase in model potential energy, is not necessarily removed from the kinetic energy of the internal wave field as modelled diffusive processes are not conservative. So there need not be any increased damping of the modelled internal waves associated with this increased deep ocean mixing.

Discussion

Global ocean models now have sufficient resolution to be used to study the large-scale near-inertial frequency part of

the internal wave spectrum. Such a study, using the OCCAM model, reveals the wind-driven inertial wave field to be dominated by waves generated at mid-high latitudes which then propagate downwards and equatorwards. These waves are characterised by remarkably uniform near-zonal crests, coherent over large distances in the along-crest direction.

In OCCAM the inertial waves are associated with a large increase in diapycnal mixing. This is due to the numerical advection scheme and could be a problem for any z-level model driven by high frequency winds. Griffies et al. (2000) described some of the problems associated with diffusion in advection schemes in ocean models. Their work was confined to models driven by monthly wind fields and it is worth noting that any problems appear to be multiplied by up to two orders of magnitude when high frequency forcing is applied. This result suggests that if ocean models are required to be run with high frequency wind fields then a less diffusive vertical advection scheme should be chosen. This may be of particular relevance in coupled ocean-atmosphere models which generally include higher frequency wind forcing of the ocean component.

No attempt has been made here to assess the realism of the modelled internal wave field by detailed comparison with observational data. One question which we are currently exploring is whether the sea surface height variations and spatial coherence seen here to be associated with inertial waves enable observation using satellite altimetry.

Acknowledgements

This work was supported by grant GST/02/1956 from the UK NERC.

References

D'Asaro, E. A., 1995: Upper-ocean inertial currents forced by a strong storm. Part II: Modeling. J. Phys. Oceanogr., 25, 2937–2952.

Fu, L. L., 1981: Observations and models of inertial waves in the deep ocean. Rev. Geophys. Space Phys., 19, 141–170.

Gill, A. E., 1982: Atmosphere–Ocean Dynamics. Academic Press.

Griffies, S. M., R. C. Pacanowski, and R. W. Hallberg, 2000: Spurious diapycnal mixing associated with advection in a z-coordinate ocean model. Mon. Weather Rev., 128, 538–564.

Sanford, T. B., 1975: Observations of the vertical structure of internal waves. J. Geophys. Res., 80, 3861–3871.

Thomson, R. E., and W. S. Huggett, 1981: Wind-driven inertial oscillations of large spatial coherence. Atmos. Ocean., 19, 281–306.

Webb, D. J., B. A. de Cuevas, and C. S. Richmond, 1997: Improved advection schemes for ocean models. J. Atmos. Oceanic Technol., 15, 1171–1187.

Thermocline Theories and WOCE: A Mutual Challenge

Geoffrey K. Vallis, GFDL/Princeton University, USA. gkv@splash.princeton.edu

This article gives a brief overview of the some recent work on the thermocline problem, and also tries to begin to make a connection between such dynamical theories and observational programmes.

WOCE is, as a whole, the most ambitious ocean observing programme to date. As the programme moves into the AIMS phase it is useful to recall its original objectives, namely: (i) To develop models useful for predicting climate change and to collect the data necessary to test them; (ii) To determine the representativeness of the specific WOCE data sets for the long-term behaviour of the ocean, and to find methods for determining long-term changes in the ocean circulation. Included in these goals is a mandate to 'determine the dynamical balance of the World Ocean Circulation'. This short article asks the questions can *observational data be effectively used to test dynamical theories of the ocean, such as thermocline theory?* and, conversely, *can dynamical theories be put into a form that can be subject to observational tests?* Although we would like to answer both questions in the affirmative, both issues appear to be more difficult and ambiguous than one would like.

Much of our theoretical understanding of the large-scale circulation of the ocean comes by way of using simplified dynamical equations, in particular (and especially for the large-scale circulation) the *planetary–geostrophic equations*, or PGE. These equations have in turn been used to construct various theories of how an idealised ocean might work – simple theories of the wind-driven circulation, thermocline theories and so forth. Thus, it seems that a worthwhile project would be to try to use observational data to test the validity of the planetary–geostrophic equations, and some of their consequences – in particular various models of the thermocline.

Dynamical theories

The planetary–geostrophic equations

The planetary–geostrophic equations follow from the primitive equations simply by neglecting the total time derivative in the momentum equations. The scaling assumptions that must be satisfied to justify this are (c.f., Pedlosky, 1987): (i) Small Rossby number; (ii) Length scales larger than the deformation radius; (iii) The Coriolis parameter must vary by O(1), else the resulting lowest-order dynamics are trivial. [On Earth, (ii) is implied by (iii).] The second of these conditions is particularly

problematic, for it explicitly excludes there being a continuous spectrum of interacting scales from the planetary scale to the mesoscale. In the Boussinesq approximation, and neglecting saline effects, the equations that result are:

$$fu = -\frac{\partial \phi}{\partial y}, fv = \frac{\partial \phi}{\partial x}, \frac{\partial \phi}{\partial z} = b, \nabla_3 \cdot \mathbf{v} = 0, \frac{Db}{Dt} = \frac{\partial}{\partial z}\kappa\frac{\partial b}{\partial z}. \quad (1)$$

Here, b is buoyancy (or temperature), ϕ is pressure divided by density, and other notation is standard. These equations were first derived as a large-scale approximation for ocean circulation by Robinson and Stommel (1959) and Welander (1959). Phillips (1963) put them in the context of other approximations to the primitive equations.

The diffusive term is not part of the planetary–geostrophic approximation per se. Rather, one is additionally assuming that small-scale turbulent motions act diffusively on the large-scale. In particular, one is implicitly assuming that small-scale turbulence has an effect on the large-scale flow, but that mesoscale turbulence does not. Unfortunately, we have few dynamical arguments to indicate whether this is really valid, or what precise value of κ is appropriate.

Theory of the thermocline

Because of the uncertainty in the approximations leading to the planetary–geostrophic approximations, and at the same time the ubiquity and importance of these equations in our theories, plainly we should seek to test their validity. We come back to this more in the next section, but for now we note that one of the consequences of the planetary–geostrophic approximation has been our current understanding of the thermocline. Historically, there have been two approaches, diffusive theories and adiabatic theories. A number of early approaches concentrated on the former, for example assuming a balance in the thermodynamic equation of

$$w\frac{\partial b}{\partial z} \approx \kappa\frac{\partial^2 b}{\partial z^2}. \quad (2)$$

Similarity theories quantified this approach, leading to a picture of the thermocline as an internal boundary layer (Stommel and Webster, 1962; Salmon, 1990; Young and Ierley, 1986). In these models, the thermocline is irreducibly diffusive; no matter how small the value of κ is, diffusion is always important. Typically, the thickness of the thermocline varies as some fractional power of κ like $\kappa^{1/2}$, the thermocline itself becoming a discontinuous front in the limit $\kappa \to 0$.

In some contrast, ideal theories assumed that the balance in the thermodynamic equation was essentially adiabatic ($\mathbf{v} \cdot \nabla b = 0$). This approach, really begun by Welander (1959), was reinvigorated by the 'LPS' theory of Luyten et al. (1983). This theory provided solutions of the equivalent layered system that combined essentially arbitrary density and (downward) Ekman pumping conditions at the upper surface with a quiescent abyss. After some years of struggle, the continuously stratified equations also finally yielded to an analogous approach (Huang, 1988). In these models, κ plays no role; the meridional profile of temperature is mapped continuously to a vertical profile, even in the limit of $\kappa = 0$. In subsequent developments, the roles of seasonal variations in surface density and mixed-layer thickness were recognised. The term "subduction", describing the theoretical vision of subtropical isopycnal layers sliding beneath one another, downward and equatorward in vast fluid sheets, has now become as common in our field as it is in plate tectonics. However, the ideal theories made no real explicit connection to the abyss.

Samelson and Vallis (1997; henceforth SV) computed numerical solutions of a planetary–geostrophic model, and found that these could be understood as a combination of the diffusive and ideal theories. In their single-basin model, the main thermocline has two dynamical regimes: an upper adiabatic region in which the dynamics are essentially those of LPS, and a lower intrinsically diffusive part, which in the limit of small κ forms an internal boundary layer (see Fig. 1). The upper, ventilated thermocline is, just as in LPS theory, a continuous mapping of a surface meridional temperature profile, but only the temperature profile across the subtropical gyre is so mapped. The temperature profile across the subpolar gyre maps to a diffusive, internal boundary layer as in the similarity theories. Furthermore, and perhaps importantly for the earth's climate, only the temperature gradient across the subpolar gyre is effective in driving the thermohaline circulation, because this circulation is buffered from the temperature gradient across the subtropical gyre by the isothermal layer at the base of the ventilated thermocline.

Arguably, SV's model can be seen as a direct consequence of the planetary–geostrophic equations, with small but non-zero vertical diffusion, convective adjustment, minimal parameterisations of lateral diffusion and friction, and certain boundary conditions of temperature and stress. An interesting question is, to what extent can the present theory of the thermocline be regarded quantitatively as the planetary–geostrophic approximation plus these or similar boundary conditions? Put another way, is the phenomenology simply the result of calculations from a planetary–geostrophic base, with the latter being the underlying theory?

Testing dynamical theories

As the planetary–geostrophic equations themselves are the foundation for our dynamical models of the large scale, it seems that they should be the starting point for observational tests. However, an objective, quantitative test of the planetary–geostrophic equations as an approximation for large-scale ocean circulation has not been achieved, forty years after their first derivation. The possible role of eddy heat and vorticity fluxes (which are excluded from the planetary–geostrophic equations) in setting the stratification of the thermocline remains a subject of active debate. Will the WOCE observations prove sufficient to settle this issue? If so, the result would be a fundamental advance in

our physical understanding of the ocean, with critical implications for future ocean climate observations and modelling programmes.

How can such a result be achieved? The most direct approach is to test the balances in the equations themselves. Some of the various approaches to inverse modelling (e.g., Bennett, 1992; Wunsch, 1996) offer the opportunity to carry out quantitative statistical hypothesis testing on the PGE approximations in this direct manner. However, the non-linearity of the PGE makes this a daunting project.

Is there an alternative to this direct approach? If so, it seems clear that it must be more phenomenologically oriented. As an analogy, consider for example the Schrödinger equation of quantum mechanics. This equation cannot be tested directly, in the manner of a weak-constraint inverse formulation, because the quantum mechanical wave-functions are not directly observable. Nonetheless, it has been tested stringently as a physical model through careful measurements of observable quantities – phenomena – that can be related to it or derived from it, in one way or another. To the extent that PGE theories predict specific, recognisable features in the ocean thermocline – such as the ventilated thermocline or the internal boundary layer – that can be compared to observations, they can and should be viewed in a similar fashion (and as the results of a similar scientific philosophy). The direct test of the dynamical equations may be as unachievable in practice for the planetary–geostrophic equations as it is in principle for the Schrödinger equation. The challenge for the practical theoretician is to quantify the planetary–geostrophic phenomenology in a way that exposes the approximations to quantitative observational tests.

Thus, we circle back to the phenomenology of the thermocline. Can the various models (ventilated, diffusive, 'two-thermocline' etc.) in and of themselves be subjected to such tests? To the extent that these theories follow from the planetary–geostrophic equations, a test of these thermocline theories is a test of the adequacy of these equations and, implicitly, the lack of importance of eddies. Thus, we would ideally like a quantitative test of the phenomena predicted by the models, but this has not yet been achieved. Of course, some progress has been made in testing the theories. For example, the relative freedom with which surface boundary conditions could be specified in the LPS theory resulted immediately in calculations that could be compared quantitatively with observations, first for the subtropical North Atlantic (Luyten et al., 1983), and, soon after, for the subtropical Pacific (Talley, 1985). Some preliminary modelling studies of the thermocline have also been made with the primitive equations (e.g., Cox, 1985) that do, in principle, allow for a continuum of scales down from the gyres to the first deformation radius. Will WOCE data allow us to do more? The two-thermocline model has a relatively rich dynamical structure that seems as well suited as anything to observational testing. For example, predictions include:

1. The formation of a thick, mode-water like, thermostad that outcrops at approximately the latitude of the mean zero wind-stress curl, separating two regions of larger vertical temperature gradient.
2. The vertical velocity should pass through zero in the lower region, that is in the internal boundary layer.

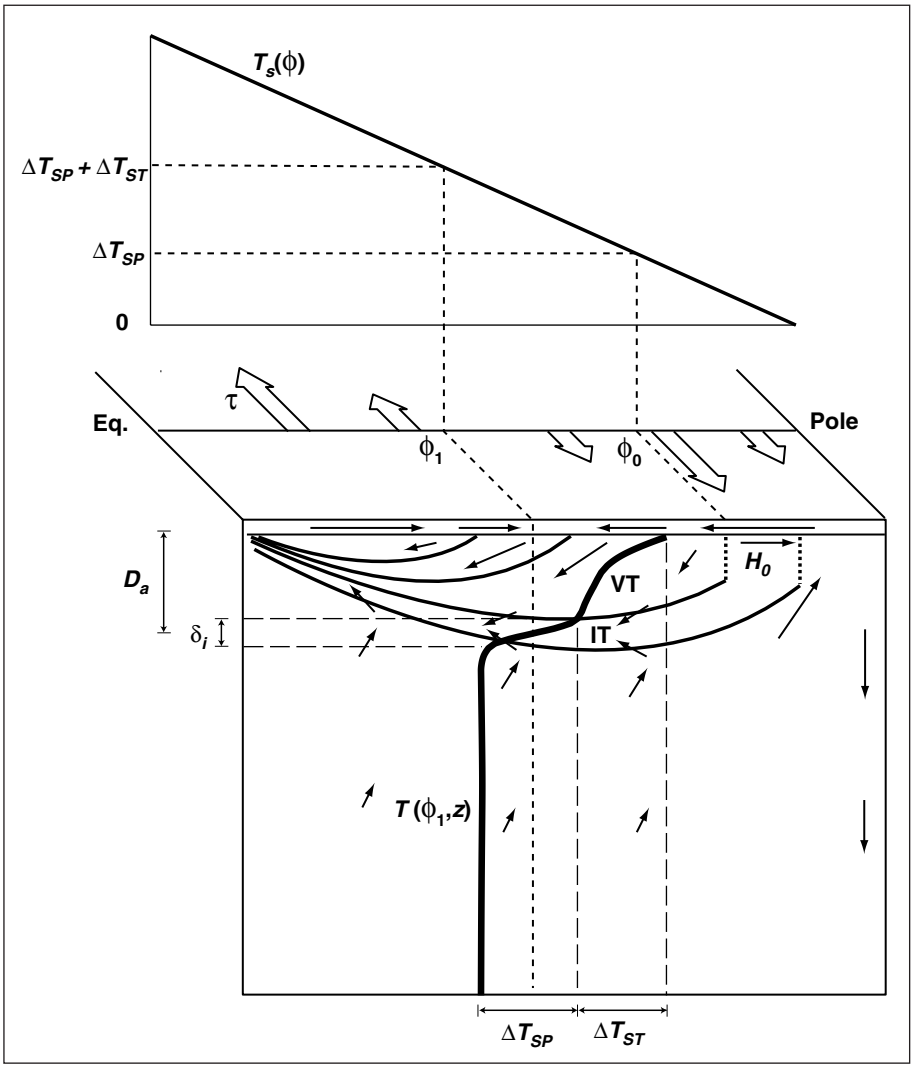

Figure 1. A schematic picture of the large-scale circulation and the thermocline regimes in a simply-connected, single-hemisphere ocean driven by wind-stress and differential heating. The idealised meridional section below is at a mid-basin longitude. The main thermocline is composed of an upper, ventilated thermocline and a lower internal boundary layer, separated by a region of mode water. From Samelson and Vallis, 1997.

3. The heat budget should be approximately closed by the large-scale fields themselves. That is, eddies should have only a small contribution. Similarly, available potential energy should dominate the energy budget. (These are related more to the adequacy of the PGE than to thermocline models per se.)
4. Specifically, in the upper thermocline (isotherms that outcrop in regions of Ekman downwelling) the heat budget should (below the surface) close on the basis of an advective balance, whereas below the region of mode water the balance is advective-diffusive.
5. Insofar as the upper part of the thermocline is a ventilated thermocline, the phenomena associated with that should be present there.

Some of these predictions may be impossible to directly test; for example, it is very difficult to directly measure vertical velocity, although tracer release experiments (as in Ledwell et al., 1993) may provide a means. Others are rather qualitative and do not directly or quantitatively test thermocline models. For example, mode water (item 1) has been the object of many observational studies (e.g., McCartney and Talley, 1982) and, in part because of strong seasonal effects, it conceivably cannot be uniquely associated with a two-thermocline model. Similarly, heat transport estimates (e.g., Hall and Bryden, 1982) indeed appear to show only small eddy effects (item 3), but this does not discount the possibility that eddies might have a cumulative influence on the large-scale fields that is impossible to detect in such diagnostics. And the specific heat budgets of item 4 may be very hard to quantitatively test, especially without exact knowledge of the variability of the vertical diffusivity.

Some of these observational tasks may ultimately be made easier by assimilating data into a primitive equation ocean model, and then testing the dynamical balances in that model. However, this may be ambiguous on various counts. In particular, such 're-analysis' products (to use a phrase common in the atmospheric sciences) unavoidably incorporate the strengths and weaknesses of the underlying numerical model, especially if observations are sparse, and so are not a direct observational test of the phenomenology. Relatedly, the primitive equation model should certainly be eddy resolving, else it is really just solving the planetary–geostrophic equations and then the thermocline solution is assured. But observations will typically not resolve the eddies, except perhaps altimeter observations of the surface only, and thus the test may end up being mainly a test of the planetary–geostrophic equation thermocline theory against another numerical model.

Summary

Although one of the goals of observations should presumably be to test dynamical theories, the non-linearity of the equations, the lack of knowledge of the value of key parameters and the sparsity of data make this difficult. Similarly, theorists should presumably seek to formulate hypotheses that are observationally testable. But this too is easier said than done. Even in the atmosphere, where the data are so much more plentiful, unresolved questions remain about such first-order questions as what determines the height of the tropopause or the latitudinal extent of the Hadley Cell. In the ocean we are both unsure about the basic level of approximation (e.g., the appropriateness of the planetary–geostrophic equations), and the dynamics that result from such equations. Because it may be near-impossible to ever directly test the dynamical balances in the equations of motion themselves, we may seek to make unambiguous phenomenological predictions from the equations of motion that in turn can be subject to observational tests. The theory of the structure of the thermocline may be a good starting point. It is then a challenging and important task for both observers and theoreticians to come up with tests that are both severe and feasible.

Acknowledgements

This article was solicited following a lecture on the large-scale circulation and thermocline dynamics given by the author at a recent conference (Vallis, 2000). I would like to thank Roger Samelson for many exchanges and ideas on this matter, and for pointing out the analogy to the Schrödinger equation.

References

Bennett, A., 1992: Inverse methods in physical oceanography. Cambridge Univ. Press, Cambridge, 346 pp.

Cox, M., 1985: An eddy-resolving model of the ventilated thermocline. J. Phys. Oceanogr., 15, 1312–1324.

Hall, M., and H. Bryden, 1982: Direct estimates and mechanisms of ocean heat transport. Deep-Sea Res., 29, 339–359.

Huang, R. X., 1988: On boundary value problems of the ideal-fluid thermocline. J. Phys. Oceanogr., 18, 619–641.

Ledwell, J., A. Watson, and C. Law, 1993: Evidence for slow mixing across the pycnocline from an open-ocean tracer-release experiment. Nature, 364, 701–703.

Luyten, J., J. Pedlosky, and H. Stommel, 1983: The ventilated thermocline. J. Phys. Oceanogr., 13, 292–309.

McCartney, M., and L. Talley, 1982: The subpolar mode water of the North Atlantic Ocean. J. Phys. Oceanogr., 12, 1169–1188.

Pedlosky, J., 1987: Geophysical Fluid Dynamics. Springer-Verlag.

Phillips, N. A, 1963: Geostrophic motion. Rev. Geophysics, 1, 123–176.

Robinson, A. R., and H. Stommel, 1959: The oceanic thermocline and the associated thermohaline circulation. Tellus, 11, 295–308.

Salmon, R., 1990: The thermocline as an "internal boundary layer". J. Mar. Res., 48, 437–469.

Samelson, R., and G. K. Vallis, 1997: Large-scale circulation with small diapycnal diffusion: the two-thermocline limit. J. Mar. Res., 55, 223–275.

Stommel, H., and J. Webster, 1962: Some properties of the thermocline equations in a subtropical gyre. J. Mar. Res., 44, 695–711.

Talley, L., 1985: Ventilation of the subtropical North Pacific and the shallow salinity minimum. J. Phys. Oceanogr., 15, 633–649.

Vallis, G. K., 2000: Large-scale circulation and production of stratification. Lecture at European Geophysical Society, Nice, April 2000.

Welander, P., 1959: An advective model of the ocean thermocline. Tellus, 11, 309–318.
Wunsch, C., 1996: The ocean circulation inverse problem. Cambridge Univ. Press, Cambridge, 442 pp.
Young, W. R., and G. Ierley, 1986: Eastern boundary conditions and weak solutions of the ideal thermocline equations. J. Phys. Oceanogr., 16, 1884–1900.

A New Approach to the Sigma-Coordinate Pressure Gradient Problem in a Terrain-Following Bottom Boundary Layer Model

A. J. George Nurser, Peter D. Killworth and S. G. Alderson, Southampton Oceanography Centre, UK. agn@soc.soton.ac.uk

It has long been known (cf. Armi and Millard, 1976) that there is a turbulent layer near the bottom, of thickness 10–50 m, whose temperature and salinity are well mixed in the vertical: the bottom equivalent of a surface mixed layer, in fact. The behaviour of water within these layers is of vital importance to the global thermohaline circulation, because outflows from areas of deep water formation, which pass over sills between basins, descend to the ocean floor as bottom boundary layers. Typical are the outflows from the Mediterranean, through the Denmark and Iceland–Faeroes Straits, areas of dense water around the Antarctic, the Deep Western Boundary countercurrents, etc., although dense bottom layers are *ubiquitous* in the ocean (Pratt and Lundberg, 1991, give a survey of sill flows).

Model intercomparisons reported by Dengg et al. (1999) indicate that the lack of a bottom layer in z-coordinate models tends to erase dense water signals in overflows. A variety of numerical approaches has been suggested, ranging from extremely simple (Campin and Goose, 1999), through medium complexity (Beckmann and Döscher, 1997) to relatively complete physics (Killworth and Edwards, 1999; Song and Chao, 2000). The flow in most of these codes is driven by pressure gradients in the bottom boundary layer (BBL). It is fair to say that most of the extant codes which include pressure gradients suffer from σ-coordinate-like difficulties. These difficulties manifest themselves as erroneous geostrophic flows near topography at mid-latitudes, but can be serious near the equator.

Here we describe modifications to the pressure gradients in the Killworth and Edwards (1999) scheme to permit it to work within a global model, and give some preliminary results. In particular, the code gives plausible results at the equator.

The scheme adds a partial layer to the bottom of each grid box as shown in Fig. 1. (Song and Chao, 2000, also permit a variable thickness bottom box, which we shall add soon.) The normal equation set for a z-coordinate model applies in the interior. In the BBL, which is connected between boxes regardless of adjacent levels, there is conservation of mass and tracers, plus momentum equations which feel a depth-averaged pressure gradient within the BBL. The thickness of the layer is predicted each time step, and then fluid entrains or detrains to bring h to a local equilibrium value given by (Zilitinkevich and Mironov, 1996)

$$\left(\frac{h}{C_n u_* / f}\right)^2 + \frac{h}{C_i^2 C_D |\mathbf{u}_m|^2 / g'} = 1$$

where u_* is the friction velocity given by $u_*^2 = C_D|\mathbf{u}_m|^2$, $\mathbf{u}$ is the horizontal velocity, C_D the quadratic drag coefficient, $g' = g(\rho_m - \rho_l)$, where ρ_l is the interior density just above the layer, a suffix m denotes values within the layer, g is the acceleration due to gravity, and C_n, C_i are constants ($C_n = 0.5$, $C_i = 20$) evaluated from Zilitinkevich and Mironov (1996). In most circumstances this gives a bulk Froude number $|\mathbf{u}_m| / (g'h)^{1/2}$ of around 0.9, which is the order observed in rapid outflows such as the Mediterranean. If h is predicted to increase by this formula, there is entrainment, and tracer and momentum from the layer above is mixed from the interior into the bottom layer. If h decreases, there is detrainment, and tracer and momentum

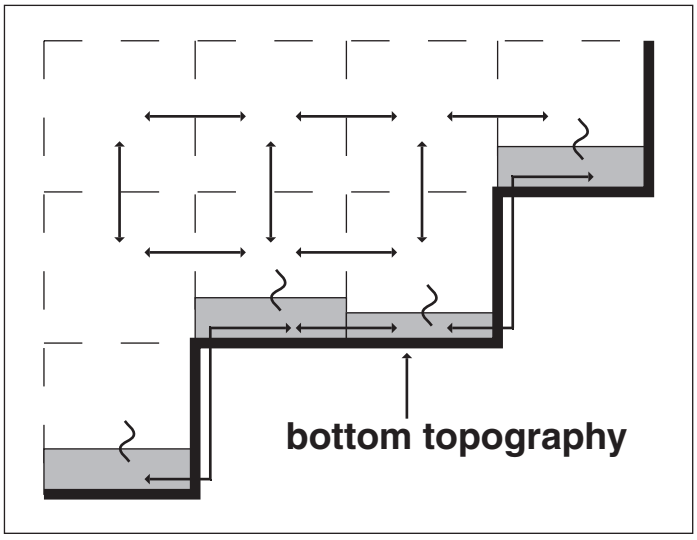

Figure 1. Schematic of the bottom boundary box in the scheme. Velocities are marked. The curly lines indicate entrainment/ detrainment.

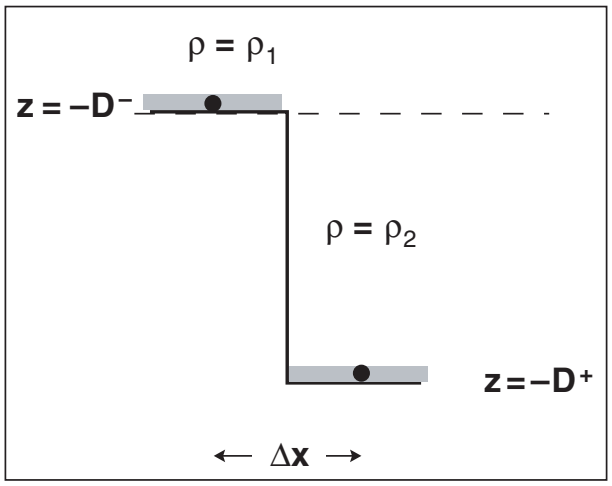

Figure 2. A thin (shaded) BBL lies above the ocean floor where it falls steeply from $z=-D^-$ to $z=-D^+$ over gridboxes Δx apart. The density distribution is vertically stratified, $\rho=\rho_1$ for $z>-D^-$; $\rho=\rho_s>\rho_1$ for $z<-D^-$.

are mixed from the bottom layer into the interior. This formulation serves as a useful surrogate for a more accurate energy equation for the bottom layer. If the predicted h falls below a prescribed minimum (10 m) then it is reset to that value.

Improving the pressure gradient

The problem we consider is how to improve the expression for the depth-averaged pressure gradient, (Killworth and Edwards, 1999):

$$\overline{\nabla p_m} = \nabla p_m - g\rho_m \nabla\left(D - \tfrac{1}{2}h\right) \qquad (1)$$

where D is the depth of the ocean, p_m is the pressure halfway down through the layer at $z=-d+\frac{1}{2}h$; so ∇p_m is the horizontal pressure gradient *along* the BBL. The second, 'depth compensation' term, $-g\rho_m\nabla(D-\frac{1}{2}h)$, represents the horizontal gradient of the difference between the pressure at constant height and that along the BBL.

We need to discretise (1). Suppose two adjacent (tracer/pressure) gridpoints at x^- and $x^+=x^-+\Delta x$. We then need to decide what value of ρ_m we should use at the (intermediate) u-point at which we evaluate the pressure gradient. The obvious solution is to use the average density, $\frac{1}{2}(\rho_1+\rho_2)$.

However this approximation can give unphysical results if the BBL depth changes rapidly from gridbox to gridbox. Suppose, for simplicity, that the BBL is thin, with $|\nabla h| << |\nabla D|$ and that the ocean floor falls steeply from $-D^-$ to $-D^+$. Suppose further – see Fig. 2 – a vertically stratified density distribution, $\rho=\rho_1$ for $z>-D^-$; $\rho=\rho_2>\rho_1$ for $z<-D^-$, and that the flow is initially motionless. Then (leaving aside compressibility effects for the moment) we would wish there to be no flow and hence no pressure gradient, but in fact

$$"\Delta_p\big|_z"= g\rho_2[D]^+_- - [D]^+_- \cdot \tfrac{1}{2}g(\rho_1+\rho_2) =$$
$$\tfrac{1}{2}g[D]^+_-(\rho_2-\rho_1)>0$$

will accelerate heavy water, density ρ_2, back up the slope.

The approach we suggest here is what might be termed an 'upstream' pressure gradient, in which we use the upstream value of ρ_m in the second 'depth compensation' term. So, using this method, if $u<0$, we use $\rho_m=\rho_2$, and

$$"\Delta_p\big|_z"= g[D]^+_-(\rho_2-\rho_2)=0.$$

This will, at least, not accelerate flow trying to bring heavy fluid up the slope. Conversely, if $u>0$, we use $\rho_m=\rho_1$, and

$$"\Delta_p\big|_z"= g[D]^+_-(\rho_2-\rho_1)>0$$

will try to slow down light waters moving down the slope, as it ought to. In the case discussed above, with $u=0$, this ensures that we choose $\rho_m=\rho_2$, so maintaining $u=0$.

Since in this formulation the pressure gradient can be very different depending on the direction of flow, care must be taken to avoid oscillations. This involves monitoring sign changes of both velocity and acceleration to ensure that the final answer approximates what would be attained with infinitesimal time steps.

Our upwind method is in fact the only consistent way to compute the pressure gradient which is energetically consistent with upwind differencing of the tracer equations in the BBL. Such upwind differencing is often employed to reduce so-called "digging", and is used in this code. On the rare occasions when u changes sign over a time step, energetic consistency is lost for that time step.

Compressibility issues must also be handled by the code, since densities are computed at differing depths. Not including this effect can induce flows of $10-20\,\mathrm{cm\,s^{-1}}$ near the equator. The code we have produced remains energetically consistent, in that gravitational potential energy plus (horizontal) kinetic energy plus the Boussinesq approximation to internal energy are conserved.

Testing the new formulation

This formulation has been tested against the original in a quasi-global 1° model using the Scripps 1° topography and fairly coarse vertical resolution (14 levels) as used in the standard distribution of MOM. Fig. 3 (page 24) shows the BBL velocity over and to the east of the Indonesian archipelago in the original code after 100 days (50 days of spin-up without BBL followed by 50 days with the BBL). Disorganised strong flow (Fig. 3a), up to $60-70\,\mathrm{cm\,s^{-1}}$, is widespread where there is large gridbox to gridbox variation in depth. Vertical motions associated with these flows eventually caused severe numerical problems, leading to surface temperatures of ~44°C after one year.

The modified code gives much more plausible flow in the BBL, even after 10 years (Fig. 3b), only reaching $20-30\,\mathrm{cm\,s^{-1}}$ at a few isolated points. The upstream pressure gradient formulation seems to have controlled these errors. These results are not directly comparable with the old run; a noisier 1° topography was employed here, taken from Sandwell and Smith (1995), together with higher vertical resolution (36 levels, chosen as in OCCAM). However, runs using the Scripps topography and coarse MOM vertical discretisation gave equally good results.

The original code also gave spurious strong, but more coherent flows in the central Equatorial Pacific in regions where the ocean bottom is level. These spurious flows were caused by the compressibility problem, associated with the dependence upon pressure of the density. The new formulation has also been tested against the old formulation in the simple channel configuration of Killworth and Edwards (1999). Results were broadly similar, but the new version required less explicit diffusivity to ensure smooth fields.

Fig. 4 (page 24) shows the global field of BBL thickness using the new formulation. Over the equatorial band f is small, and BBL velocities also tend to be greater, so the homogeneous-ocean depth scale u^*/f is large. Other regions of thick BBL lie along the continental slopes where again BBL velocities are large. Over most of the deep ocean the difference in temperature between the bottom gridbox and the BBL is small and positive, showing slightly stable conditions. Where BBL flows are strong however, particularly on the continental slopes, the temperature difference can reach 4°C or even greater, showing that the BBL is transporting waters with considerably different properties to those just above it.

Conclusions

The code thus appears stable and well-behaved. Any erroneous equatorial flows appear to be small, and the BBL is 'active' in physically sensible regions. Further improvements will involve isopycnal mixing (to further reduce smearing of dense water masses in overflows) as well as variable depth bottom boxes. The work will be coordinated with an ad hoc group (DOME) which is investigating the general problem of bottom mixing in a variety of models (DOME: Dynamics of Overflow Mixing and Entrainment;

http://www.gfdl.gov/~rwh/DOME/dome.html)

Acknowledgements

This work was carried out under agreement FS2/2040/12 under the Gassiot system, to insert the BBL code into the UK Met. Office Unified Model. We also acknowledge the encouragement from the DOME community.

References

Armi, L., and R. C. Millard, 1976: The bottom boundary layer of the deep ocean. J. Geophys. Res., 81, 4983–4990.

Beckmann, A., and R. Döscher, 1997: A method for improved representation of dense water spreading over topography in geopotential-coordinate models. J. Phys. Oceanogr., 27, 581–591.

Campin, J. M., and H. Goosse, 1999: Parameterization of density-driven downsloping flow for a coarse-resolution ocean model in z-coordinate. Tellus, 51, 412–430.

Dengg, J., C. Böning, and U. Ernst, 1999: Effects of an improved model representation of overflow water on the subpolar North Atlantic. Int. WOCE Newsl., 37, 10–15.

Killworth, P. D., and N. R. Edwards, 1999: A turbulent bottom boundary layer code for use in numerical ocean models. J. Phys. Oceanogr., 29, 1221–1238.

Pratt, L. J., and P. A. Lundberg, 1991: Hydraulics of rotating strait and sill flow. Ann. Rev. Fluid Mech., 23, 81–106.

Sandwell, D. T., and W. H. F. Smith, 1995: Marine gravity from satellite altimetry. Scripps Institutution of Oceanography, La Jolla, CA, USA (digital file, Version 7.2), anonymous ftp to baltica.ucsd.edu, Rep.

Song, Y. T., and Y. Chao, 2000: An embedded bottom boundary layer formulation for z-coordinate ocean models. J. Atmos. Oceanic Technol., 17, 546–560.

Zilitinkevich, S., and D. V. Mironov, 1996: A multi-limit formulation for the equilibrium depth of a stably stratified boundary layer. Boundary Layer Meteorol., 81, 325–351.

WOCE Hydrographic Program Office Report

James H. Swift, Director; Danielle M. Bartolacci, Data Analyst; Stephen C. Diggs, Data Manager; and Jerry L. Kappa, Publications Manager: all at Scripps Institution of Oceanography, USA. jswift@ucsd.edu

The WOCE Hydrographic Program Office at the UCSD Scripps Institution of Oceanography has three overriding and ongoing tasks:

- gather, merge, and make widely available all relevant data from the WHP,
- improve the adherence of WHP data to recommended format and content specifications, and
- assemble and provide all relevant documentation to accompany the WHP data.

The ultimate goal is to supply all WHP data and documentation to the WOCE Archive.

WHP Office resources during 1998–1999 focused primarily upon making the maximum number of data files available to the community via acquisition of new

files, replacements and updates to existing files, and merging of WHP tracer data into the bottle data files. Related to this has been assembling information and documentation about the cruises. Except for problem cases, the One-Time Survey data files are close to up to date at this time. There was a temporary lull during early 2000 in placing most new Repeat Hydrography data on line due to a focus on completing mergers of the One-Time data, but rapid progress on placing Repeat data on line has resumed. There are many more Repeat Hydrography data now available than previously.

Some WHP data remain "non public". This means that the data originators for the data in question do not yet wish that their data be usable by others without their knowledge and specific consent. The number of non-public data files has, however, greatly decreased during 2000.

Tables of detailed information on all WHP cruises are on line at the WHPO web site (http://whpo.ucsd.edu) and on WHP CD-ROMs, one click away from the summary information page for each cruise. These tables are now updated directly from the WHPO internal database of cruise information. These include the file history, listing all receipts and updates after the write date of the Version 1 WHP CD-ROM. The web site also includes a list of changed files.

The WHP Office continues to create documentation directories to be used in the files sent to the WOCE Archive. The archived versions will contain in addition to all the reports an ASCII version of the web site tables (including the detail tables and file histories), so that in the future a person who has access to the WOCE Archive will have all relevant information received and assembled by the WHP Office. The WHPO plans that cruise files at the WOCE Archive will be citable (authors, title, traceable reference, and year).

Data inconsistencies

There remain an alarming number of file format and content inconsistencies in WHP data. These are not easy to discover at times, let alone to repair in a timely manner. One problem for the WHPO is that many WHP data do not follow the "acquisition, processing, submittal, DQE, adjustment, archive" process envisioned by the WHP planners. Instead there is a semi-chaotic process where "preliminary" files and subsequent updates are received in near random order (for the various parameters) over a period of years, with some new files referenced to out of date versions of old companion files. Sometimes it is required from a data management standpoint to let a cruise lie until all the "submitted for DQE" versions of the files or accompanying tracer data arrive. (This sometimes means that an out-of-date file stays on the web site longer than desired.)

Some things can be said:

(1) All .sum, .sea., and .ctd files the SIO WHPO has sent out for DQE have gone through format checking and adjustment.

(2) The WHPO has begun a systematic format check and adjustment of all One-Time Survey files.

(3) Some inter-file inconsistencies were not picked up by earlier file checks, which concentrated on individual files. [The .sum and .sea files were matched, and the .sum and .ctd files matched, to the point of successful reading, but the .sea. and .ctd files were not compared previously.]

(4) The most seriously defective files are sometimes held off-line but can be provided to users in "as is" condition on request. The data detail tables on the WHP web site and CDs contain information about problems and repairs.

When tracer data (CFC, He/Tr, ^{14}C, CO_2 parameters) arrive at the WHPO, they may be based on the shipboard files, or on some internal file or format from the tracer laboratory, rather than to be based on a clean up version of the 'core' files the WHPO has prepared. Common issues include changed bottle or sample numbers, evidence of investigators working with data within their laboratories in their traditional (non-WOCE) format, tracer samples reported for stations, casts, and/or bottles not in the S / O_2 / nutrient file, and indexing by depth/pressure instead of station, cast, and bottle/sample number.

There are several sources of information about file format problems. When data arrive at the WHPO ftp site, the Data Manager makes a quick check for readability, during which the more obvious problems show up. When possible, there ensues a brief exchange with the data provider to see if a resubmission or other on-the-spot fix is feasible. Data users are effective sources of information about data and format problems. It is not always possible to take advantage of this information in a timely manner, but e-mails regarding such problems are archived, and often noted in the detailed data status tables that accompany each cruise.

Another type of discrepancy has arisen – the WOCE Data Information Unit noted earlier this year inconsistencies in EXPOCODE, cruise dates, and other data information across the overall WOCE programme and recommended a reconciliation, namely that a list of changes be instituted immediately. For the upcoming WOCE Version 2 CD-ROM set it was possible for the WHPO only to bring the information accompanying the data files (most importantly the EXPOCODE listed in the browsable cruise information tables) up to date with DIU recommendations, but due to the last minute nature of these changes it was not possible to write over all the EXPOCODEs inside the data files themselves. This will be fixed soon on the WHPO web site.

As noted, highest priority for the WHPO staff has been making the data and information available. But now that the WOCE programme is complete, and most of the data are at the WHPO, the effort is shifting to a systematic file clean up.

WHP "clean" file formats

The WHPO and many users have found that some of the WHP .sum (summary/header) files, even when corrected for repairable deficiencies, can still fail a file import application which is not robust enough. There is too much information which can be missing, and the WHPO, unlike a data user, cannot simply fill in values to make to-be-archived data look good.

A pragmatic solution discussed recently with the WOCE Data Products Committee is to instead have the WHPO create bottle and CTD data products which have the most-used information. In the clean bottle data files the .sum and .sea/.hyd files are in effect combined into one file adhering tightly to a spreadsheet-like comma-delimited ASCII standard to be published by the WHPO. Similarly for the .sum and .ctd files. WHP data files soon to be available in other formats such as netCDF will first be written in this "clean" WOCE format. It will take through summer 2000 to complete this for the One-Time Survey. The original WHP-format files will be archived at the WOCE Archive, so there will be no loss of information. But most future users will likely use only the clean files. See the WHPO web site for additional information, including small sample files.

Building Version 2.0 of WOCE Global Data on CD-ROM: A Summary of the Data Products Committee Meeting in April 2000

N. P. Holliday, Southampton Oceanography Centre, UK. penny.holliday@soc.soton.ac.uk

The WOCE Data Products Committee (DPC) met at Texas A&M University in early April 2000 to discuss the design of the second version of the WOCE data resource on CD-ROMs, and to discuss the future directions of the data system. The DPC members are a lively mix of data centre managers and scientists all keen to maximise the use of the WOCE data, not just by accumulating and assessing the data and metadata in data centres, but by finding ways to make the resource available to the wider community. To that end a second version of the WOCE data on CD-ROMs is being produced this year, following the first version distributed in 1998.

Why produce an interim version of the WOCE data on CD-ROM now? Well an important aspect is the increased data holdings of all the data centres; since Version 1.0 in 1998 the amount of data available has increased substantially, and new products have been created. In addition the DPC is committed to creating a truly integrated data archive from which a user will be able to search and extract data from across the wide variety of WOCE data sets with greater ease. The interim Version 2.0 makes an important step towards that goal by providing the majority of data files in a self-describing binary format, netCDF. This move will make it simpler for users to read the data files and search them on common variables. The advantage of netCDF is that the files do not have to have complex specified formats; each file contains its own format description in the header, enabling software to immediately read it. The DPC has carefully defined consistent variable names, and formats for such parameters as time and location to aid searching. NetCDF files can be read by many commonly used software packages and the CD package will include software to create ASCII files as well as a Primer for first-time users.

The DPC spent considerable time reviewing the contents of the Version 2.0 CD-ROMs. Some problems identified with Version 1.0 have been resolved thanks to feedback from users. Additional CDs will be included in the new package, including satellite surface wind fields from CERSAT, IFREMER, and an electronic atlas of WOCE bottle and profile data from R. Schlitzer at AWI. The new CD set will be published and distributed in September 2000; all recipients of the Version 1.0 CD set will automatically receive the new version, and further copies will be available from US-NODC who are funding the reproduction of the sets. The third and final version of the WOCE Global Data will be produced in time for the final WOCE Conference. Version 3.0 will have even greater levels of integration, with all data in netCDF or similar, and with search-and-retrieve facilities.

How to maintain the momentum of improvement that the WOCE data system has brought to the traditional oceanographic data management scene is a topic close to the hearts of DPC members. As the environment in which we make oceanographic observations changes with the development of more operational programmes and with wider applications for research data, the way in which data are managed and distributed is also changing. A far greater emphasis is being placed on real-time delivery of data and increased openness in data sharing. Projects like CLIVAR, GODAE and the Global Observing Systems all have specific requirements in terms of delivery of data and products, and the DPC is actively providing input to the development of new global data resources by liasing with planning committees. Some data facilities developed during WOCE will continue to provide a important contribution to global oceanographic data management, while others will no longer be required. The DPC is continuing to review its own activities in relation to developing programmes.

The next meeting of the DPC will be early in 2001.

The Global Ocean Data Assimilation Experiment

Michele Rienecker, NASA Goddard Space Flight Centre, USA; and Neville Smith, Bureau of Meteorology Research Centre, Australia. nsmith@bom.gov.au

The Global Ocean Data Assimilation Experiment (GODAE) is a partnership among agencies and research and development groups with an interest in operational oceanography and, in particular, in using and applying advanced models and data assimilation. They share a vision for

> "A global system of observations, communications, modelling and assimilation, that will deliver regular, comprehensive information on the state of the oceans, in a way that will promote and engender wide utility and availability of this resource for maximum benefit to the community."

The GODAE Strategic Plan (http://www.bom.gov.au/bmrc/mrlr/nrs/oopc/godae/Strategic_Plan.pdf) outlines the intended strategy (note this document is still in draft form). A more general description can be seen at http://www.bom.gov.au/OceanObs99/Papers/LeTraon.pdf. The concept of a GODAE was borne out of the conviction that

- The development and maturity of remote sensing and in situ observing systems now make global real-time observation feasible; and
- Steady advances in scientific knowledge meant that we were ready to model the global ocean and assimilate data in real-time.

The period 2003–2005 was seen as a good time to mount a demonstration of feasibility and practicality of this concept.

Objectives

The two primary objectives of GODAE are to:

1. Apply state-of-the art ocean models and assimilation methods to produce short-range open-ocean forecasts, boundary conditions to extend predictability of coastal and regional subsystems, and initial conditions of climate forecast models.
2. Provide global ocean analyses to develop improved understanding of the oceans, improved assessments of the predictability of ocean systems, and as a basis for improving the design and effectiveness of the global ocean observing system.

GODAE is a practical demonstration of real-time global ocean data assimilation for operational global oceanography and will be characterised by:

- Regular comprehensive depictions of the ocean circulation
- High temporal and spatial resolution;
- Consistency with a suite of remote and direct measurements; and
- Consistency with appropriate dynamical and physical constraints.

Integration is an over-riding theme. Each of the input data streams, like altimetry or *Argo*, have enormous power individually but, interpreted together, their power and utility will increase. There is also an integrated approach in terms of applications: the GODAE participants believe high-performance ocean model data assimilation centres can provide products that will serve multiple purposes, thus delivering efficiency in both our ability to exploit data and in our ability to process it effectively for broad user communities. CLIVAR has taken a similar approach to the climate problem: beyond TOGA, it was believed that an integrated, global approach to the coupled climate problem was the most appropriate. While it has not been stated explicitly, CLIVAR has also approached its observing requirements in this way as well.

Anticipated outcomes

To some, GODAE seems overly ambitious. To the GODAE participants, the broad applicability and utility of potential GODAE products, and their long-term legacy, are seen as powerful and positive. The anticipated outcomes include:

- improved predictability of coastal and regional subsystems through the provision of suitable oceanic boundary conditions,
- better initial conditions for climate predictions
- improved open ocean nowcasts and forecasts,
- integrated analyses or re-analyses for research programmes
- description of the ocean circulation and physics upon which more specialised systems can be developed and tested,
- a foundation for hypothesis testing, process studies , etc.
- improved availability and utility of ocean data,
- a methodology for systematic handling, quality control and consistent scientific interpretation (analysis) of special data sets,
- assessments of the observing system and of the utility of new ocean data sets,
- model testing and improvement through data assimilation,
- a viable, long-term observing system for GOOS; and
- development of an enhanced user base and suite of applications.

Guiding principles

The generation of globally consistent fields of upper ocean temperature, salinity and velocity through the synthesis of multivariate satellite and in situ data streams with models

is an identifying characteristic of GODAE. The concept of a GODAE Common is being used to foster free and open exchange among the participants. The Common comprises data, products, processing systems, models and assimilation tools available to and shared among all GODAE Partners.

The GODAE strategy also seeks to build upon, work with, and leverage off existing research and operational capabilities. The guiding principle in determining relevance of activities is that it must make a significant contribution to the development of the GODAE Common.

Inputs

GODAE has worked very closely with remote sensing agencies, through CEOS and through the Integrated Global Observing Strategy Partners, to develop the case for sustained remote measurements. The current status is reflected in the papers of the OceanObs Conference. These same agencies continue to value GODAE as an effective mechanism for maximising the value and effect of their efforts.

GODAE has (naturally) also worked closely with GOOS, particularly for the development of in situ contributions. GODAE, along with CLIVAR and its UOP, took a leading role in developing *Argo* and continues to work closely with the *Argo* ST on relevant scientific issues. *Argo* is seen as the only viable route toward a truly global in situ T and S measurement programme. GODAE is also initiating a project to develop high-resolution (space and time) SST products (see http://www.bom.gov.au/bmrc/mrlr/nrs/oopc/godae/4thIGST/Prospectus_HiResSST.htm for the draft prospectus for that project).

Ocean models are required to interpret, interpolate and extrapolate, in both space and time, the incomplete information provided by the in situ and remote data streams. The implementation of state estimation tools will often be model-specific, and it can be anticipated that a hierarchy of models and assimilation methods will be invoked. The typical GODAE model will be eddy-resolving and global, have many vertical levels (~50), include advanced upper ocean physics, possess high numerical performance, and be capable of interfacing efficiently interfaces with other models. Ocean state estimation methods will vary from the sophisticated to relatively simply, depending upon the primary use. Observing system sensitivity experiments have already been conducted for *Argo* and will be a key part of the GODAE tool set.

The unique nature of GODAE outputs

GODAE will contribute to, and in some cases lead, the development of more coherent, organised data sets through

- More effective assembly and availability;
- Improving data utility; and
- Improving data quality.

The processing stream outputs will include synoptic ocean analyses, short-range ocean forecasts, re-analyses, statistical characterisation of products (i.e., quantified error). The Strategic Plan gives further detail and discusses the functional components and the strategy for assuring progress and effective performance.

Synergy with CLIVAR

There are many areas where the applied activities of GODAE and the research of CLIVAR will overlap. In terms of applications, initial conditions for climate forecasts and re-analyses are obvious areas of common interest. There are also scientific and technical issues such as:

- Improvement in data quality, definition of covariance errors, developing/testing improved processing techniques, improvements in forcing fields, etc.,
- Development of advanced models and efficient/effective ocean assimilation schemes, and
- Understanding the (ocean) predictability of coastal/regional systems and thus the impact of improved boundary conditions derived from global models,

that will benefit from collaboration (indeed, because of the large intersection of the communities such collaboration will occur naturally).

Discussion

GODAE has large challenges it must face if it is to realise its ambitions. It has formally been in existence now for over 2 years and, while there has been satisfying progress in some areas, it has probably fallen behind schedule in other key areas. It draws strength from its Partners and Patrons – it is a bottom-up initiative, not a creation from the top. GODAE needs significant intellectual investment as well as investment in the data and model systems; computing power is looming as a major factor.

H. U. Sverdrup Symposium Announcement

The Role of Ocean, Sea Ice, Atmosphere Interaction in Polar and Sub-Polar Climate, Tromsø, Norway, 21–24 September 2000

The Norwegian Polar Institute (NPI) and the Fram Committee will be the hosts of an international symposium commemorating the Maud Expedition to the Arctic, which was concluded 75 years ago. Professor H. U. Sverdrup, who later become director of Scripps Institution of Oceanography and thereafter of the NPI, was responsible for the scientific aspects of the expedition. His name is also recognised by the American Meteorological Society, which awards the Harald U. Sverdrup Medal for outstanding scientific contributions.

Scientific Steering Committee

Jochem Marotzke, UK
Petter Haugan, Norway
John Calder, USA
Gennadi Matishov, Russia
Olav Orheim, Norway

Topics

The Intent of the symposium is to provide a current assessment of the role of the ocean/sea ice/atmosphere interaction in polar and sub-polar climate. The topics will include mixing and exchange processes, fluxes, deep-water formation and shelf processes. There will be invited papers, as well as other papers. There will be a limited poster display and brief oral poster presentations. Posters will have the same status as the oral papers in the published proceedings.

Workshop

As part of the Symposium a workshop will be organised with the aim of developing a broad international Arctic Ocean climate programme.

The workshop themes will cover the following subjects: Circumarctic fluxes (incl. fresh water), Paleoclimate, Processes. It will also include modelling input on what we need to know, and a session on new innovative technology and observing systems.

Submission of Abstracts for Papers and Posters

Participants who want to contribute to the symposium should submit an abstract of their proposed paper in English. This abstract must contain sufficient details to enable the scientific steering committee to form a judgement on the scientific merit and relevance of the proposed paper.

Send abstracts to Anne Kibsgaard, at kibsgaard@npolar.no preferably by e-mail. **LAST DATE FOR RECEIPT OF ABSTRACTS IS 15 AUGUST**.

Participation

The booking form for registration and accommodation can be downloaded from the Sverdrup Symposium web page: http://www.npolar.no/E/Cover/SverdrupSymp/Default.htm where more information on registration fees can be found.

The form and accompanying payments should be returned to the H. U. Sverdrup Symposium, c/o Norsk Polarinstitutt, Polarmiljøsenteret, N-9296 Tromsø, Norway, in accordance with instructions given, **before 20 August 2000**.

Conference Location

Tromsø has the midnight sun in summer, 2 metres of snow in winter, and the world's most northerly university with 6000 students. The city is located on a small island, surrounded by mountains. Airline communications include about a dozen daily direct flights from Oslo to Tromsø. The flying time is 1h 45 min.

The climate in Tromsø throughout the year is mild, due to the influence of the North Atlantic Current. Summer temperatures vary, with a mean temperature for August/ September of about 10°C. This time of the year is usually fairly dry, but we suggest you bring clothing for all conditions.

Accommodation

The principal symposium hotels will be Amalie Hotel and Comfort Hotel Saga. The hotels are within walking distance of the conference location. Please indicate your first and second choice on the enclosed form.

Further information

To find out more, please contact:

H. U. Sverdrup Symposium
c/o Norsk Polarinstitutt
Polarmiljøsenteret
N-9296 Tromsø, Norway.
E-mail: kibsgaard@npolar.no
Tel: + 47 77 75 06 16
Fax: + 47 77 75 05 01

Or visit the Sverdrup Symposium web page:
http://www.npolar.no/E/Cover/SverdrupSymp/Default.htm

WCRP/SCOR Workshop on Intercomparison and Validation of Ocean–Atmosphere Flux Fields (Washington, DC, USA, 21–25 May 2001)

The WCRP/SCOR Workshop on Intercomparison and Validation of Ocean–Atmosphere Flux Fields, to be held in Washington, DC, USA, **(21-25 May 2001),** is the second meeting encouraging interaction and dialogue between the diverse scientific communities involved in producing and using air–sea fluxes.

Following the landmark First WCRP Workshop on Air–Sea Flux Fields for Forcing Ocean Models and Validating GCMs held at ECMWF, Reading, in October 1995, a joint WCRP/SCOR Working Group on Air–Sea Fluxes was set up to continue to foster interdisciplinary consultations in this area, and to catalogue and keep under review available surface flux and flux-related data sets. The Final Report of the Working Group is a substantial document assessing the present state of the art in regard to air sea flux determination ("Intercomparison and Validation of Ocean–Atmosphere Energy Fluxes" shortly to be published in the WCRP report series). The report can be accessed at

http://www.soc.soton.ac.uk/JRD/MET/WGASF

Aims of the Workshop are to:

- bring together the different scientific communities interested in air–sea fluxes and working on their development and application through modelling, remote sensing and in-situ measurements;
- stimulate discussion by a wide spectrum of the research community on the issues raised in the WGASF report, consider group recommendations and discuss priorities for future activities in the areas identified as significant knowledge gaps;
- consider the need for any continuing internationally coordinated initiative in air–sea flux studies.

A focus of the Workshop will be to summarise recent developments of in-situ, remotely sensed and model output fields for flux and flux related parameters. Particular attention will be devoted to assessing the uncertainties inherent in the various fields. Although primarily concerned with global-scale flux climatologies, emphasis will also be given to the development of flux parameterisations, and to field experiments and other high quality in-situ flux data, designed to refine those parameterisations. Contributions dealing with global and basin-scale energy balances, and the variability of ocean–atmosphere fluxes will also be welcome.

The Workshop is intended to promote feedback and encourage dialogue between the producers and users of surface flux and related data. Following an introductory presentation of the WGASF report, sessions will address the key topics using a combination of invited, oral and poster papers. Break-out groups will be tasked with considering an effective and balanced strategy for making further progress in the study and utilisation of ocean–atmosphere fluxes.

Workshop organisers (Frank Bradley, Sergey Gulev – organising committee chair, David Legler – local organising committee chair, Roger Newson, Joerg Schulz, Peter Taylor, and Glenn White) invite all interested scientists to send statements of interest, abstracts of papers (if you are going to present one) and submittal information (name, address, e-mail, telephone, fax) should be sent on e-mail, mail or fax by the deadline of **15 January 2001** to Sergey Gulev (P.P. Shirshov Institute of Oceanology, RAS, 36 Nakhimovsky ave., 117851 Moscow, Russia, e-mail: gul@gulev.sio.rssi.ru, fax: +7-095-1245983, tel.: +7-095-1247985). Further information about the Workshop will be available shortly at

http://www.soc.soton.ac.uk/JRD/MET/WGASF

MEETING TIMETABLE

2000

21–24 September	H.U. Sverdrup Symposium: The Role of Ocean, Sea-Ice, Atmosphere Interaction in Polar and Sub-Polar Climate	Tromsø, Norway
27–30 September	47th Annual Eastern Pacific Oceanography Conference (EPOC)	Victoria, Canada
9–11 October	CLIVAR-JSC Working Group on Coupled Modelling	La Jolla, USA
9–12 October	CLIVAR Workshop on Shallow Tropical–Subtropical Overturning Cells (STC) and Interaction with Atmosphere	Venice, Italy
16-27 October	Latin America School in Ocean and Climate Modelling	Concepcion, Chile
17–20 October	WOCE/CLIVAR Representativeness and Variability Workshop	Fukuoka, Japan
20–28 October	PISCES 9th Annual Meeting	Hakodate, Japan
21–22 October	WOCE-27	Fukuoka, Japan
12–14 November	CLIVAR Ocean Observing Panel Meeting	Perth, Australia
13–15 November	CLIVAR Indian Ocean Workshop	Perth, Australia
15–17 November	Jason/Topex Science Working Team	Miami Beach, USA
16–18 November	CLIVAR Southern Ocean Workshop	Perth, Australia
28 November–1 December	Chapman Conference on NAO	Orense, Spain
1-2 December	CLIVAR Atlantic Implementation Panel Meeting	Orense, Spain
15–19 December	AGU Fall Meeting	San Francisco, USA

2001

22–25 January	CLIVAR Pacific Implementation Panel	Hawaii, USA
26–30 March	EGS XXVI General Assembly	Nice, France
14–18 May	CLIVAR SSG-10	Toulouse, France
21–25 May	WCRP/SCOR Workshop on Intercomparison and Validation of Ocean–Atmosphere Flux Fields	Washington, DC, USA
29 May–2 June	AGU 2001 Spring Meeting	Boston, USA
25–29 June	WOCE Ocean Transport Workshop	Southampton, UK
10–13 July	IGBP Open Science Conference	Amsterdam, NL
20–24 August	Climate Conference 2001	Utrecht, NL
21–28 October	IAPSO-IABO 2001: an Ocean Odyssey	Mar del Plata, Argentina
10–14 December	AGU 2001 Fall Meeting	San Francisco, USA

The WOCE International Newsletter is published by the WOCE International Project Office.

Editor:
Roberta Boscolo

Compilation and layout:
Sheelagh Collyer

The International WOCE Newsletter is distributed free-of-charge upon request thanks to the funding contributions from France, Japan, UK, and WCRP.

This Newsletter provides a means of rapid reporting of work in progress related to the Goals of WOCE as described in the WOCE Scientific and Implementation Plan.

Requests to be added to the mailing list and changes of address should be sent to:
WOCE IPO
Southampton Oceanography Centre
Empress Dock
Southampton SO14 3ZH
United Kingdom
Tel. +44 23 8059 6205
Fax. +44 23 8059 6204
e-mail: woceipo@soc.soton.ac.uk

Contents of past issues together with the electronic PDF version can be found at:
http://www.soc.soton.ac.uk/OTHERS/woceipo/acrobat.html

Articles, letters, announcements and reviews are welcome and should be addressed to the editor.

Printed by Technart Ltd.
Southern Road
Southampton SO15 1HG
United Kingdom.

If undelivered please return to:

WOCE IPO
Southampton Oceanography Centre
Empress Dock
Southampton SO14 3ZH
United Kingdom.

CONTENTS OF THIS ISSUE